Protein Engineering for Targeted Delivery of Radionuclides to Tumors

by
Kelly Davis Orcutt

B.S., Chemical Engineering
Johns Hopkins University, 2004

Submitted to the Department of Chemical Engineering
in partial fulfillment of the requirements for the degree of

DOCTOR OF PHILOSOPHY IN CHEMICAL ENGINEERING

at the

MASSACHUSETTS INSTITUTE OF TECHNOLOGY

[February 2010]
December 2009

Signature of Author: _____
Department of Chemical Engineering
Dec 15, 2009

Certified by: _____
K Dane Wittrup
C.P. Dubbs Professor of Chemical and Biological Engineering
Thesis Supervisor

Accepted by: _____
William M. Deen
Professor of Chemical Engineering
Chairman, Committee for Graduate Students

Protein Engineering for Targeted Delivery of Radionuclides to Tumors

by
Kelly Davis Orcutt

Submitted to the Department of Chemical Engineering on December 15, 2009 in partial fulfillment of the requirements for the degree of Doctor of Philosophy in Chemical Engineering

ABSTRACT

Traditional cancer treatment strategies include systemic chemotherapy, external beam radiation, and surgical excision. Chemotherapy is nonspecific, and targets all rapidly dividing cells. External beam radiation and surgery only target known cancer sites. However, targeted therapeutics, such as antibodies, will bind to all cancer cells that express the targeted antigen, including small metastases that are invisible by current imaging technology. In the past decade, nine antibodies have been approved for the treatment of cancer and are demonstrating moderate success in the clinic. Some of these antibodies have intrinsic toxic effects and block the interaction of growth factors or induce cell death. Other antibodies are conjugated to drugs, toxins, or radioactive isotopes. Unfortunately, antibodies exhibit slow clearance from the body and exposure of healthy tissues to toxins or radiation can result in undesirable side effects that limit the doses that can be safety administered to the patient.

We have used rational engineering design and mathematical modeling to develop a novel pretargeted radioimmunotherapy (PRIT) approach for the treatment of cancer. In PRIT, a bifunctional antibody is administered and allowed to bind to a cancer antigen. After sufficient tumor uptake of the antibody, a small molecule carrying a radionuclide is administered and captured by the pretargeted antibody while unbound molecules clear rapidly from the body. PRIT combines the high binding specificity of antibodies with the rapid clearance properties of small molecules. We have identified a small molecule metal chelate, DOTA, which exhibits rapid whole-body clearance and that has demonstrated safety in humans. We engineered a high-affinity antibody fragment specific to DOTA and subsequently engineered a novel bispecific antibody (bsAb) construct with specificity for both DOTA and carcinoembryonic antigen (CEA). The bsAb exhibits retention of parental affinities, *in vivo* stability, and tumor targeting. The engineered PRIT approach was tested in a mouse tumor model and demonstrates excellent DOTA capture at the site of the tumor with the best 48 hour tumor to blood and tumor to kidney ratios reported to date for CEA targeting. The PRIT approach developed here can be easily applied to other disease targets and has the potential to impact clinical cancer radioimmunotherapy.

Acknowledgements

My advisor, Dane Wittrup, has been a phenomenal mentor to me. His patience, advice, and guidance have been invaluable. The independence he has given me has allowed me to grow and develop my confidence as an independent researcher.

I want to thank my thesis committee members, Dr. Bill Deen, Dr. George Stephanopoulos, Dr. Tony Parker and Dr. John Frangioni. I always looked forward to my thesis committee meetings and the helpful insights and feedback that came from them. I thank Dr. Tony Parker for his invitation to attend the Joint Program in Nuclear Medicine seminars at Harvard Medical School through which I have gained breadth in the fields of nuclear medicine and molecular imaging. I am especially grateful to Dr. Frangioni for inviting me into his lab as a research student at Beth Israel Deaconess Medical Center and giving me the opportunity to study our engineered proteins in mouse tumor models. Working in his lab has been an amazing opportunity for me to learn radiochemistry, preclinical animal experimentation, and state-of-the-art small animal imaging. The *in vivo* data presented throughout this thesis would not exist without Dr. Frangioni's support and mentoring.

My research assistants Gabriel Tobon, Ben Ruiz-Yi, Maryelise Cieslewicz, Adrian Slusarczyk, Gaurav Gulati, and David Levary have all worked very hard and contributed to the work presented here. Their inquisitiveness and thoughtful suggestions have challenged me to think about research problems in new and exciting ways.

I want to thank all of the graduate students and post docs of the Wittrup lab who have helped me during my time there and created a friendly and stimulating lab culture. Stefan Zajic, Shaun Lippow, Andy Rakestraw, Ginger Chao, Wai Lau, Dasa Lipovsek, Andrea Piatesi, Pankaj Karande, Greg Thurber, Shanshan Howland, Steve Sazinsky, Margie Ackerman, Annie Gai, Ben Hackel, Eileen Hingham, and Mike Schmidt all welcomed me into the lab and taught me molecular biology and protein engineering. I also want to thank David Liu who joined the lab when I did, and the younger students, Jordi Mata-Fink, Jamie Spangler, Chris Pirie, John Rhoden, Xiaosai Yao and Tiffany Chen with whom I have enjoyed discussing science, sharing reagents, and collaborating on projects. I especially thank Don McGaffigan for administrative assistance.

I also want thank all of the Frangioni lab members, who have been so incredibly helpful and supportive; Lori Moffitt, Eugnia Trabucchi, Khaled Nasr, Preeti Misra, Kumar Bhushan, Hak Soo Choi, Jeong Heon Lee, Summer Gibbs-Straus, Sanjeev Mathur, Sylvain Gioux, Rafiou Oketokoun, Yoshi Ashitate, Kazu Inoue, Fangbing Liu, Merlijn Hutteman, Alan Stockdale, and Barbara Clough. I especially want to thank David Whitehead and Lainey Lunsford for helping to collect some of the animal data presented here.

I want to acknowledge Vladamir Voynov of the Trout lab for helpful discussions and assistance with mammalian cell culture and the MIT Flow Cytometry Core Facility for technical assistance.

I want to thank collaborators Steve Larson and Peter Smith-Jones at Memorial Sloan Kettering Cancer Center and Paul Yazaki at the City of Hope.

I especially want to thank my parents and my brother for their unconditional love and support and for encouraging me to always follow my passion and my dreams.

Last but not least, I'd like to thank my husband, Jason. If it weren't for him, I wouldn't be writing this thesis. He kept me sane throughout the frustrations of research.

Table of Contents

List of Figures

List of Tables

1. INTRODUCTION

1.1. Antibodies in Cancer Treatment

Traditional cancer treatment strategies include chemotherapy, external beam radiation and surgical excision. Chemotherapy is nonspecific and targets all rapidly dividing cells resulting in undesirable side effects. In addition, tumors can become resistant to chemotherapy. External beam radiation and surgery are only able to target known tumor sites, and will miss undetectable metastases. In the past decade, the development of targeted antibody therapeutics has demonstrated significant improvements in cancer treatment, increasing the number of patient responses to treatment for several types of cancer (Hudson and Souriau 2003; Nayeem and Khan 2006; Tassev and Cheung 2009; Weiner et al. 2009).

Antibodies are proteins made by the immune system to target foreign pathogens. Each antibody is highly specific for a particular antigen or target. Antibodies can be engineered with specificity to surface receptors on cancer cells. These antibodies can either be naked or conjugated to drugs, toxins, or radioactive metal atoms. Naked antibodies can target cancer cells for recognition and destruction by the immune system (Iannello and Ahmad 2005). Naked antibodies can also block the interaction of growth factors and signaling molecules with cancer cell receptors, reducing proliferation and metastasis (Capdevila et al. 2009). Unfortunately, similar to chemotherapy, cancer can become resistant to antibody therapy over time and certain aggressive forms of cancer show no response at all (Garber 2003; Hopper-Borge et al. 2009).

There are current efforts to conjugate tumor-targeting antibodies to chemotherapeutics, toxins, and radioisotopes. It is believed that antibody-mediated delivery of these substances will increase tumor toxicity and decrease normal tissue toxicity. Most chemotherapeutics and toxins need to be delivered to the cytoplasm of a cell to induce cell death. This requires the targeting of each individual cancer cell, a relatively daunting task due to tumor vascular heterogeneity, high tumor pressure limiting convection, and non-functional and transiently-functional blood vessels. Therapeutic

radioisotopes, however, have path lengths on the order of 10 to 1000 cell diameters (Cutler et al. 2000) and therefore not every cell would require antibody targeting in order to deliver cytotoxic doses of ionizing radiation to the entire tumor. Therapy using radioisotope-conjugated antibodies, or radioimmunotherapy, is thus a very active area of research.

1.2. Radioimmunotherapy

Ibritumomab tiuxetan and tositumomab are two radioimmunotherapy agents currently approved by the FDA for the treatment of certain types of Non-Hodgkin's lymphoma. These agents are both radioisotope-conjugated antibodies specific to the cell surface antigen CD20 and have demonstrated patient responses in CD20-positive B-cell Non-Hodgkin's lymphoma when chemotherapy and rituximab, a naked antibody, fail (Horning et al. 2005; Park and Press 2007). However, despite the clinical responses to ibritumomab tiuxetan and tositumomab, most chemotherapy- and rituximab-resistant patents relapse and die.

The radioactive dose that can be delivered to a tumor is limited by the dose-limiting organ. In radioimmunotherapy of Non-Hodgkin's lymphoma, the bone marrow is the dose-limiting organ due to the radiosensitivity of bone marrow and long antibody circulation times in the blood, resulting in significant blood cumulative activity. In addition, low levels of CD20 expression have been observed in marrow, and marrow involvement occurs in some patients. A time course of radioimmunotherapy imaging of a patient with Non-Hodgkin's lymphoma is shown in Figure 1.1. Note the high activity in the heart and large blood vessels at early times indicating high blood activity. The tumor is not visible above background until after several days. It is thought that if the administered radioactivity could be cleared faster from non-tumor tissues, higher doses could be administered, higher tumor radioactive doses could be achieved, and significantly more cancer cures would be observed in the clinic.

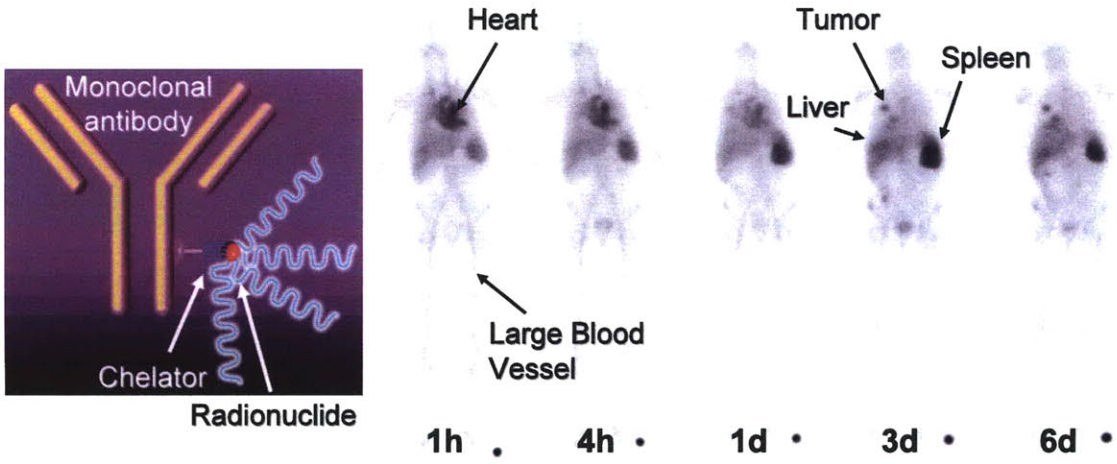

Figure 1.1 Radioimmunotherapy. A schematic of a radioimmunotherapy agent (left) and a radioimmunotherapy imaging time course of a Non-Hodgkin's lymphoma patient (right). Figure courtesy of Dr. Tony Parker.

In addition to improving treatment for Non-Hodgkin's lymphoma, a blood cancer, higher tumor radioactive doses may allow radioimmunotherapy to successfully treat solid tumors. Solid tumors are significantly more challenging to treat with antibody-based technology, due to high intra-tumoral pressure (Baxter and Jain 1989) resulting in transport limitations of the antibody crossing the capillary wall (Thurber et al. 2008). Because of the low permeability coefficient of antibodies across the vasculature, large antibody concentrations are needed to obtain sufficient solid tumor penetration. Systemic exposure of healthy tissues to radiation due to the slow antibody plasma clearance mentioned above limits the dose that can be safely administered.

If the delivery of the targeting antibody could be separated from the delivery of the radioisotope, significantly higher tumor to non-tumor ratios could be achieved. If one could wait until after the antibody had localized to the tumor (day 3 or later in Figure 1.1) to "turn on" or deliver the radiation, higher tumor doses and lower nonspecific doses would be realized. Thus, we are interested in a technology called pretargeted radioimmunotherapy (PRIT).

1.3. Pretargeted Radioimmunotherapy

PRIT decouples the pharmacokinetics of antibody targeting and radionuclide delivery, and has been shown to increase efficacy and decrease toxicity in both

preclinical (Kraeber-Bodere et al. 1999; Axworthy et al. 2000; Gautherot et al. 2000; Pagel et al. 2003; Sharkey et al. 2003; Karacay et al. 2005) and clinical models (Knox et al. 2000; Kraeber-Bodere et al. 2006). In PRIT, the antibody is administered first and allowed to bind to the targeted surface receptor on the cancer cells. Then, a chelated radionuclide is administered and "captured" by the antibody retained at the site of the cancer (Figure 1.2). With this two step process, the small radionuclide molecule diffuses rapidly throughout the body and is cleared quickly, significantly reducing the non-specific radiation associated with directly-conjugated antibodies.

The idea of PRIT was originally published over 20 years ago (Goodwin et al. 1988). The first PRIT technology was based on the high affinity binding of streptavidin and biotin for radionuclide capture (Paganelli et al. 1991). While this system has demonstrated excellent proof of concept, there are several major reasons why this strategy is not clinically viable. Streptavidin is a bacterial protein and is highly immunogenic in humans. Endogenous levels of biotin (also known as vitamin H) compete with biotinylated metal-chelate-conjugates (Hamblett et al. 2002). In addition, streptavidin exhibits high uptake in the kidney, where it remains accessible to binding by biotinylated hapten (Forster et al. 2006). A seminal clinical trial of pretargeted radioimmunotherapy using streptavidin resulted in delayed nephrotoxicity and several patient deaths due to kidney toxicity (Knox et al. 2000).

In light of these issues, bispecific antibodies with alternative capture methods are under development. One system involves an antibody fragment specific to ^{111}In-DTPA in a chemically conjugated Fab-based bispecific antibody format (Barbet et al. 1998; Kraeber-Bodere et al. 2006). However, the anti-DPTA antibody fragment exhibits significantly lower affinity to chelated metals other than indium, limiting the utility of this system. Another pretargeted system developed recently uses a Fab specific to a small peptide hapten and a novel protein domain tethered Fab-based bispecific antibody construct (Sharkey et al. 2003). However, nontrivial synthesis of the peptide chelate and bispecific antibody is required. In addition, the biodistribution and safety of the peptide chelate is unknown in humans. Both of these pretargeted radioimmunotherapy systems use relatively small bispecific antibody constructs with no Fc domain (antibody constant

region). Published experimental data demonstrate that IgG-like molecules with retained Fc domain result in significantly higher tumor uptake than smaller fragments.

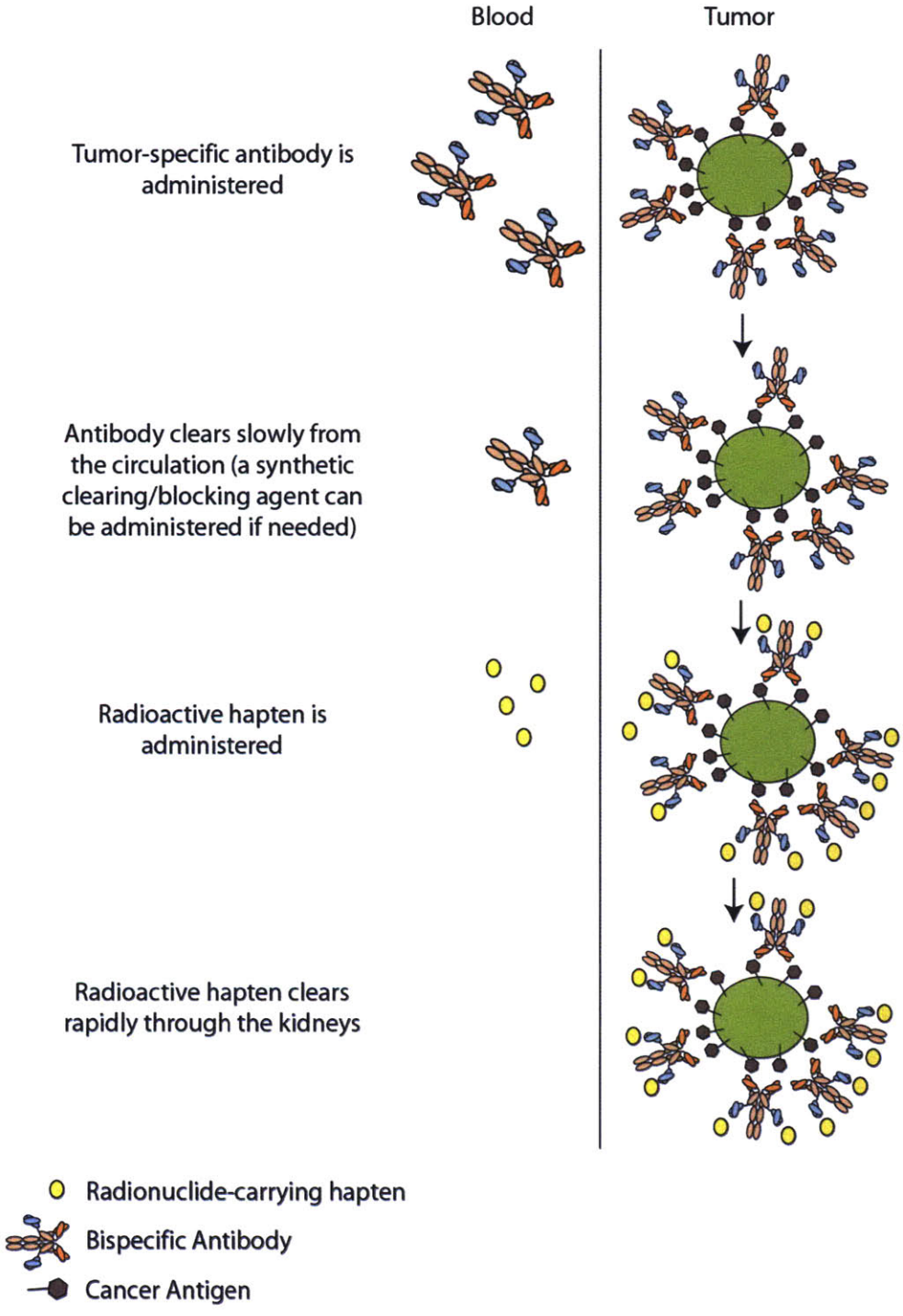

Figure 1.2 A schematic of pretargeted radioimmunotherapy.

1.4. Introduction to the Thesis

In this thesis, we present a new approach to pretargeted radioimmunotherapy, based on rational engineering design and mathematical modeling.

DOTA (Figure 1.3) was selected as the radionuclide-carrying hapten, due to its ability to chelate trivalent metal cations and its favorable clearance properties and demonstrated safety in humans. DOTA chelated to gadolinium (Gd-DOTA) has extensive clinical history as a magnetic resonance imaging (MRI) contrast agent and has an excellent safety profile (Le Mignon et al. 1990; Bourrinet et al. 2007). Gd-DOTA diffuses rapidly, and exhibits rapid renal clearance.

To use DOTA for PRIT, a high-affinity antibody to DOTA metal chelates is needed. An anti-DOTA antibody with relatively weak affinity has been previously isolated and characterized (Goodwin et al. 1994; Corneillie et al. 2003; Corneillie et al. 2003). We synthesized a single chain variable fragment (scFv) from the variable domains of this antibody and used yeast surface display and directed evolution to affinity mature the scFv. The end goal for the affinity maturation was determined by mathematical modeling. Mathematical modeling and subsequent affinity maturation are described in Chapter 2.

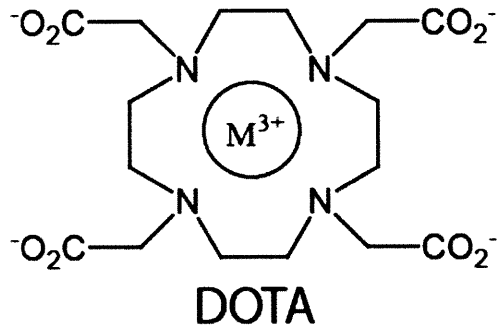

Figure 1.3 Molecular structure of DOTA. DOTA chelates trivalent metal cations (M^{3+}).

The next step in developing a pretargeted radioimmunotherapy system is the design of a bispecific antibody with tumor targeting properties. In chapter 3 of this thesis, we describe a novel IgG-like bispecific antibody topology constructed as an scFv fusion to the C-terminus of an IgG light chain. A bispecific antibody of this format was

synthesized containing the engineered high affinity DOTA-binding scFv and an IgG specific to carcinoembryonic antigen (CEA), a tumor antigen expressed in about 50% of colorectal, stomach, liver, and pancreatic carcinomas.

In an effort to minimize hapten retention in normal tissues, a series of DOTA-based derivatives were evaluated for blood clearance and organ biodistribution *in vivo*. ^{177}Lu-labeled DOTA, DOTA-biotin, a di-DOTA tyrosine lysine peptide, and DOTA-aminobenzene were evaluated. This study is described in Chapter 4.

We tested our rationally designed system in a mouse xenograft tumor model and demonstrate tumor targeting of the bsAb, and DOTA capture at the site of the tumor, which are presented in Chapter 5. An IgG-like bsAb will result in high tumor uptake but also slow systemic clearance resulting in residual bsAb in the blood. We thus engineered a novel dextran-based blocking agent to reduce DOTA binding to residual bispecific antibody. We determine tumor to background ratios for our engineered three-step approach and present quantitative biodistribution data and SPECT/CT images.

Affinity maturation of the anti-DOTA scFv described in chapter 2 resulted in an antibody fragment that binds with different affinities to DOTA, depending on the coordination chemistry of the chelated metal and the absence or presence of a small benzene adduct to one of the carbons of the macrocycle. This effect resulted in an excellent system to study the impact of affinity on small molecule tumor targeting *in vivo*. Using two different isotopes and two different DOTA-based derivatives, we were able to analyze the affect of affinity over three orders of magnitude in a systematic fashion *in vivo* in tumor-bearing mice (presented in chapter 5). This type of systematic study of the effect of affinity on small molecule tumor uptake *in vivo* has not been possible previously.

2. AFFINITY MATURATION OF DOTA-SPECIFIC ANTIBODY

2.1. Abstract

We aim to engineer high-affinity binders to DOTA chelates for use in PRIT applications. We mathematically modeled antibody and hapten pharmacokinetics to analyze hapten tumor retention as a function of hapten binding affinity. Modeling predicts that for high antigen density and saturating bsAb dose, a hapten binding affinity of 100 picomolar (pM) is needed for near-maximal hapten retention. Motivated by model predictions, we used directed evolution and yeast surface display to affinity mature the 2D12.5 antibody to 1,4,7,10-tetraazacyclododecane-1,4,7,10-tetraacetic acid (DOTA), reformatted as a single chain variable fragment (scFv). Affinity maturation resulted in a 1000-fold affinity improvement to biotinylated DOTA-yttrium, yielding an 8.2 ± 1.9 picomolar binder. The high-affinity scFv binds DOTA complexes of lutetium and gadolinium with similar picomolar affinity and indium chelates with low nanomolar affinity. When engineered into a bispecific antibody construct targeting carcinoembryonic antigen (CEA), pretargeted high-affinity scFv results in significantly higher tumor retention of a ^{111}In-DOTA hapten compared to pretargeted wild-type scFv in a xenograft mouse model. We anticipate that this engineered versatile, high-affinity DOTA-chelate-binding scFv will prove useful in developing pretargeted imaging and therapy protocols.

2.2. Introduction

The first PRIT reagents used the high-affinity binding of streptavidin to biotin for radionuclide capture. However, this approach is limited by streptavidin immunogenicity, kidney localization, and endogenous biotin binding to streptavidin. Second generation PRIT approaches employ bispecific antibodies (bsAb) with specificity for both cancer antigen and chelated radionuclide (Goldenberg et al. 2007). An approach with a bispecific antibody recognizing an indium EDTA derivative has been studied previously (Stickney et al. 1991). Because antibodies to metal chelates generally exhibit relatively weak binding, researchers have taken advantage of avidity and developed bivalent haptens to improve tumor retention of the radiometal chelate (Le Doussal et al. 1989; Janevik-Ivanovska et al. 1997; Sharkey et al. 2003; Kraeber-Bodere et al. 2006; Goldenberg et al. 2007). Another approach to improve hapten tumor retention uses an engineered redox-reactive group in the radiometal chelate to attach covalently to a free thiol in the antibody (Corneillie et al. 2004). However, it remains a challenge to maintain the free thiol during antibody production, purification and delivery.

We present here an alternative approach using DOTA as the radionuclide-carrying hapten. DOTA-metal-complexes are essentially irreversible under physiological conditions and demonstrate higher thermodynamic stability than linear DTPA and EDTA complexes for many metals including gadolinium, yttrium, and lutetium (Camera et al. 1994; Byegard et al. 1999; Penfield and Reilly 2008). DOTA-gadolinium (DOTA-Gd) has extensive clinical history as an MRI contrast agent (Le Mignon et al. 1990). DOTA-Gd diffuses rapidly, and exhibits rapid renal clearance. A monoclonal DOTA-binding antibody, 2D12.5, was previously isolated from an immunized mouse (Goodwin et al. 1994; Lubic et al. 2001). 2D12.5 binds to DOTA chelates of all lanthanides with similar nanomolar affinity (Goodwin et al. 1994; Corneillie et al. 2003) and to DOTA chelated to indium and copper with weaker affinity (Corneillie et al. 2004). This promiscuity in binding is an unusual property, as other anti-metal-chelate antibodies generally bind only one or two chelated metals with significant affinity (Love et al. 1993; Blake et al. 2001).

The goal of the present study was to develop a high-affinity antibody to DOTA chelates, starting from the 2D12.5 antibody. A high-affinity DOTA binder will enable the use of simply DOTA as the pretargeted hapten.

There are many display systems used to engineer proteins to increase affinity, specificity, and stability, including phage, mRNA, and bacterial display. These display systems provide a direct connection between genotype and phenotype by linking the protein of interest with its genetic encoding material. We have chosen to use yeast surface display in our affinity maturation efforts presented here. In yeast surface display, a plasmid containing the gene of interest is contained episomally within the yeast cell while the encoded protein is expressed on the surface. Yeast surface display allows the use of the eukaryotic expression bias of yeast, allowing for engineering of complex proteins that require posttranslational modifications such as foldase and chaperone mediated assembly. A recent study showed that yeast display allows for the selection of proteins that are nonfunctional when expressed on phage (Bowley et al. 2007). In addition to eukaryotic expression, yeast surface display allows for fluorescence activated cell sorting (FACS) to be used allowing for high throughput quantitative screening of protein expression and antigen binding in real time. Normalization for protein expression used with two-color FACS allows for fine affinity discrimination between clones (VanAntwerp and Wittrup 2000). In addition, expedient characterization of binding kinetics as well as thermal stability of proteins can be performed without time consuming soluble expression and purification.

2.3. Materials and Methods

2.3.1. Mathematical Modeling

The PRIT models developed here are straightforward extensions of two model systems developed and described by Thurber and colleagues (Thurber et al. 2007). The micrometastasis model uses spherical geometry and assumes diffusion-only transport. The vascularized tumor model uses cylindrical geometry around capillaries. Numerical simulations were performed in MATLAB (The MathWorks, Framingham, MA). Details of the mathematical models are provided in the appendix (section 7.1).

PRIT simulations were performed for a 1 g vascularized tumor and a 400 μm diameter micrometastasis assuming a 70 kg human with 3.5 L of plasma volume. An IgG-like bispecific antibody is given as a bolus dose of 7 μmol at time zero. The hapten is given as a bolus dose of 350 nmol with 5 GBq initial activity at 72 h. The model implements a clearing/blocking step 24 h before hapten dosing, in which 99.9% of bsAb hapten binding sites are blocked in the blood compartment. After hapten dosing, unbound hapten concentration in the blood is calculated as the initial hapten concentration minus hapten binding sites in the blood from unblocked residual antibody. The model assumes a ^{90}Y radionuclide that has a residualization half life of 120 h after cellular internalization.

2.3.2. Synthesis of DOTA Compounds

DOTA (Macrocyclics M-140) and DOTA-Bn (S-2-(4-Aminobenzyl)-1,4,7,10-tetraazacyclododecane tetraacetic acid; Macrocyclics B-200) were dissolved in 0.4 M sodium acetate, pH 5.2, as stock solutions.

DOTA-Bn-biotin was synthesized by dissolving Amine-PEG_3-Biotin (Pierce 21347) and p-SCN-Bn-DOTA (S-2-(4-Isothiocyanatobenzyl)-1,4,7,10-tetraazacyclododecane-tetraacetic acid; Macrocyclics B-205) in dimethyl sulfoxide (DMSO) with a 10-fold molar excess of triethylamine (VWR #EM-TX1200-5). The reaction mixture was vortexed at room temperature for 3 h, and then purified by high performance liquid chromatography (HPLC). HPLC purification was performed on a C-18 reverse-phase

column (Agilent Model 1100 HPLC, 1 x 25 cm, buffer A = 0.05% trifluoroacetic acid (TFA), buffer B = 0.0425% TFA in 80% acetonitrile, 2 – 100% B gradient for 98 min). Flow through was monitored by absorbance detection at 280 nm. Fractions containing DOTA-Bn-biotin were confirmed using matrix assisted laser desorption instrument time of flight (MALDI-TOF) mass spectrometry (Applied Biosystems Model Voyager DE-STR). Chemical purity was assessed by analytical HPLC (Agilent Model 1100 HPLC, 2.1 x 150 mm, buffer A = 0.05% TFA, buffer B = 0.0425% TFA in 80% acetonitrile, 2-100% B gradient for 45 min). DOTA-Bn-biotin concentration was determined using a biotin quantitation kit (Pierce 28005) following the manufacturer's instructions.

(+)-(2S)-2-(4-Aminobutyl)-1,4,7,10-tetra-azacyclododecane-1,4,7,10-tetrayltetra-acetic acid (DOTA-alkyl) has been synthesized previously (Cox et al. 1990). Here, it was synthesized following the procedure of Takenouchi et al. (Takenouchi et al. 1993) starting with the compound H-Lys(Boc)-OMe (Bachem, E-1620). H-Lys(Boc)-OMe was treated stepwise with methyl bromoacetate and diethylenetriamine to obtain *tert*-butyl 4-(3,12-dioxo-1,4,7,10-tetraazacyclododecan-2-yl)butylcarbamate. Borane·THF complex (Ashweek et al. 2003) was used to reduce the carboxylic amides followed by trifluoroacetic acid Boc deprotection to obtain 4-(1,4,7,10-tetraazacyclododecan-2-yl)butan-1-amine. This compound was subsequently reacted with biotin-xx, SSE (Invitrogen, B-6352) in DMSO with a 10 fold molar excess of triethylamine for 3 h vortexing at room temperature to form DOTA-alkyl-biotin. In all synthesis steps compounds were purified by HPLC and their identity and purity confirmed by mass spectrometry with a Waters (Milford, MA) LCT electrospray time-of-flight (ES-TOF) liquid chromatography mass spectrometry (LC/MS) or by MALDI-TOF as described above.

Metal complexes of each DOTA derivative (see Figure 2.2 for chemical structures) were prepared as follows. Yttrium nitrate hexahydrate, lutetium (III) chloride hexahydrate, indium (III) chloride, gallium (III) nitrate hydrate, and gadolinium (III) chloride hexahydrate were purchased from Sigma and prepared as stock solutions in 0.4 M sodium acetate pH 5.2. To a 2 mM (for DOTA and DOTA-Bn) or 400 μM (for DOTA-Bn-biotin) solution of the chelating agent, a 5-fold molar excess of the metal

stock solution was added and chelated by overnight rotation at room temperature. The pH was adjusted to 7 with 10 M NaOH and the complex was diluted with phosphate buffered saline with 0.1% bovine serum albumin (PBSA) to a final concentration of 1 mM (for DOTA and DOTA-Bn) or 200 μM (for DOTA-Bn-biotin). For gadolinium chelates, an identical metal loading procedure was used except that the complexation reaction took place at 80°C for 12 h in a thermocycler. Complete complexation of the chelator was confirmed by LC/MS using a 75 μm x 150 mm C18 column (Magic C18 from Michrom Bioresources).

2.3.3. Kinetic Characterization

K_D Measurements for DOTA-Bn-biotin-metal

Equilibrium dissociation constants (K_D) for binding of yeast surface-displayed scFv to biotinylated DOTA complexes at 37°C were determined in triplicate by titration as described by Chao et al. (Chao et al. 2006). Briefly, yeast expressing an scFv clone on their surface were grown, washed with PBSA and incubated with various concentrations of DOTA-Bn-biotin-metal long enough to allow for at least a 95% approach to equilibrium. Generally, 5 x 10^5 induced cells were used for each concentration point. When antigen concentrations less than 10 pM were assayed, the titration was performed with 2.5 x 10^4 induced and 7.5 x 10^5 non-induced cells to ensure antigen excess over the scFv without requiring impractically large volumes. The addition of non-induced cells aids pelleting during centrifugation (Hackel et al. 2008). When antigen concentrations greater than 100 nM were used, non-specific antigen binding to the yeast surface was taken into account. Yeast expressing an irrelevant scFv on their surface were treated in the same manner as the yeast displaying the scFv of interest, and mean total phycoerythrein fluorescence (MFU_{tot}) due to non-specific binding was measured by flow cytometry and averaged over three replicates. This value was subtracted from the MFU_{tot} for the yeast of interest, and the data was fit by least-squares regression.

K_D Measurements for DOTA-metal and DOTA-Bn-metal

To determine the K_D for scFv binding to nonbiotinylated haptens, the above protocol was modified to a competition-based assay as follows. After determining the K_D for scFv binding to DOTA-Bn-biotin-Y, a titration was set up with 100 pM DOTA-Bn-biotin-Y, 2.5 x 10^5 cells per tube, and varying concentrations of the nonbiotinylated complex. Incubation, staining, and flow cytometry analysis was the same as that for biotinylated antigen. MFU_{tot} as a function of the concentration of the nonbiotinylated antigen ([Ag]), normalization constant (MFU_{range}), minimal total mean fluorescence (MFU_{min}), K_D for DOTA-Bn-biotin-Y ($K_{D,biot}$), DOTA-Bn-biotin-Y concentration ($[Ag_{biot}]$), and K_D for the antigen of interest (K_D) follows this modified equation:

$$MFU_{tot} = MFU_{\min} + \frac{MFU_{range} \times [Ag_{biot}]}{K_{D,biot} + [Ag_{biot}] + \left(\frac{K_{D,biot}}{K_D}\right)[Ag]}$$

The data was fit by least squares regression as before, varying MFU_{min}, MFU_{range} and K_D.

Dissociation Kinetics

To determine the dissociation rate, k_{off}, for DOTA-Bn-biotin complexes, cells were induced and washed as above, and 1 x 10^7 cells were incubated in 1 mL PBSA with 1 nM DOTA-Bn-biotin-metal for 1 h to reach saturation. Subsequently, the yeast were washed with 1 mL PBSA, resuspended in 1 mL PBSA with 1 μM (excess) non-biotinylated antigen as competitor and split into 100 uL aliquots. These aliquots were incubated at 37°C for different lengths of time, then washed with cold PBSA and left on ice. All samples were simultaneously stained with streptavidin-phycoerythrein for 10-20 min and analyzed by flow cytometry. The data was fit to the following equation by least squares regression, varying MFU_{min}, MFU_{range} and k_{off}:

$$MFU_{tot} = MFU_{\min} + MFU_{range} e^{-k_{off} t}$$

For nonbiotinylated antigens, the procedure was identical except that initial saturation was with the nonbiotinylated antigen and DOTA-Bn-biotin-metal was used as competitor. The data followed the expression:

$$MFU_{tot} = MFU_{\min} + MFU_{range} \left(1 - e^{-k_{off} t}\right)$$

2.3.4. Affinity Maturation

The 2D12.5 scFv served as our starting point and was subjected to nine rounds of directed evolution by random mutagenesis and subsequent selection for improved binding using yeast surface display as described by Chao and colleagues (Chao et al. 2006) and adapted as follows.

Mutagenesis

To counteract the mutational bias of error-prone PCR, mutagenesis at each round was also performed with the Mutazyme mutagenesis kit (Stratagene) according to the manufacturer's instructions, and the resulting mutagenized DNA was pooled with that obtained by error-prone PCR. All other steps were carried out as described (Chao et al. 2006).

Selection

Each round of mutagenesis resulted in a library size of 0.5–4 $x10^7$ and was sorted 2-3 times by flow cytometry for improved binders. At least five times the estimated library diversity was labeled for cell sorting. Staining was performed by equilibrium incubation at a biotinylated DOTA-Y concentration of approximately 1/3 of the average K_D of the previous library (in early rounds) or by saturation with antigen followed by dissociation for 2-3 dissociation half-times (in later rounds), and subsequent labeling with streptavidin-phycoerythrein. To label for full-length scFv expression, the yeast were also stained with a mouse anti-HA (clone 12CA5, Roche Applied Science) or a mouse anti-cmyc (clone 9e10, Covance) primary antibody and a goat anti-mouse Alexa-647 (Invitrogen) secondary antibody. Yeast expressing the best 0.01–0.1% of binders were collected. Periodically, the antigen was alternated between DOTA-Bn-biotin-Y and DOTA-alkyl-biotin-Y.

Disulfide stabilization and glycosylation knockout.

The N-linked glycosylation site in the heavy chain of the scFv was removed and a disulfide bond between the heavy and light chain was introduced during the seventh

mutagenesis of the affinity maturation. This was accomplished by introducing through PCR site-directed mutagenesis the mutations N88E or N88D, Q111C, and L179C (numbering corresponds to the scFv sequence; Figure 2.3C).

Selection of clones.

Individual clones were isolated by transforming XL-1 blue chemically competent E. coli (Stratagene) with plasmid DNA isolated from the yeast library (Zymoprep II Kit, Zymo research) and plating on agar plates containing ampicillin. Individual colonies were picked and grown in liquid medium overnight and plasmid DNA was isolated using the Qiagen Miniprep kit. The plasmid DNA was sequenced and transformed back into yeast with the EZ yeast transformation kit (Zymo Research). Clonal yeast cultures were grown and their kinetic parameters determined.

2.3.5. Bispecific Antibody Construction

An IgG-like bispecific antibody that binds to CEA and DOTA was engineered from a high-affinity Sm3e antibody (Graff et al. 2004) and the C8.2.5 scFv. Characterization of this bispecific antibody is described in Chapter 3. An analogous bispecific antibody with the wild-type 2D12.5ds scFv was also constructed by ligating the 2D12.5ds scFv into the light chain plasmid between the Nhe1 and Sal1 restriction sites. The bispecific antibodies were produced in transient HEK293 culture and purified by protein A chromatography as described in Chapter 3.

2.3.6. Radiolabeling

The HPLC/mass spectrometry platform used for purification of radioactive small molecules has been described in detail (Humblet et al. 2006; Misra et al. 2007). DOTA-Bn was dissolved at 5 mM in ammonium acetate pH 5.5. 1-2 mCi $^{111}InCl_3$ (Cardinal Health, Dublin, OH) were added to the metal chelate and incubated for 1 h at 90°C. The radiolabeled compound was purified by RP-HPLC with gamma detection on a 4.6 x 75 mm Symmetry C18 column using a linear gradient from 0% to 100% B over 15 minutes, at a flow rate of 1 mL/min, where A = water and B = acetonitrile with 0.1% formic acid.

2.3.7. Xenograft Mouse Model

All animal handling was performed in accordance with Beth Israel Deaconess Medical Center (BIDMC) Institutional Animal Care and Use Committee (IACUC). LS174T human colorectal carcinoma cells (CL 188) were obtained from American Type Culture Collection and maintained under standard conditions and confirmed to be negative for mycoplasma and mouse pathogens by the Yale Virology Lab. Xenografts were established in 5-6 week-old male NCRU-nu/nu mice (Taconic Farms) by subcutaneous injection of 1-2 x 10^6 LS174T cells into the flank of the mouse. After 8-10 days, tumors were 0.1 – 0.5 g in size. 30 ug of bispecific antibody was injected intravenously followed 24 h later by intravenous injection of 1.3 pmol ^{111}In-labeled DOTA-Bn. Mice were euthanized 24 h later by intraperitoneal injection of pentobarbital, a method consistent with the recommendations of the Panel on Euthanasia of the American Veterinary Medical Association. Tumors were resected, washed in PBS, weighed, and counted with a model 1470 Wallac Wizard (Perken Elmer, Wellesley, MA) 10-detector gamma counter. A Students t-test was used to examine the differences between the experimental groups.

2.4. Results

2.4.1. Mathematical Modeling

We mathematically modeled the effect of DOTA-binding affinity on the delivery of ionizing radiation in PRIT. Two mathematical models were implemented that simulate PRIT based on previously validated models, one that simulates antibody distribution in vascularized tumors and the other in micrometastases (Thurber et al. 2007). These two types of tumors were considered separately due to different modes of transport. For micrometastases, antibody and hapten diffuses into the tumor mass from the surrounding interstitial fluid. While there may be some transport from surrounding interstitial fluid into the edges of large vascularized tumors, the majority of antibody and hapten transport occurs across the tumor vasculature.

We extended both models to account for hapten kinetics, assuming an IgG-like bsAb with specificity to CEA, with a 15 h internalization half-time (Schmidt et al. 2008). We used a bsAb blood concentration of 2 μM as an input variable. We expect this initial concentration to essentially saturate the antigen binding sites for vascularized tumors from both modeling predictions and from Fenwick and colleagues (Fenwick et al. 1989), who demonstrated that antibody doses of several hundreds of micrograms, or more, are required to obtain saturation in a mouse xenograft model. PRIT model timing and dosing parameters are similar to that of a recent Phase II human trial (Knox et al. 2000) with bsAb dosing at time 0, followed by a clearing/blocking step at 48 h and hapten dosing at 72 h, with an initial hapten blood concentration of 100 nM. Our model predicts that this hapten dose will saturate the pretargeted bsAb binding sites in the vascularized tumor. Note that bsAb and hapten doses are orders of magnitude above those predicted to saturate micrometastases. The model assumes a 70 kg man and 2-compartment pharmacokinetic parameters for antibody and hapten. A detailed description of all model parameters is provided in the appendix (section 7.1.4).

PRIT model simulations were run, varying the hapten dissociation rate while keeping the association rate constant. We simulated hapten concentration in the tumor as a function of time and total cumulative activity assuming a ^{90}Y radionuclide over a time

interval of 15 days. Hapten retention in vascular tumors (Figure 2.1A) and micrometastases (Figure 2.1B) were predicted over a hapten K_D range of six orders of magnitude. The half-time of residualization of DOTA chelates after internalization is assumed to be 120 h (estimated from (Shih et al. 1994)). We examined the effect of varying the association rate while maintaining a constant K_D and found no significant difference in hapten retention for typical hapten association rates ($5x10^5 - 5x10^7$ $M^{-1}s^{-1}$), demonstrating that the relevant parameter is K_D.

For the aforementioned PRIT conditions, we predict that a hapten K_D greater than 100 pM will allow significant hapten retention for both vascularized tumors and micrometastases. This prediction is in agreement with other modeling analyses of tumor targeting of small molecules (Schmidt and Wittrup 2009).

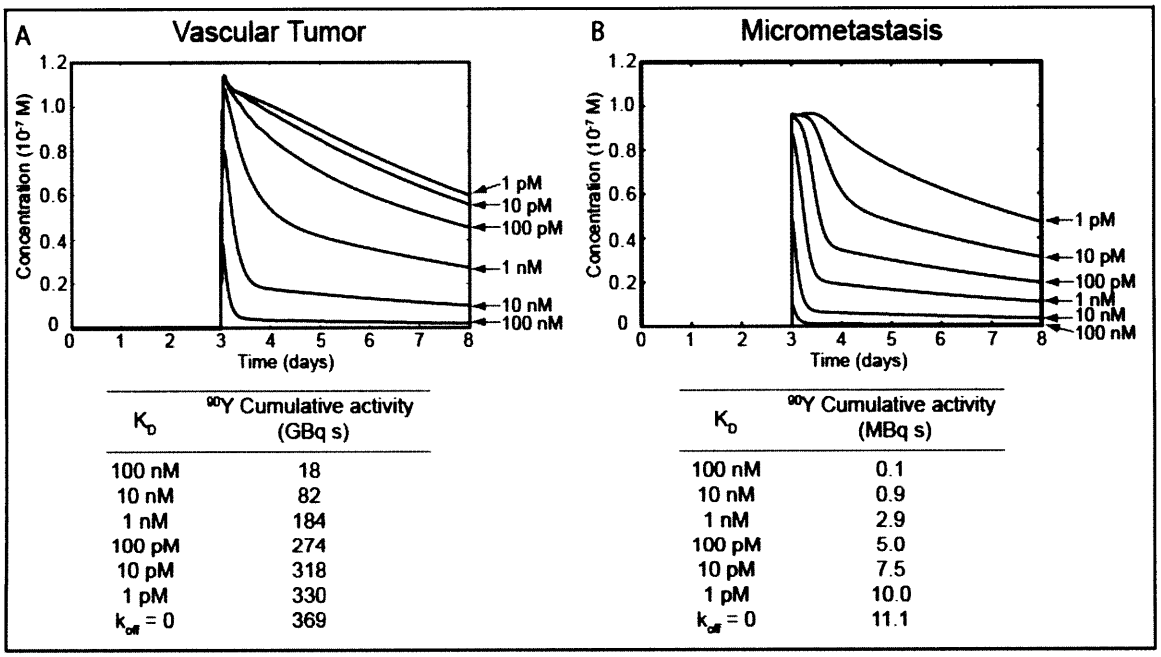

K_D	^{90}Y Cumulative activity (GBq s)
100 nM	18
10 nM	82
1 nM	184
100 pM	274
10 pM	318
1 pM	330
$k_{off} = 0$	369

K_D	^{90}Y Cumulative activity (MBq s)
100 nM	0.1
10 nM	0.9
1 nM	2.9
100 pM	5.0
10 pM	7.5
1 pM	10.0
$k_{off} = 0$	11.1

Figure 2.1 Hapten retention in tumors as a function of hapten binding affinity. PRIT simulations were performed assuming a vascularized tumor (A) and a small micrometastasis (B) with human pharmacokinetic parameters. The hapten concentration in the tumor as a function of time was plotted for various dissociation constants (indicated by arrows). The cumulative activity for a ^{90}Y radionuclide is tabulated for various K_D values and also for a theoretical k_{off} equal to zero. Cumulative activity units are gigabecquerel seconds (GBq s) for the vascularized tumor and megabequerel seconds (MBq s) for micrometastases.

2.4.2. Affinity Maturation

We affinity matured the 2D12.5 antibody fragment against biotinylated DOTA-Y by directed evolution. We used biotinylated DOTA-Y in order to probe binding using a streptavidin-fluorophore secondary label and flow cytometry, as DOTA-Y itself possesses no intrinsic fluorescent properties. The gene encoding the variable domains of the 2D12.5 DOTA-binding antibody in an scFv format (Figure 2.3C) was synthesized from its published sequence (Corneillie et al. 2003). The scFv was subsequently subjected to nine rounds of affinity maturation. Yeast expressing 2D12.5 scFv variants were labeled for expression and with either DOTA-Bn-biotin-Y or DOTA-alkyl-biotin-Y (Figure 2.2) followed by streptavidin-phycoerythrein and sorted by flow cytometry to select the highest affinity clones. The antigen was periodically switched to minimize selection of variants with mutations that conferred binding improvement to the linker region. During the seventh mutagenesis, we introduced an intramolecular disulfide bond between the heavy and light variable regions of the scFv (Reiter et al. 1996) and removed the N-linked glycosylation site in the heavy chain. These additional mutations may improve stability and result in simpler downstream processing of the scFv.

Sequences and kinetic constants were determined for several clones from libraries 8.2 (8 rounds of mutagenesis followed by 2 sorts) and 9.3 (9 rounds of mutagenesis and 3 sorts). All clones from library 9.3 had lost the disulfide bond between the heavy and light chain and were consequently discarded. Of the clones from library 8.2, C8.2.5 retained the disulfide bond and bound most tightly to DOTA-Bn-biotin-Y.

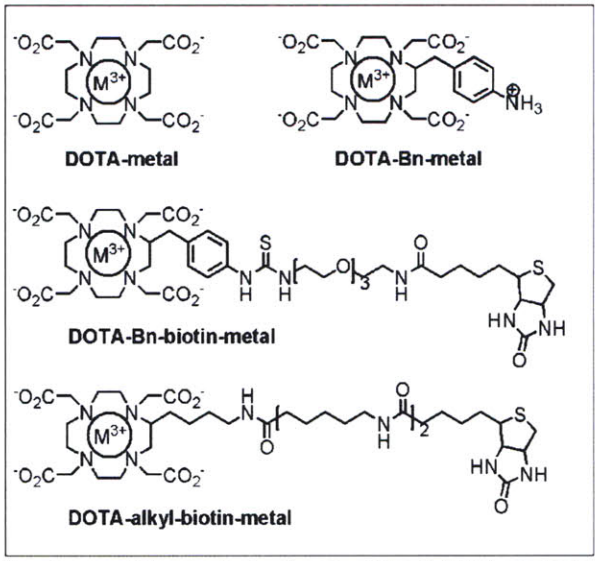

Figure 2.2 Chemical Structures. Chemical structures of the DOTA variants used in this study with trivalent metal cations.

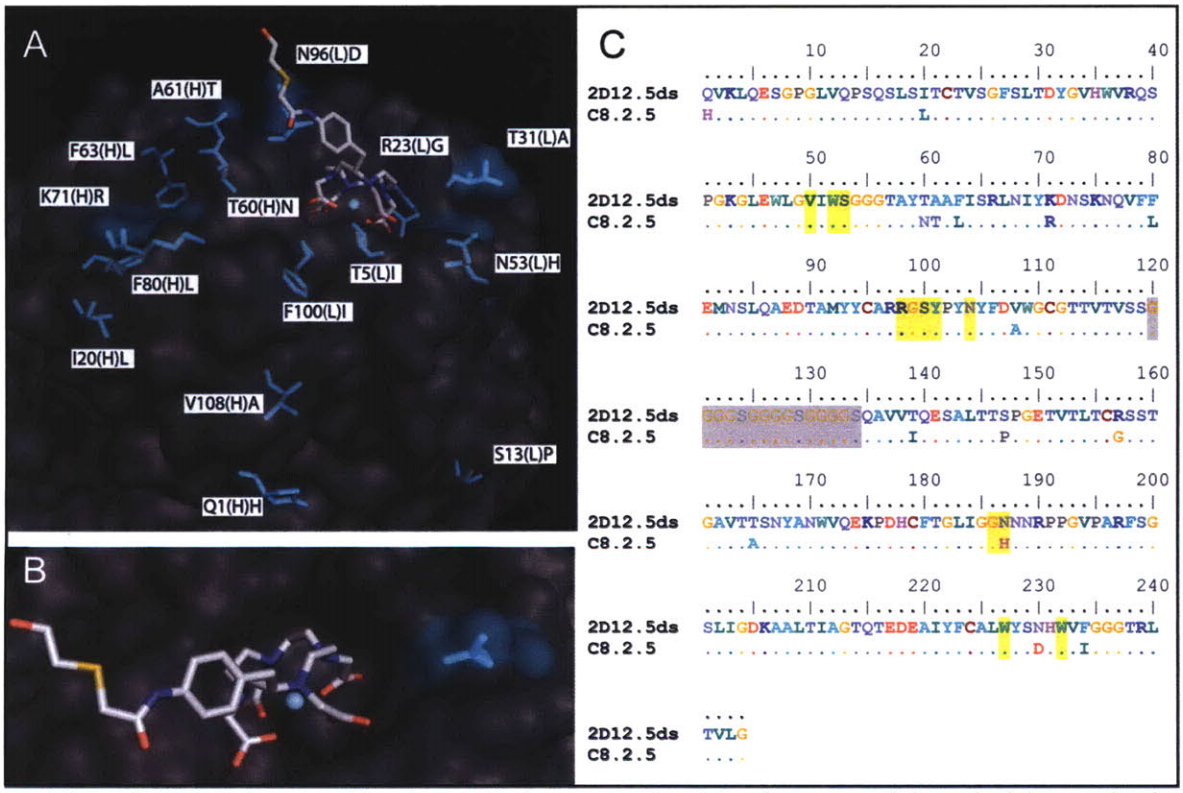

Figure 2.3 Mutations resulting from affinity maturation. Mutations accrued through eight rounds of affinity maturation are highlighted in blue in the x-ray crystal structure of the 2D12.5 Fab (A) and a magnified view of the binding pocket (B). Panels A and B were generated with PyMol based on the research collaboration for structural bioinformatics (RCSB) protein data bank entry 1NC2 (Corneillie et al. 2003). Panel C shows the sequence alignment of the 2D12.5ds and C8.2.5 scFvs. Residues within 5 Angstroms of the hapten from the 2D12.5 crystal structure are highlighted in yellow; the $(Gly_4Ser)_3$ linker is highlighted in grey. Note that the residue numbering is different from that for the crystal structure of the Fab.

2.4.3. C8.2.5 Mutant

The sequence (Figure 2.3C) of the high-affinity C8.2.5 scFv differs from 2D12.5ds (the original 2D12.5 scFv with the addition of the intramolecular disulfide bond and removed glycosylation site) at 15 amino acid positions. The spatial distribution in the crystal structure of wild-type 2D12.5 is depicted in Figure 2.3A and 2.3B. Only one mutation, N53(L)H (numbering corresponds to the 2D12.5 antigen-binding fragment (Fab) for which the crystal structure was determined (Corneillie et al. 2003)), occurred within 5 Angstroms of the bound hapten, indicating that most mutations enhanced affinity via subtle structural perturbations remote from the binding interface.

2.4.4. Kinetic Characterization

The kinetic properties of both 2D12.5ds and C8.2.5 were characterized and are summarized in Tables 2.1 and 2.2 and in Figures 2.4 and 2.5. The affinity of the scFv to DOTA-Bn-biotin-Y was improved by 3 orders of magnitude, from nanomolar to single-digit picomolar. The dissociation half-time for DOTA-Bn-biotin-Y increased from 5.5 min for 2D12.5ds to just over 5 hours for C8.2.5 (Table 2.2 and Figure 2.5).

Table 2.1 Equilibrium dissociation constants for various DOTA compounds

scFv	Hapten	Metal	K_D*			n
2D12.5ds	DOTA-Bn-Biotin	Y	3.7	± 3.6	nM	3
C8.2.5	DOTA-Bn-Biotin	Y	8.2	± 1.9	pM	3
	DOTA-Bn	Y	15.4	± 2.0	pM	3
		Lu	10.8	± 2.5	pM	3
		Gd	34.0	± 5.3	pM	2
		In	1.01	± 0.04	nM	2
		Ga	52	± 12	nM	2
	DOTA	Y	103	± 35	pM	3
		Lu	390	± 14	pM	2
		Gd	149	± 6	pM	2
		In	23.7	± 3.7	nM	2
		Ga	216	± 26	nM	2

*K_D given as mean ± SD.

Table 2.2 Dissociation half-lives for various DOTA compounds

Dissociation halflives for yeast surface displayed scFvs bound to DOTA complexes

scFv	Hapten	Metal	Dissociation halflife *
2D12.5ds	DOTA-Bn-Biotin	Y	5.5 ± 1.3
C8.2.5	DOTA-Bn-Biotin	Y	302 ± 13
	DOTA-Bn	Y	53.1 ± 2.3
	DOTA	Y	3.5 ± 0.7
		Lu	3.8 ± 0.4

*Calculated as $\ln(2)/k_{off}$ and given in minutes as mean ± SD for n=3 experiments.

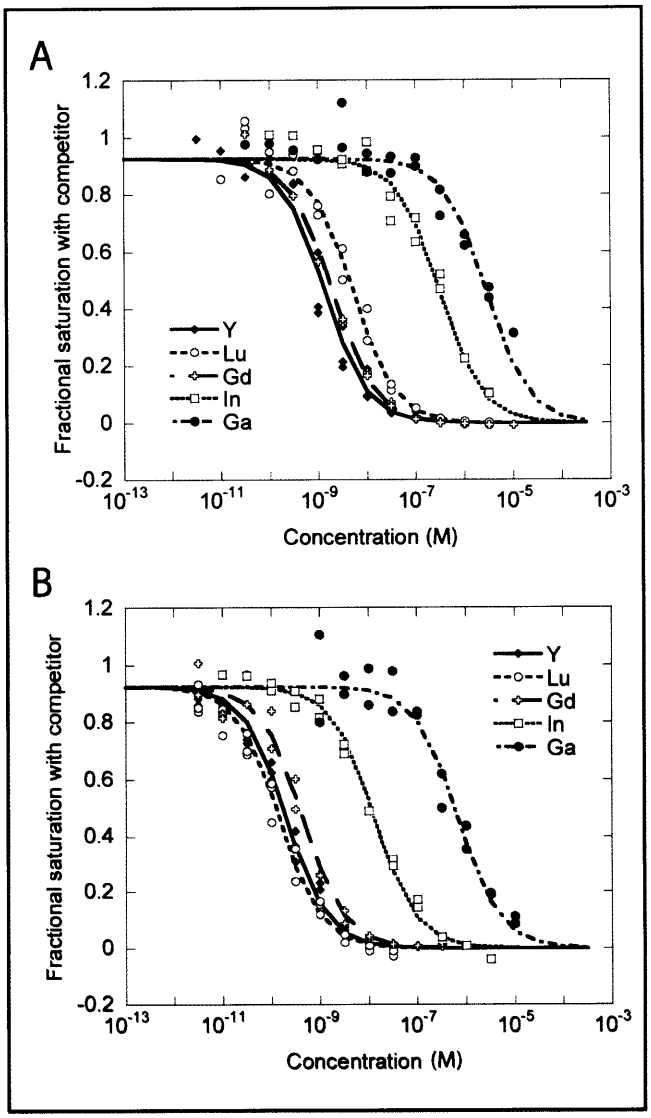

Figure 2.4 Metal specificity of improved mutant. Competition equilibrium isotherms for C8.2.5 scFv displayed on the surface of yeast for binding to DOTA-metal (A) and DOTA-Bn-metal (B) complexes measured with a competition-based assay. It should be noted that 100 pM DOTA-Bn-biotin-Y is the detected label. The binding constant for the competitor will follow a Cheng-Prusoff relationship as described in Materials & Methods.

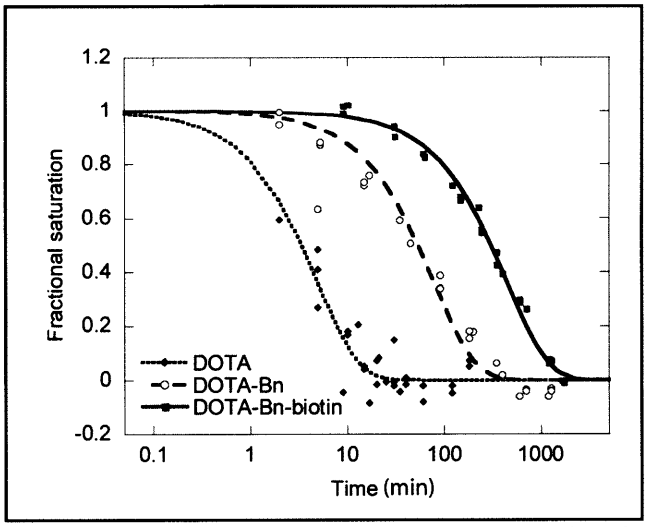

Figure 2.5 Improved mutant dissociation curves to DOTA variants. Dissociation curves for C8.2.5 scFv and yttrium complexes of different DOTA variants. For the nonbiotinylated haptens, the fractional saturation plotted is 1-(fractional saturation with competitor (DOTA-Bn-biotin-Y)).

The high-affinity clone C8.2.5 binds DOTA-Bn-biotin-Y, DOTA-Bn-Y, and DOTA-Y with equilibrium dissociation constants of 8.2 ± 1.9 pM, 15.4 ± 2.0 pM, and 103 ± 35 pM, respectively. The addition of the benzene ring and biotin moiety may change the charge distribution of the DOTA epitope, altering the affinity. It is also possible that there are some binding interactions between the scFv and the benzene ring and biotin linker region. The affinity differences between these various yttrium chelates are reflected in their dissociation half-lives (Table 2.2 and Figure 2.5).

DOTA complexes of lutetium and gadolinium were bound by C8.2.5 similarly to those of yttrium (Table 2.1 and Figure 2.4). The high-affinity scFv also binds indium and gallium chelates with nanomolar affinity. All DOTA-metal chelates were bound by C8.2.5 with about an order of magnitude weaker affinity than the respective DOTA-Bn metal chelate.

Complete metal complexation of DOTA was confirmed using LC/MS as described in the materials and methods. However, LC/MS may not be able to distinguish the thermodynamically stable complex from intermediates that may form (Moreau et al. 2004). To confirm that the kinetic characterization described above was not influenced by the presence of intermediate complexes, the DOTA-Bn metal complexes were incubated for an additional 12 h at 80°C; the measured binding affinities of these DOTA-Bn

complexes to C8.2.5 were essentially the same as those described above (data not shown).

2.4.5. Analysis of Tumor Targeting *In Vivo*

The C8.2.5 scFv was engineered into an IgG-like bispecific antibody as a C-terminal fusion to the light chain of a CEA-targeting Sm3e IgG (Chapter 3). The bispecific antibody retains parental affinities of both the C8.2.5 scFv and Sm3e IgG and also exhibits IgG-like blood clearance and tumor targeting *in vivo* (Chapter 3). Mice injected with 30 ug C8.2.5 bispecific antibody 24 hours prior to ^{111}In-DOTA-Bn administration exhibit significantly greater tumor uptake of the hapten 24 hours later, compared to an analogous bispecific antibody containing the wild-type 2D12.5ds scFv and ^{111}In-DOTA-Bn only (Figure 2.6), demonstrating improved retention of the ^{111}In-DOTA-Bn at the site of the tumor for the affinity matured scFv.

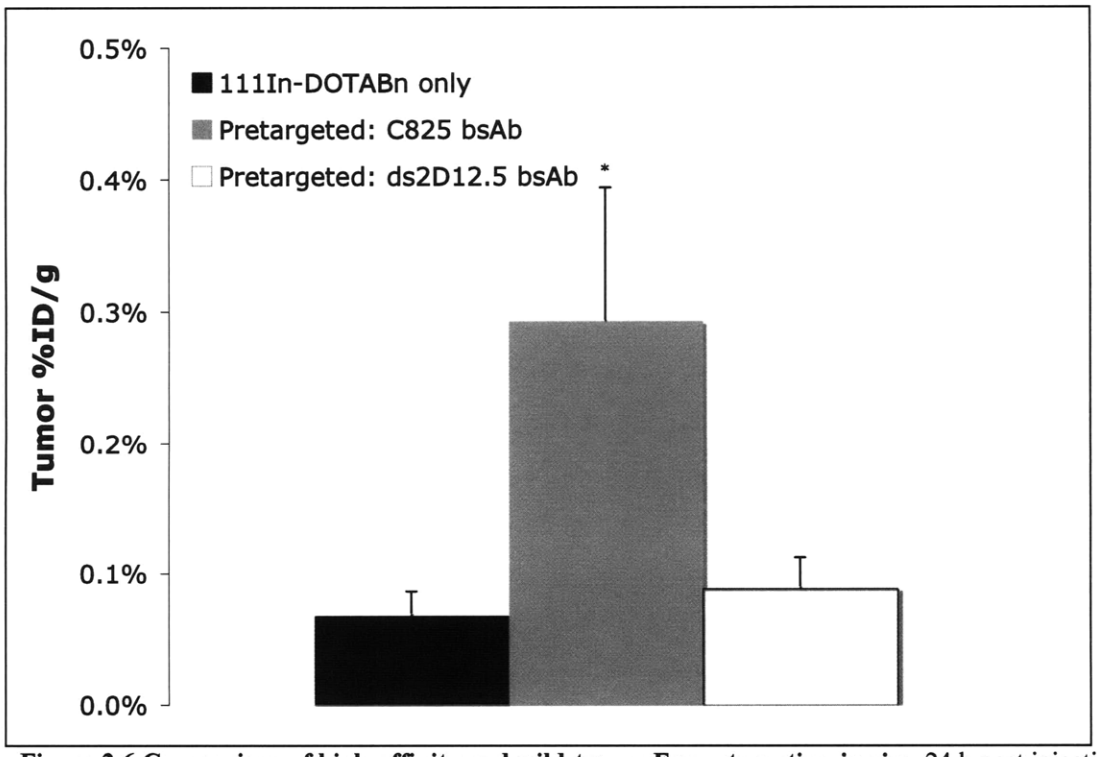

Figure 2.6 Comparison of high-affinity and wild-type scFv pretargeting *in vivo*. 24 h post injection hapten tumor retention in xenograft mice pretargeted with C8.2.5 bispecific antibody compared to 2D12.5ds bispecific antibody and ^{111}In-DOTA-Bn hapten alone. n = 3, error bars are s.d.; * $P < 0.05$.

2.5. Discussion

In this study, we have used a mathematical model of PRIT to predict the maximum achievable cumulative activity in the tumor as a function of antibody binding affinity to the radiometal chelate. While other mathematical models of PRIT have been developed (Zhu et al. 1998; Liu et al. 2007), for the present work we exclusively used published measured parameters without any curve fitting. Hapten retention at the site of the tumor depends on a large number of factors, including the hapten dissociation rate, rebinding of dissociated hapten, diffusion rate, capillary permeability, hapten pharmacokinetics in the blood, and antigen internalization. For therapeutic applications, it is desired that the hapten is retained at the site of the tumor until the majority of radioactive decays have occurred.

From predicted hapten tumor concentrations, we have calculated tumor cumulative activities for a ^{90}Y radionuclide. It would be straightforward to further calculate doses to the tumor assuming spherical geometry and published S-values for ^{90}Y (Siegel and Stabin 1994). However, we have not presented dose estimates, as we expect the model to provide qualitative trends but due to significant heterogeneity in many of the model parameters, we do not expect accurate predictions of true clinical doses.

Motivated by mathematical modeling, we used directed evolution and yeast surface display to affinity mature the 2D12.5 scFv to biotinylated DOTA-Y with a goal of low picomolar affinity. The resulting high-affinity clone not only binds DOTA-Y chelates but also lutetium and gadolinium chelates with low picomolar affinity and indium and gallium chelates with nanomolar affinity. While the 2D12.5 Fab binds the DOTA chelates of all lanthanides with similar nanomolar affinity and indium DOTA chelates with micromolar affinity (Butlin and Meares 2006), it was not *a priori* obvious that this versatility would persist throughout the affinity maturation. The engineered high-affinity clone possesses mutations that significantly improve binding to several metal chelates, despite selective pressure only toward the yttrium chelate. This promiscuous binding is highly advantageous in further preclinical and clinical development of a bispecific agent

containing the C8.2.5 scFv for pretargeting, as it allows metals (with their different radioactive properties) to be varied and used with the same bsAb.

Interestingly, the metals whose complexes are bound by C8.2.5 most tightly – yttrium, lutetium, and gadolinium – are chelated by DOTA with identical coordination chemistry, having a coordination number of 9 with one crystalline water molecule in the complex. Indium and gallium, in contrast, are chelated by DOTA with coordination numbers of 8 and 6, respectively. This leads us to hypothesize that C8.2.5 may bind all lanthanides with low-picomolar affinities, as they are known to form nonacoordinate chelates with DOTA. This suggests further potential biotechnological applications for C8.2.5, exploiting for example the luminescence of Tb and Eu.

The nature of the accumulated mutations in C8.2.5 is similar to that previously observed for engineering extremely high-affinity binders from a moderate binder to the same antigen (Midelfort et al. 2004). Most mutations occurred away from the binding interface, many of them at second-shell residues, and are conservative with respect to physicochemical properties. This indicates that enhanced binding stems from slight structural adjustments, rather than novel direct binding contacts to the hapten. Determining a crystal structure for C8.2.5 bound to DOTA-Y would enable a more detailed analysis of the binding interactions.

Based on our model, we predict that our high-affinity scFv will effect approximately 4-fold higher cumulative activities in vascularized tumors and 8-fold higher cumulative activities in micrometastases when compared to the wild type 2D12.5 antibody (for ^{90}Y radionuclides) for the model conditions. We also predict that any further improvement in affinity to yttrium chelates would result in no more than a two-fold increase in cumulative activity in micrometastases and would have no significant effect in vascularized tumors. Four-fold and eight-fold improvements in cumulative activity may seem modest for an affinity improvement of three orders of magnitude. However, these predictions are based on the selection of a highly expressing cancer antigen and saturating bsAb and hapten doses (similar to optimized doses tested previously in pretargeted radioimmunotherapy studies in the clinic (Knox et al. 2000)). While sub-

saturating bsAb doses, lower antigen densities, and smaller hapten doses would result in more striking cumulative activity increases for hapten affinity improvements, they would also result in significantly lower tumor cumulative activities overall.

We demonstrate that the *in vitro* affinity maturation of 2D12.5 results in a significant improvement in hapten retention *in vivo* in a xenograft mouse model, where we compare bispecific antibodies constructed with the high-affinity C8.2.5 scFv and the wild-type 2D12.5 scFv (Figure 2.6). We have utilized a bispecific antibody that is a C-terminal scFv fusion to the light chain of an IgG (chapter 3).

While IgG-like bispecific antibodies are expected to result in significantly higher tumor accumulation than smaller antibody fragments due to slower blood clearance (Olafsen et al. 2006; Schneider et al. 2009), a considerable amount of antibody will likely remain in the blood at the time of hapten dosing. Thus a clearing/blocking step will be necessary to minimize hapten binding to residual bsAb in the blood. While three-step pretargeted radioimmunotherapy is more complex than proposed two-step approaches (Barbet et al. 1998; Sharkey et al. 2003), it may result in higher tumor doses for a given amount of bispecific antibody (due to a higher concentration of hapten binding sites accumulating in the tumor) and possible antibody dependent cell-mediated cytotoxicity (ADCC) and complement dependent cytotoxicity (CDC) due to the retained Fc domain.

Based on the model results, hapten retention is expected to be similar for DOTA-Bn-Y with a 10 pM affinity and DOTA-Y with a 100 pM affinity under antigen saturation for highly expressed tumor targets. Either DOTA or DOTA-Bn could be used with this system; in Chapter 4 we show that ^{177}Lu-DOTA-Bn exhibits similar blood clearance and biodistribution as ^{177}Lu-DOTA.

We have engineered a versatile, DOTA-chelate-binding scFv with picomolar binding to yttrium, lutetium, and gadolinium chelates and nanomolar binding to indium and gallium chelates. Our approach comprised mathematical modeling of the pharmacokinetics of the bsAb and the metal chelate for the treatment of both micrometastatic disease and vascularized tumors to derive design specifications, and

protein engineering via directed evolution using yeast surface display to achieve the desired outcome experimentally. We anticipate that the high-affinity DOTA-binding C8.2.5 scFv will prove useful for pretargeted imaging with positron emission tomography using ^{86}Y and single photon emission computed tomography using ^{111}In and pretargeted therapy with beta-emitters ^{177}Lu and ^{90}Y. C8.2.5 may also be useful for targeted MRI with multivalent macromolecular contrast agents containing DOTA-Gd.

3. IGG-LIKE BISPECIFIC ANTIBODY TOPOLOGY

3.1. Abstract

Here we present a bispecific antibody (bsAb) format in which a disulfide-stabilized scFv is fused to the C-terminus of the light chain of an IgG to create an IgG-scFv bifunctional antibody. When expressed in mammalian cells and purified by one-step protein A chromatography, the bispecific antibody retains parental affinities of each binding domain, exhibits IgG-like stability, and demonstrates *in vivo* IgG-like tumor targeting and blood clearance. We demonstrate here that the light chain of an IgG can be extended with an scFv without affecting IgG function and stability. This format serves as a standardized platform for the construction of functional bispecific antibodies.

3.2. Introduction

While monoclonal antibodies have shown success in the clinic for a variety of diseases (Hudson and Souriau 2003), multi-specific antibodies, with an ability to bind to more than one target, may further improve clinical efficacy via novel mechanisms. Multi-specific antibodies have been engineered for a variety of applications including enhanced antibody-dependent cell-mediated cytotoxicity (ADCC) (Garcia de Palazzo et al. 1992; McCall et al. 2001), tumor surface-receptor blocking and downregulation (Lu et al. 2005), simultaneous binding to two soluble effector molecules (Wu et al. 2007), and pretargeting tumor cells for the subsequent capture of radionuclides (Boerman et al. 2003), drugs (Ford et al. 2001), and prodrugs (Bagshawe 2006).

Early efforts to produce bispecific antibodies included chemical conjugation of two antibodies or fragments thereof (Graziano and Guptill 2004) or co-expression of two antibodies with different specificities through the hybrid hybridoma technique (Menard et al. 1989). Unfortunately, the conditions required for chemical conjugation can inactivate, unfold, or aggregate the bsAb, while the hybrid hybridoma technique not only produces the desired bsAb but also undesired products from mispairing necessitating complex purification schemes. In 1996, Carter and colleagues described a "knobs into holes" method, wherein different but complementary mutations introduced into the CH3 domains favor heterodimerization. In the past decade, several other formats of multi-specific antibodies have been synthesized by recombinant methods to produce scFv fusions or diabodies, scFv Fc fusions, and single variable domain IgGs, among others (Coloma and Morrison 1997; Kontermann 2005; Marvin and Zhu 2005; Shen et al. 2007; Wu et al. 2007). In addition, Goldenberg and colleagues have developed a "dock and lock" method for creating multi-specific antibodies, in which one antibody fragment is fused to a peptide regulatory subunit of cAMP-dependent protein kinase and another antibody fragment to a peptide anchoring domain of A kinase anchor protein, where the two peptides have natural affinity for each other (Rossi et al. 2006; Goldenberg et al. 2008). A recent format that appears to possess good stability is the dual-variable-domain IgG that extends both the heavy chain and the light chain with the N-terminal addition of a second set of variable domains; however, the physical proximity of the two binding

sites may be sterically problematic for certain pairs of antigen binding domains (Wu et al. 2007). In addition, the authors mention that significant construct optimization is often required to preserve the parental affinities as both the orientation of the variable domains and the linkers between them appear to be critical to functional and expression.

We present here a novel bispecific antibody design as a C-terminal fusion of a disulfide-stabilized scFv to the light chain of an IgG. It can be expressed in mammalian cell culture and purified to homogeneity by protein A chromatography. Here, we test three different versions of this new bsAb construct with specificity to different cell surface protein targets and small molecule haptens. Simultaneous binding, affinity, and *in vitro* stability are assessed, as are *in vivo* blood clearance and tumor targeting.

3.3. Materials and Methods

3.3.1. Construction of Bispecific Antibodies

The bispecific format was designed as an scFv fusion to the C-terminus of the light chain of an IgG. The heavy chain is the same as that of an IgG1 and was subcloned into the mammalian expression vector gwiz, purchased from Aldevron (Fargo, ND). The light chain is constructed as leader-FLAG-VL-Cκ-$(Gly_4Ser)_2$-scFv-cmyc, where VL is the variable light domain, Cκ is the kappa light chain constant domain, and FLAG and cmyc are N- and C-terminal epitope tags, respectively. It was cloned into a separate gwiz plasmid. Both plasmids were transiently co-expressed in HEK293 cells (cat. no. R790-07) purchased from Invitrogen (Carlsbad, CA). HEK293 cells were grown in flasks on an orbital shaker platform at 140 rpm at 37°C, 5% CO_2 and subcultured following the manufacturer's protocol. Co-transfection was performed with polyethyleneimine (PEI) as the transfection reagent. Briefly, HEK293 cells were subcultured to a cell density of 0.5 – 0.7 x 10^6 cells/mL 24 h before transfection. Immediately before transfection, cell density was adjusted to 1 x 10^6 cells/mL. 500 μg of each purified plasmid (1 mg/mL) was added to 19 mL Optipro (Invitrogen). 2 mL of 1 mg/mL PEI pH 7.0 (MW 25,000) purchased from Polysciences (Warrington, PA) dissolved in water was added to 18 mL Optipro. Both solutions were incubated at room temperature for 5 min. The DNA/optipro solution was added to the PEI/optipro solution and incubated for 10 min at room temperature and added drop-wise to 1 L HEK293 culture. The supernatant was collected 6-8 d after transfection. Antibodies were purified by protein A chromatography (Thermo Fisher Scientific, Rockford, IL) following the manufacturer's instructions.

Specific constructs were made by overlap extension PCR and QuikChange mutagenesis. The Sm3e/C825 bsAb was cloned and produced as described above using the VH and VL domains from the affinity-matured anti-CEA Sm3e scFv (Graff et al. 2004) and the disulfide-stabilized C8.2.5 scFv. The Sm3e/4m5.3 bsAb substituted a 4m5.3 scFv that is a femtomolar fluorescein binder (Boder et al. 2000) disulfide-stabilized by introducing two cysteine residues, S43C in the VL domain and Q105C in the VH domain (Reiter et al. 1996). The A33/4m5.3 bsAb uses the VH and VL domains

from an A33 humanized Fab fragment (Rader et al. JBC 2000) for the IgG binding domains. Sm3e IgG and A33 IgG plasmids were produced by introducing two stop codons in the light chain immediately following the Cκ sequence via QuikChange PCR. The C-terminus of the A33 IgG light chain was extended by an 18 amino acid peptide ($(G_4S)_2$LPETGGSG), to make the construct A33 IgG + peptide. A33 IgG + peptide was disulfide stabilized by introducing two different pairs of cysteine residues, VL G100C and VH G44C (ds1) and VL V43C and VH Q105C (ds2) (Reiter et al. 1996). The appendix (section 7.2) contains sequence information for all constructs.

3.3.2. Gel Electrophoresis and Western Blotting

Culture expression media was analyzed by Western blot using a horseradish peroxidase (HRP) conjugated goat anti-human Fc antibody (Thermo Fisher Scientific) and an HRP conjugated goat anti-human κ light chain antibody purchased from AbD Serotec (Raleigh, NC). Purified bsAb and IgG were analyzed by SDS-PAGE and quantified by absorbance at 280 nm.

3.3.3. Synthesis of Small Molecule Compounds

DOTA-biotin was synthesized by adding p-SCN-Bn-DOTA (S-2-(4-Isothiocyanatobenzyl)-1,4,7,10-tetraazacyclododecane-tetraacetic acid) purchased from Macrocyclics (Dallas, TX) to Amine-PEG_3-Biotin (Thermo Fisher Scientific) in dimethyl sulfoxide (DMSO) purchased from Sigma Aldrich (St. Louis, MO) with a 10-fold molar excess of triethylamine (TEA) purchased from VWR (West Chester, PA). The reaction mixture was vortexed at room temperature for 3 h, and purified by high performance liquid chromatography (HPLC) on a C-18 reverse-phase column (Agilent Model 1100 HPLC, 1 x 25 cm, buffer A = 0.05% trifluoroacetic acid (TFA), buffer B = 0.0425% TFA in 80% acetonitrile, 2 – 100% B gradient for 98 min). Flow through was monitored by absorbance detection at 280 nm. Fractions containing DOTA-biotin were confirmed using matrix-assisted laser desorption/ionization - time of flight (MALDI-TOF) mass spectrometry (Applied Biosystems Model Voyager DE-STR).

DOTA-647 was synthesized by adding 1 mM p-SCN-Bn-DOTA to 1 mM Alexa Fluor 647 cadaverine (Invitrogen) in DMSO with 40 mM TEA overnight at room temperature, with rotation. DOTA-647 was purified by HPLC as described above. Yttrium complexes of DOTA conjugates were prepared by incubating a molar excess of yttrium nitrate hexahydrate (Sigma Aldrich) with the DOTA conjugates in 0.4 M sodium acetate pH 5.2 buffer overnight at room temperature. The pH was adjusted to 7.0 with 10 M sodium hydroxide and the solution was diluted with PBSA.

Fluorescein-647 (Fl-647) was synthesized by adding 1 mM fluorescein-5-EX, succinimidyl ester (Invitrogen) to 1 mM Alexa Fluor 647 cadaverine in DMSO with 40 mM TEA and rotating overnight at room temperature and used without further purification.

3.3.4. Simultaneous Binding Assay

10^5 trypsinized LS174T cells were washed with 500 μL PBS with 0.1% bovine serum albumin (PBSA) and incubated with 50 nM bsAb or IgG for 1 h at room temperature. Cells were subsequently incubated with 100 nM fluorescein (Fl) purchased from Invitrogen, 100 nM DOTA-biotin chelated with yttrium (DOTA-Y-biotin), 50 nM bsAb, or 100 μL PBSA, followed by incubation with 20 nM DOTA-Y-647 or FITC-647 and analysis by flow cytometry. All incubations were performed for 30 min on ice followed by washing once with PBSA unless otherwise indicated.

3.3.5. Affinity Measurements

CEA binding affinities for the Sm3e/C825 bsAb and Sm3e IgG were measured using fixed LS174T cells incubated with varying concentrations of bsAb or IgG overnight at 37°C. Cells were subsequently incubated with a 1:200 dilution of protein A Alexa Fluor 647 (Invitrogen) and analyzed by flow cytometry. The affinity of the Sm3e/C825 bsAb for DOTA-yttrium (DOTA-Y) was measured by incubating 100 nM bsAb on the surface of fixed LS174T cells for 1.5 h at room temperature. Cells were incubated with varying concentrations of DOTA-647 loaded with yttrium (DOTA-Y-647) for 2 h at 37°C before

analysis by flow cytometry. Yeast expressing the C8.2.5 scFv on their surface were grown and induced as described (Chao et al. 2006). Cells were incubated with varying concentrations of DOTA-Y-647 for 2 h at 37°C and analyzed by flow cytometry. All affinities are reported as mean ± standard deviation calculated from at least two replicates.

3.3.6. Fast Protein Liquid Chromatography

IgG purified from human plasma (Sigma Aldrich), and purified Sm3e IgG and Sm3e/C825 bsAb were analyzed by FPLC size exclusion chromatography (Pharmacia Biotech Superdex 200 column) and monitored by absorbance at 280 nm and data were normalized.

3.3.7. Thermal Stability Assay

IgG and bsAb were incubated in PBSA for various times at 37°C. Antigen binding activity was analyzed with a magnetic bead flow cytometry assay. 20 nM IgG or bsAb was incubated with Protein A beads (Invitrogen) at room temperature for 1 h. Beads were washed and incubated with 20 nM biotinylated CEA (Graff et al. 2004) or 620 nM A33-HIS6 followed by incubation with 1:200 dilution of anti-his Alexa Fluor 647 (Qiagen, Valencia, CA) or streptavidin Alexa Fluor 647 (Invitrogen), and analyzed by flow cytometry. A33-HIS6 was synthesized by transient HEK cell transfection as described above with 1 mg A33-HIS6 gwiz plasmid transfected per liter of culture. A33-HIS6 was purified by TALON metal affinity resin (Clontech, Mountain View, CA) following the manufacturer's protocol. The A33-HIS6 gwiz plasmid was constructed by cloning the A33 signal sequence and gene from a bacculovirus plasmid (Joosten et al. 2004) and inserting a C-terminal hexahistidine.

3.3.8. Serum Stability Assay

Sm3e IgG and Sm3e/C825 bsAb were incubated in either PBSA or 50% mouse serum (Invitrogen) in PBSA for various times at 37°C. Binding activity was analyzed with a

magnetic bead flow cytometry assay where 8.1 x 10^6 biotin binder beads (Invitrogen) were incubated with 20 nM biotinylated CEA in 300 µL PBSA overnight at 4°C with rotation. 10^5 CEA-coated beads were washed and incubated with 50 nM IgG or bsAb for 1 h at room temperature followed by incubation with 20 nM DOTA-Y-647 or 1:100 dilution of chicken anti-cmyc (Invitrogen) followed by incubation with 1:200 dilution of goat anti-chicken Alexa Fluor 647 (Invitrogen). Beads were washed and analyzed by flow cytometry.

3.3.9. Radiolabeling

IgG and bsAb protein were conjugated to p-SCN-Bn-DTPA (Macrocyclics) as described (Cooper et al. 2006). Concentrated DTPA-labeled protein was incubated with ~ 1 mCi $^{111}InCl_3$ (Cardinal Health, Dublin, OH) for 30 min at room temperature. The protein was diluted with 500 µL saline and concentrated to approximately 50 µL using Vivaspin 5000 MWCO spin columns (Sartorius Stedim Biotech, Aubagne, France). The ^{111}In-labeled protein was diluted with 500 µL saline and concentrated twice more.

3.3.10. *In Vivo* Blood Clearance and Tumor Uptake

All animal handling was performed in accordance with BIDMC IACUC guidelines. LS174T human colorectal carcinoma cells (CL 188) were obtained from American Type Culture Collection (Manassas, VA) and C6 rat glioma cells were obtained from Brian W. Pogue (Dartmouth Medical School). Both cell lines were maintained under standard conditions and confirmed to be negative for mycoplasma and mouse pathogens by the Yale Virology Lab. Xenografts were established in 5-6 week-old male NCRU-nu/nu mice (Taconic Farms, Hudson, NY) by subcutaneous injection of 1-2 x 10^6 LS174T cells into the left flank and 1-2 x 10^6 C6 cells into the right flank of each mouse. After 8-10 days, tumors were 0.1 – 0.5 g in mass. 500 µg of ^{111}In-labeled protein was injected intravenously in 100 µL saline. Blood samples of 10-15 µL were collected from the tail vein at various times and counted on a model 1470 Wallac Wizard (Perken Elmer, Wellesley, MA) 10-detector gamma counter. Mice were euthanized by intraperitoneal injection of pentobarbital, a method consistent with the recommendations of the Panel on

Euthanasia of the American Veterinary Medical Association. Tumors were resected, washed in PBS, weighed, and counted as described above.

3.4. Results

3.4.1. Plasmid Design and Expression in HEK293 Cells

We have designed a bispecific antibody as a C-terminal fusion to the light chain of an IgG (Figure 3.1). The heavy chain is identical to that of an IgG. The light chain is constructed by extending an IgG light chain with a C-terminal $(Gly_4Ser)_2$ linker followed by an scFv. In this study, the light chain is constructed with an N-terminal FLAG tag and C-terminal cmyc tag for characterization purposes. The fully assembled bsAb contains two heavy and two light chains, and is tetravalent with two IgG binding domains and two scFv binding domains.

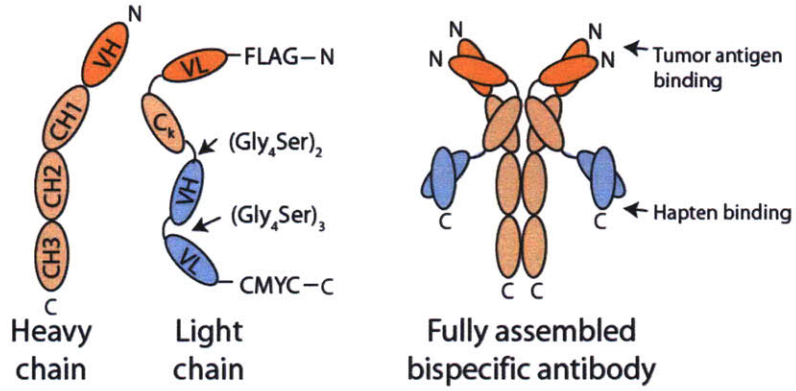

Figure 3.1 Design of IgG light chain C-terminal scFv fusion. Pictorial representation of heavy chain, light chain, and fully assembled bsAb with indicated N- and C- termini. The light chain is modified with an scFv fusion to the C-terminus, while a completely naïve heavy chain is preserved.

We synthesized a bsAb of this format that binds to the carcinoembryonic antigen (CEA) and to complexes of the metal chelate, DOTA. The Sm3e/C825 bsAb was constructed from an Sm3e IgG and a DOTA-binding scFv, C8.2.5, by cloning heavy and light variable domains from the picomolar affinity Sm3e scFv (Graff et al. 2004) into a plasmid containing human IgG1 constant heavy domains and kappa constant light chain domain. The C8.2.5 scFv was subsequently cloned into the light chain plasmid immediately following the C-terminus of the Cκ gene. The heavy and light chain expression plasmids were transiently co-transfected into HEK293 mammalian cells. Secreted antibody was purified from cell culture supernatants by protein A chromatography. Yields of both Sm3e IgG and Sm3e/C825 bsAb were ~5-7 mg/L.

Non-reducing SDS-page gel electrophoresis of purified bsAb displays a species with a molecular weight of ~200 kDa (Figure 3.2A). Under reducing conditions, the bsAb gives rise to two bands, both at around 50 kDa, as the scFv fusion increases the molecular weight of the light chain to ~50 kDa. Size exclusion chromatography of purified bsAb shows a single dominant peak with a small amount of higher molecular weight species, similar to that observed for recombinant IgG and for IgG purified from human plasma (Figure 3.2B).

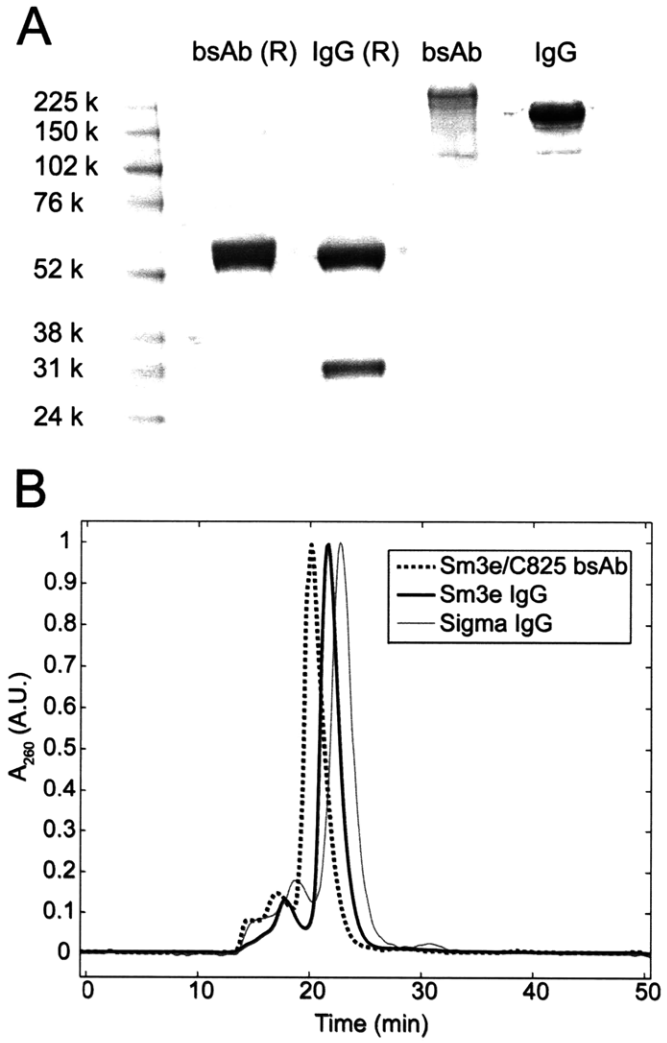

Figure 3.2 Characterization of bispecific antibody construct. Gel electrophoresis of reduced (R) and nonreduced Sm3e/C825 bsAb and Sm3e IgG (A). Size exclusion chromatography of Sm3e/C825 bsAb, Sm3e IgG, and IgG purified from human plasma (B).

3.4.2. Simultaneous Binding to Tumor Surface Antigen and Soluble Hapten

Bispecific antibody function was tested using CEA-expressing LS174T cells incubated with Sm3e/C825 bsAb followed by Alexa Fluor 647 conjugated DOTA loaded with nonradioactive yttrium (DOTA-Y-647). These samples exhibited a positive 647 signal, demonstrating bsAb simultaneous binding of both cell-surface CEA and soluble DOTA-Y-647. Control samples in which CEA or hapten epitopes were blocked showed no significant fluorescence (Figure 3.3A). Similarly, LS174T cells incubated with monospecific Sm3e IgG followed by DOTA-Y-647 exhibited no significant fluorescence.

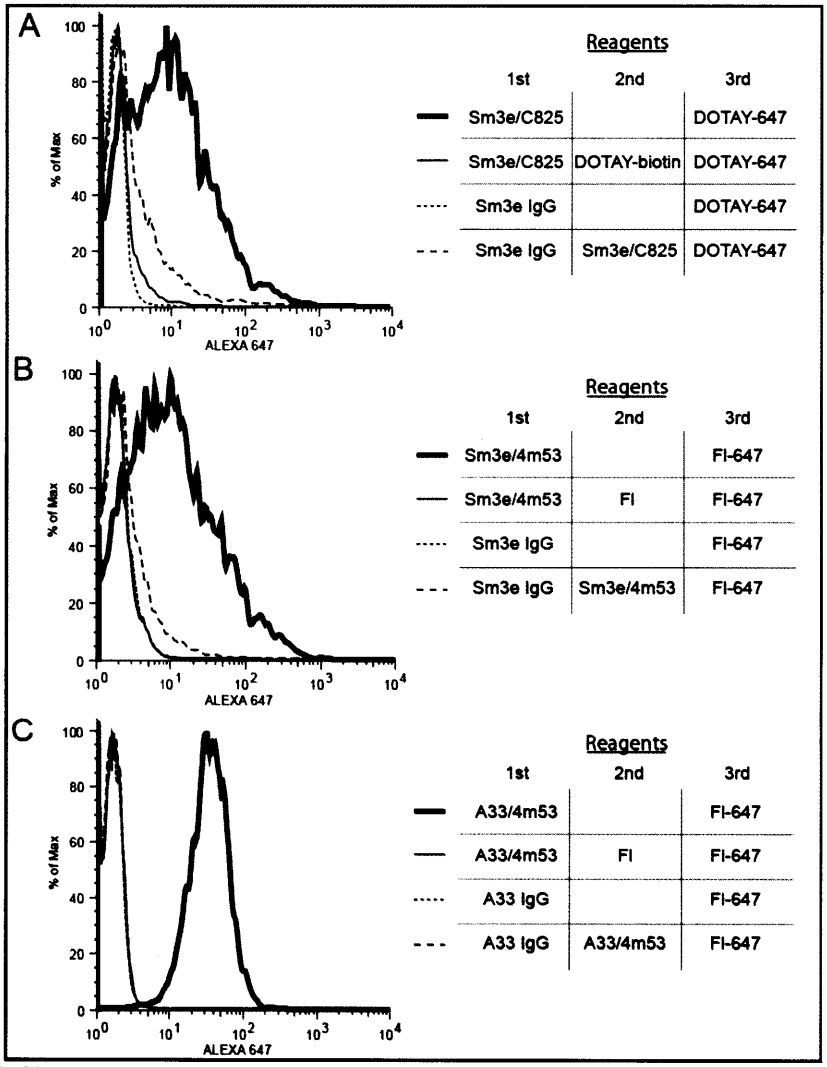

Figure 3.3 Simultaneous binding to cell surface antigen and hapten. Flow cytometry data of Sm3e/C825 bsAb (A), Sm3e/4m5.3 (B), and A33/4m5.3 (C) binding to cell surface antigen expressed on LS174T cells and soluble hapten. Legends show labeling scheme for sequential incubations.

We produced two additional bsAbs of the same format. Sm3e/4M5.3 binds to CEA and fluorescein, and A33/4M5.3 binds to the A33 antigen, a colon cancer immunotherapy target (Welt et al. 1990), and fluorescein. The 4M5.3 scFv was constructed by disulfide stabilizing the femtomolar fluorescein binding scFv 4M5.3 (Boder et al. 2000). Introduction of the disulfide bond does not significantly affect the binding affinity of the scFv (data not shown). The A33/4M5.3 bsAb was made by fusing an A33 antibody to ds4m5.3. The A33 IgG was constructed with heavy and light variable domains from an A33 humanized rabbit Fab (Rader et al. 2000). Both the Sm3e/4M5.3 (Figure 3.3B) and A33/4M5.3 (Figure 3.3C) bsAbs exhibited simultaneous binding to tumor surface antigen and soluble hapten.

3.4.3. Inter-Chain Disulfide Bond Formation

It was observed that when both IgG and bsAb were boiled prior to Western blot analysis, the molecules dissociate and exhibit a laddering effect with bands observed at molecular weights that correspond to the fully assembled molecule with two heavy chains and two light chains (H2L2) and partially assembled molecules (H2L and H2) (data not shown). The laddering of the bsAb is more significant compared to that of the IgG, likely due to more incomplete disulfide bond formation between the light and heavy chains of the bsAb due to the fusion of the scFv domain to the C-terminal Cκ cysteine.

To test this theory, we synthesized the A33 IgG with a light chain C-terminal Gly_4Ser based 18 amino acid peptide, which exhibited the same laddering effect as the bsAb under boiling conditions (Figure 3.4). In order to restore covalent linkage between the heavy and light chains, a disulfide bond was introduced between the A33 IgG variable light and variable heavy domains (the IgG portion of the bsAb). Two different pairs of cysteine mutations were tested (Reiter et al. 1996). This alternative site of disulfide stabilization significantly reduced the laddering effect such that it was similar to that observed for the IgG and suggests that variable domain disulfide stabilization of the IgG allows formation of a covalent bond between the heavy and light chains that can substitute for the normal position at the Cκ C-terminus.

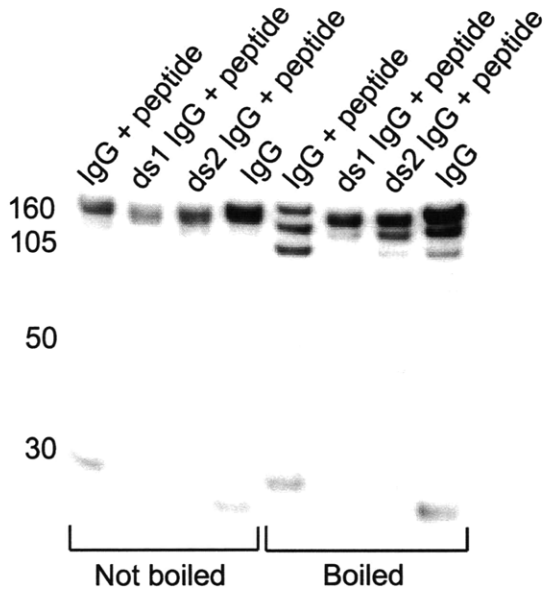

Figure 3.4 Disulfide stabilization of IgG. Western blot analysis detecting heavy and light chains of A33 IgG and A33 IgG extended by an 18 amino acid peptide (IgG + peptide) shows that extension of the light chain beyond the C-terminal Cκ cysteine disrupts disulfide bond formation. Two different pairs of cysteine mutations (ds1 and ds2) introduce disulfide stabilization of the IgG variable domains and demonstrate reformation of a covalent linkage between light and heavy chains.

3.4.4. Sm3e/C825 Retains Binding Affinity of Parent IgG and scFv

The affinity of IgG and scFv binding domains for the Sm3e/C825 bsAb were measured using cell binding assays. The bsAb binding affinity for CEA expressing LS174T cells was similar to that of the Sm3e IgG and the scFv binding affinity for soluble DOTA-Y-647 was similar to that of the scFv alone, expressed on the surface of yeast (Table 3.1).

Likewise, the affinity of the A33/4M5.3 bsAb to A33 antigen expressing LS174T cells was measured to be 647 ± 108 pM, within 2-fold to that measured for the A33 IgG, 303 ± 9 pM.

Table 3.1 Equilibrium dissociation constants

	CEA K_D	DOTA-Y-647 K_D	A33 antigen K_D
Sm3e/C825 bsAb	87 ± 55 pM	1.7 ± 0.2 pM	-
Sm3e IgG	54 ± 21 pM	-	-
C825 scFv	-	5.5 ± 0.1 pM	-
A33/4m5.3 bsAb	-	-	647 ± 108 pM
A33 IgG	-	-	303 ± 9 pM

3.4.5. Bispecific Antibodies Retain Stability of Parent IgGs

The thermal stability of the bsAb construct was tested by incubation at 37°C in PBSA. Both Sm3e/C825 and Sm3e/4M5.3 bispecific antibodies exhibited similar CEA binding activity as the Sm3e IgG after 7 days (Figure 3.5A). A33/4M5.3 also exhibited similar stability as the A33 IgG (Figure 3.5B).

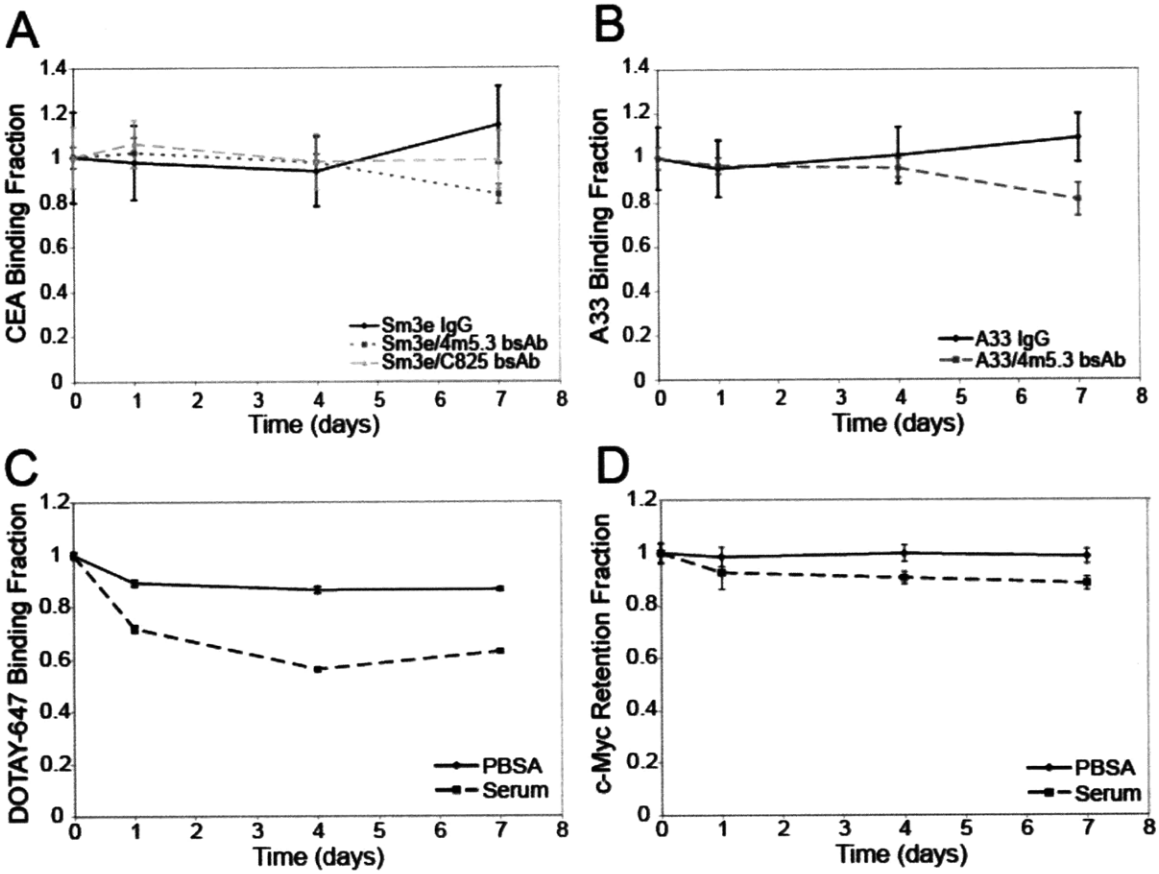

Figure 3.5 Bispecific antibody thermal and serum stability. Thermal stability of various IgGs and bsAbs over 7 days at 37°C in PBSA detecting CEA binding (A) or A33 antigen binding (B). Serum stability of Sm3e/C825 bsAb over 7 days at 37°C in 50% mouse serum detecting cmyc retention (C) or DOTA-Y-647 binding (D).

3.4.6. Stability of Bispecific Antibody Construct in Serum

Serum stability of the Sm3e/C825 bsAb was tested by incubation at 37°C in 50% mouse serum and compared to bsAb incubated in PBSA. After 7 days in PBSA, bsAb bound to CEA coated beads showed no loss of the C-terminal cmyc tag and retained about 90% of its DOTA-binding activity (Figures 3.5C and 3.5D), indicating thermal stability of the scFv and retention of assembled bsAb with simultaneous binding function.

After 7 days in serum, the bsAb retained approximately 90% of the c-Myc tag, and about 60% of initial DOTA-binding activity, indicating proteolytic stability but lower scFv stability in serum.

3.4.7. *In Vivo* Blood Clearance and Tumor Uptake

^{111}In-labeled Sm3e/C825 bsAb was injected intravenously into nude mice bearing both LS174T and C6 tumors. LS174T cells express ~ 4 x 10^5 CEA antigen per cell (Thurber and Wittrup 2008). C6 tumors have been used previously as an internal CEA negative control (Kenanova et al. 2005). Blood samples were taken at various times over 24 h and the activity measured by gamma counting. The blood half-life of the Sm3e/C825 bsAb is very similar to that of the Sm3e IgG (Figure 3.6), indicating *in vivo* stability of the bispecific construct and that the addition of the scFv does not interfere with FcRn binding (Olafsen et al. 2006). The tumor uptake of the Sm3e/C825 bsAb and Sm3e IgG were also measured at 24 h and found to be very similar with 19 ± 3 %ID/g and 15 ± 3 %ID/g for the CEA positive LS174T tumors, respectively. The tumor uptake in the CEA negative C6 tumors was 5.3 ± 1.7 %ID/g and 4.0 ± 1.6 %ID/g for the bsAb and IgG, respectively.

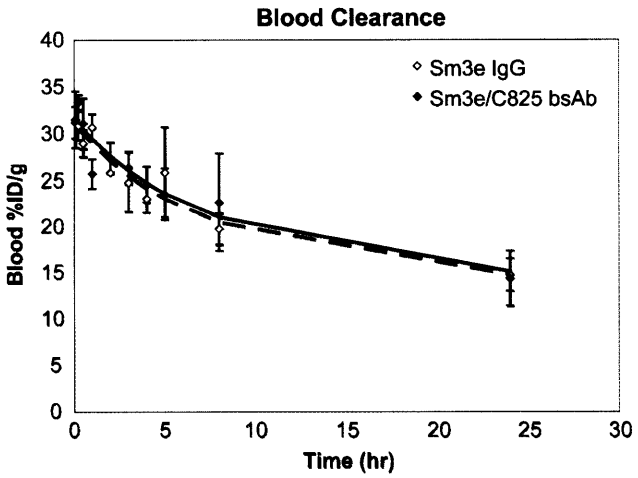

Figure 3.6 Blood clearance of Sm3e/C825 and Sm3e IgG in mice. Blood activity (mean ± s.d.) time profile of Sm3e IgG (open diamonds) and Sm3e/C825 (closed diamonds) after a 500 μg intravenous dose in male nude mice, n = 3. The blood curves were fit by least squares regression to a biexponential function for Sm3e IgG (dotted line) and Sm3e/C825 (solid line).

3.5. Discussion

We have engineered a novel bispecific antibody construct as an scFv fusion to the C-terminus of the light chain of an IgG. Fusing the scFv in this way should minimize steric hindrance that could obstruct simultaneous binding of both target antigens that might result from an N-terminal fusion to the light and/or the heavy chain. To date, we have synthesized several versions of the construct with various IgG and scFv domains, and all molecules bind simultaneously to their respective targets and retain parental affinities within two-fold. No linker-length optimization is required for expression and retention of scFv and IgG binding. The bispecific construct also exhibits IgG-like stability, blood clearance and *in vivo* tumor targeting. The bsAb construct appears to work generally to pair any stable and functionally expressing IgG and scFv into a bispecific format, while retaining IgG-like properties. However, it should be noted that all of the bsAb constructs tested in this study have IgG domains that bind to cell surface proteins and scFv domains that bind to haptens. While we believe that this bsAb construct will also work when the scFv specificity is a protein target due to flexibility in the Gly_4Ser-based linker and in the hinge region of the IgG, this has yet to be tested.

Coloma and Morrison also used an scFv for introducing additional specificity to an IgG, by attaching it to the C-terminus of the heavy chain of an IgG3 (Coloma and Morrison 1997). They report excellent results obtaining fully-assembled monomeric functional protein from transfectoma supernatants. However, the IgG-scFv fusion results in notably faster clearance in an *in vivo* mouse model compared to the parent IgG. This may be due to a decrease in FcRn binding possibly from steric hindrance of the attached scFv.

We are interested in bispecific antibodies for PRIT applications. It is desirable to preserve the Fc region in a bsAb for pretargeting applications, which will result in prolonged plasma retention due to FcRn binding and hence increased tumor penetration (Olafsen et al. 2006; Thurber et al. 2008). Full IgG molecules have demonstrated significantly higher tumor accumulation compared to minibodies, diabodies, and scFvs (Schneider et al. 2009). The addition of the scFv to the C-terminus of the IgG light chain

does not impact blood clearance, indicating that the scFv does not affect FcRn binding to the bispecific construct. The Fc binding domain may also retain FcγR binding, leading to ADCC resulting in the potential for additional therapeutic benefit.

The long circulating half-life of the bsAb will result in increased tumor uptake as discussed above but may also result in significant residual antibody retention in the blood at the time of hapten dosing. Thus, a clearing agent to quickly clear antibody from the blood prior to hapten dosing will be necessary to accelerate hapten clearance from the body. Rapid hapten clearance is necessary for high tumor to background ratios for imaging and low off-target radiation for therapy.

The Sm3e/C825 bsAb retains approximately 90% of its c-Myc tag at 37°C in serum after seven days, indicating little if any protease cleavage of the Gly_4Ser linker. However, the binding activity of the C8.2.5 scFv decreases to about 60% after seven days, with a rapid decrease during the first 24 hours followed by a plateau. The decreased binding activity does not appear to be pH-mediated as the pH of the serum solution remains neutral for the length of the experiment (data not shown). Nor does it appear to be simply due to thermal instability, because 90% of binding is retained after similar incubation at 37°C in PBSA. Thus, the loss of activity may be due to serum protein binding or protein- or enzyme-assisted denaturation.

One aspect of the bsAb format is an intermolecular disulfide bond between the variable heavy and variable light domains of the scFv. The open conformation of an scFv can be prone to aggregation (Reiter et al. 1994; Worn and Pluckthun 2001). Disulfide stabilization of the scFv should prevent the scFv from assuming an open conformation and hence reduce the risk of aggregation. In addition, as one would expect, the stability of the scFv in the bispecific format is limited by the stability of the parent scFv. Thus, it is important to select highly stable scFvs.

It is interesting to note that attaching an scFv, or even an 18 amino acid flexible peptide, to the C-terminus of the light chain appears to disrupt formation of the disulfide bond between the light chain and the heavy chain of the human IgG1. This disulfide bond

naturally exists at the C-terminal cysteine of the C_κ domain in IgG1 molecules. It does not appear to be necessary for function or stability of the bsAb, as all bsAbs tested retain parental affinities and exhibit excellent serum stability, even after protein A purification with acidic pH elution. We nevertheless added a disulfide bond between the heavy and light variable domains of the A33 IgG with peptide to determine if an interdomain disulfide bond can be introduced in this region to reform a covalent linkage between the LC and HC. Indeed, both disulfide stabilized versions of the A33 IgG with peptide exhibited significantly reduced dissociation after boiling, confirming that a covalent bond between the LC and HC can be reformed. While in this study, a covalent linkage between the heavy and light chains does not appear necessary for bsAb function or stability, it is possible that other IgGs may be less stable and require interdomain disulfide stabilization for stable bsAb construction.

While we have designed this bispecific format to be used for pretargeting approaches, this platform may be beneficial for other applications requiring bispecific antibodies. We demonstrate that the light chain of an IgG can be extended with an scFv without affecting IgG function and stability. Other proteins or peptides, such as affibodies (Nygren 2008), single variable domains (Harmsen and De Haard 2007), and peptide toxins could be attached to IgGs in this site specific manner, to yield homogenous IgG fusion products for targeted delivery. This platform could be used in a straightforward fashion to modify current FDA-approved antibodies to add additional functionalities. Production and purification should scale directly with current antibody manufacturing methods. As a robust modular platform, this bispecific antibody format obviates the need for extensive optimization of each new combination of binding domains and retains IgG-like properties both *in vitro* and *in vivo*.

4. CHARACTERIZATION OF DOTA-BASED HAPTENS

4.1. Abstract

In an effort to minimize hapten retention in normal tissues and determine the effect of various chemical adducts on *in vivo* properties, a series of DOTA-based small molecule derivatives were evaluated. Biodistribution and whole-body clearance were evaluated for ^{177}Lu-labeled DOTA, DOTA-biotin, a di-DOTA peptide, and DOTA-aminobenzene in normal CD1 mice. Kidney, liver, and bone marrow doses were estimated using standard Medical Internal Radiation Dose (MIRD) methodology. All haptens demonstrated low tissue and whole-body retention, with 2-4% of the injected dose remaining in mice 4 h post-injection. The kidney is predicted to be dose-limiting for all ^{177}Lu-labeled haptens tested with an estimated kidney dose of approximately 0.1 mGy/MBq. We present here a group of DOTA-based haptens that exhibit rapid clearance and exceptionally low whole-body retention 4 h post-injection.

4.2. Introduction

One very important step in the development of PRIT approaches is the selection of the hapten. The hapten must be nontoxic, not endogenous, not metabolized, and must clear rapidly from the blood with minimal normal tissue retention (Figure 4.1). While many small peptides exhibit fast renal clearance, most exhibit significant non-specific tissue retention (Sharkey et al. 2003; Chen et al. 2004; Chen et al. 2005; Schmitt et al. 2005; Wild et al. 2006; Garrison et al. 2007; Zhang et al. 2007). This background retention is typically 10-30 %ID at 2 to 4 h post-injection (summarized in Table 4.1). Significant whole-body retention results in background activity limiting signal-to-background ratios (SBRs) for imaging and contributing to nonspecific radiation limiting the maximum tolerated dose for therapy applications. Identifying small molecules with low whole-body retention is thus necessary for improving both imaging and therapy with radioisotopes.

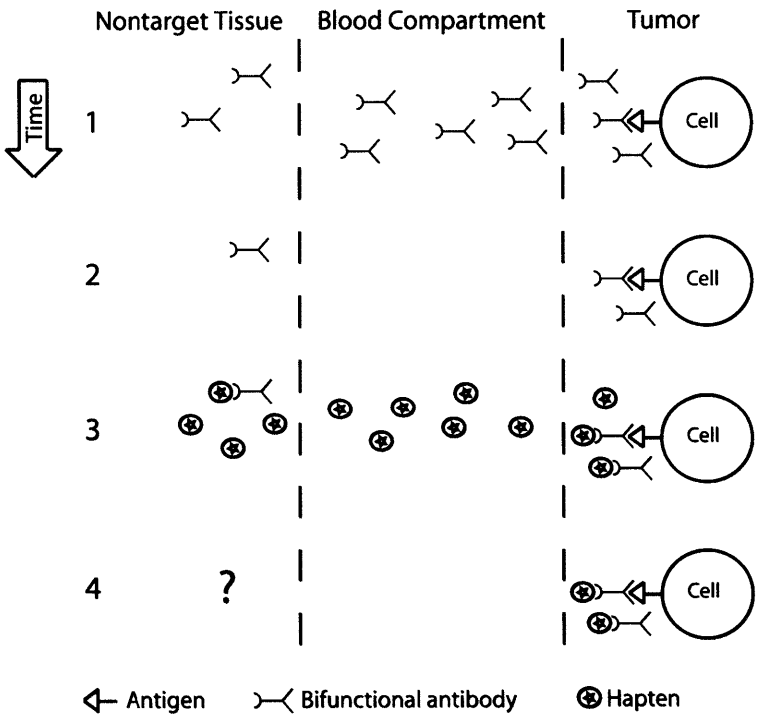

Figure 4.1 Schematic of PRIT. A pictoral representation of PRIT where a bifunctional antibody is administered in step 1. In step 2, the antibody is cleared from the body over time and/or with the help of a synthetic clearing agent (clearing agent not depicted). In step 3, a radiolabeled hapten is administered. In step 4, the hapten is cleared from the body over time; in this study, we investigate tissue and whole-body retention of various haptens.

Table 4.1 Estimation of whole-body retention at 4 hours post-injection for previously published small peptides

Molecule	%ID (retained in the body)	Reference
^{64}Cu-DOTA-RGD	> 15	(Chen et al. 2004)
^{64}Cu-DOTA-PEG-E(c(RGDyK))$_2$	> 6.7	(Chen et al. 2005)
^{64}Cu-DOTA-8-AOC-BBN	> 35	(Garrison et al. 2007)
^{64}Cu-CB-Te2A-8-AOC-BBN	> 13	(Garrison et al. 2007)
^{67}Ga-DOTA-PESIN	> 8.9	(Zhang et al. 2007)
^{177}Lu-DOTA-PESIN	> 8.8	(Zhang et al. 2007)
^{99m}Tc-depreotide	> 31	(Schmitt et al. 2005)
^{111}In-DTPA-octreotide	> 13	(Schmitt et al. 2005)
Lys$_{40}$(Ahx-DTPA-^{111}In)NH$_2$ exendin-4	> 93	(Wild et al. 2006)
^{111}In-IMP-241	> 1.4[a]	(Sharkey et al. 2003)
^{99m}Tc-IMP-243	> 24[a]	(Sharkey et al. 2003)
^{99m}Tc-IMP-245	> 2.6[a]	(Sharkey et al. 2003)

[a] 3 h %ID

The present study focuses on the use of DOTA as a possible hapten for PRIT because of its ability to chelate a wide variety of isotopes useful for imaging and therapy (Cutler et al. 2000) and its history of safe use in humans as an MRI contrast agent (chelated to Gd) (Le Mignon et al. 1990; Bourrinet et al. 2007). DOTA-Gd is nontoxic, not endogenous, not metabolized, and exhibits rapid blood clearance.

In this chapter, we are interested in investigating the *in vivo* biodistribution and clearance of various small molecule haptens to determine the effects of various adducts on the *in vivo* properties of DOTA. Currently, it is not known *a priori* how the addition of chemical groups will affect the *in vivo* properties of small molecules. Even small chemical modifications can drastically change retention and background (Banerjee et al. 2008). Our efforts are two-fold: 1) to increase the knowledge base of *in vivo* behavior of various DOTA-based compounds in an effort to develop a more comprehensive understanding to aid in the future development of molecular imaging and therapeutic agents with low background, and 2) to determine what form(s) of the DOTA chelate will result in the fastest blood clearance and lowest whole-body and kidney retention for PRIT applications. This quantitative analysis is crucial in moving towards an end goal of minimizing radioisotope retention in normal tissues.

4.3. Materials and Methods

4.3.1. Reagents

1,4,7,10-Tetraazacyclododecane-1,4,7,10-tetraacetic acid (DOTA), *S*-2-(R-Aminobenzyl)-1,4,7,10-tetraazacyclododecane tetraacetic acid (DOTA-Bn), DOTA-biotin-sarcosine (DOTA-biotin), and 1,4,7,10-Tetraazacyclododecane-1,4,7,10-tetraacetic acid mono(N-hydroxysuccinimide ester (DOTA-NHS) were purchased from Macrocyclics (Dallas, TX). Tyrosine-lysine peptide was purchased from Anaspec (San Jose, CA). All other chemicals were purchased from Sigma-Aldrich (St. Louis, MO) or Thermo Fisher Scientific (Waltham, MA).

4.3.2. DOTATyrLysDOTA Synthesis

DOTATyrLysDOTA was synthesized by reacting a 10-fold molar excess of DOTA-NHS with tyrosine-lysine peptide in DMSO in the presence of a 20-fold molar excess of triethylamine. The reaction was vortexed for 3 h at room temperature. To confirm completion of the reaction, the reaction mixture was analyzed by reverse-phase HPLC as described previously (Humblet et al. 2006) using a Waters 4.6 x 150 mm Symmetry C18 column and a linear gradient from 0% to 40% B in 25 minutes at 1 mL/min with A = water + 0.1% formic acid and B = acetonitrile + 0.1% formic acid. DOTATyrLysDOTA eluted at a retention time (R_t) = 9.6 minutes as detected by evaporative light scatter detector (ELSD), with the mass confirmed by electrospray time-of-flight (ES-TOF) mass spectrometry, calculated m/z 1082.53 $[M+H]^+$, found 1083.19 $[M+H]^+$. Preparative purification was performed on an HPLC system using a 19 x 150 mm Symmetry C18 column with a linear gradient of 0% B to 40% B in 35 minutes with A = water + 0.1% formic acid and B = acetonitrile + 0.1% formic acid. DOTATyrLysDOTA eluted at R_t = 5.6 minutes using ELSD detection. Fractions containing product were pooled and lyophilized. Purity was confirmed by analytical HPLC.

4.3.3. Radiolabeling

The HPLC/mass spectrometry platform used for purification of radioactive small molecules and peptides has been described in detail (Humblet et al. 2006; Misra et al. 2007). Compounds were dissolved at 0.5 mM in ammonium acetate pH 5.6. 1-2 mCi $^{177}LuCl_3$ (PerkinElmer, Waltham, MA) were added to the metal chelate and incubated for 1-2 h at 85-95°C. The radiolabeled compounds were purified by RP-HPLC with gamma detection on a 4.6 x 75 mm Symmetry C18 column using a linear gradient from 0% to 90% B over 15 minutes, at a flow rate of 1 mL/min, where A = water and B = acetonitrile. The compounds were then dried under vacuum, resuspended in saline, and filter-sterilized.

4.3.4. Mouse Model

All animal handling was performed in accordance with BIDMC IACUC guidelines. CD1 male mice were purchased from Taconic Farms (Germantown, NY). For biodistribution and clearance testing, 50-150 μCi ^{177}Lu-labeled hapten was injected intravenously into the mice. Blood was collected from the tail vein using micro-capillary tubes and counted on a model 1470 Wallac Wizard (Perkin Elmer, Wellesley, MA) 10-detector gamma counter. Mice were euthanized by intraperitoneal injection of pentobarbital followed by cervical dislocation, a method consistent with the recommendations of the Panel on Euthanasia of the American Veterinary Medical Association. Whole-body retention of radioactivity was measured in a dose calibrator after removing the bladder en masse. Organs were resected, washed in PBS thrice, weighed, and counted as described above.

4.3.5. Dosimetry

Radiation doses absorbed by normal tissues other than the red marrow were calculated according to the MIRD scheme. Percent injected activity in kidneys, liver, and whole-body were calculated from activity measurements. Isotope decay-adjusted activity was integrated over time, with a conservative assumption that the 24 h organ %ID remained constant thereafter for the liver, kidneys, and whole-body. *S* values (the

absorbed dose per unit cumulated activity) for ^{90}Y, ^{131}I, and ^{177}Lu were used to calculate dosimetry estimates in an adult male reference (Stabin and Siegel 2003). The blood activity data was fit to a biexponential function and used to determine the red marrow dose as described (Wessels et al. 2004) from blood activity measurements. The activity in the whole-body was used to estimate the total body cumulative activity used for cross-dose calculations.

4.3.6. Estimation of Whole-body Retention for Published Haptens

For each molecule, a lower bound for the whole-body %ID was calculated by summing the %ID of each measured organ from the published average %ID/g multiplied by the organ weight. Where organ weight information was unavailable, we assumed a 25 g mouse with the following distribution of organ weight percent: blood 8%, skin 11.2%, adipose 20%, muscle 40%, bone 7.5%, heart 0.43%, lung 0.56%, spleen 0.42%, liver 6.4%, kidneys 1.5%, stomach 0.9%, large intestine 1.78%, small intestine 2.75%, pancreas 0.3%, and brain 1.38%.

4.4. Results

The *in vivo* blood clearance and organ biodistribution of four ^{177}Lu-labeled DOTA haptens (Figure 4.2) were studied to determine how various small molecule appendages (aminobenzene, biotin, and a small peptide) affect *in vivo* tissue retention and clearance of DOTA. Serial blood samples were taken to determine blood clearance of the haptens (Figure 4.3). DOTA cleared faster from the blood than the other haptens tested; blood activity was not distinguishable from background after 2 h. The blood activity for all other haptens tested was not distinguishable above background after 3 h. Mice were sacrificed 4 h and 24 h post-injection to determine organ biodistribution (Figure 4.4). Tissue uptake was relatively low for all haptens. The %ID remaining in the whole animal was approximately 2-4% at 4 hours and 1-3% at 24 hours for the haptens, significantly lower than many other small molecule radioisotopes reported in the literature (summarized in Table 4.1).

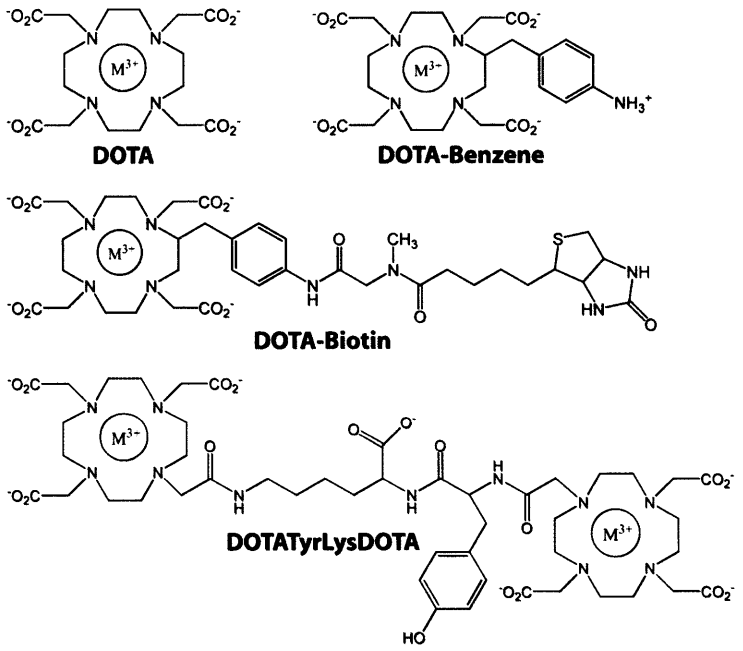

Figure 4.2 Chemical structure of DOTA-based small molecule haptens. Chemical structures of DOTA-based haptens. M^{3+} = trivalent cation metal = ^{177}Lu in all experiments presented here.

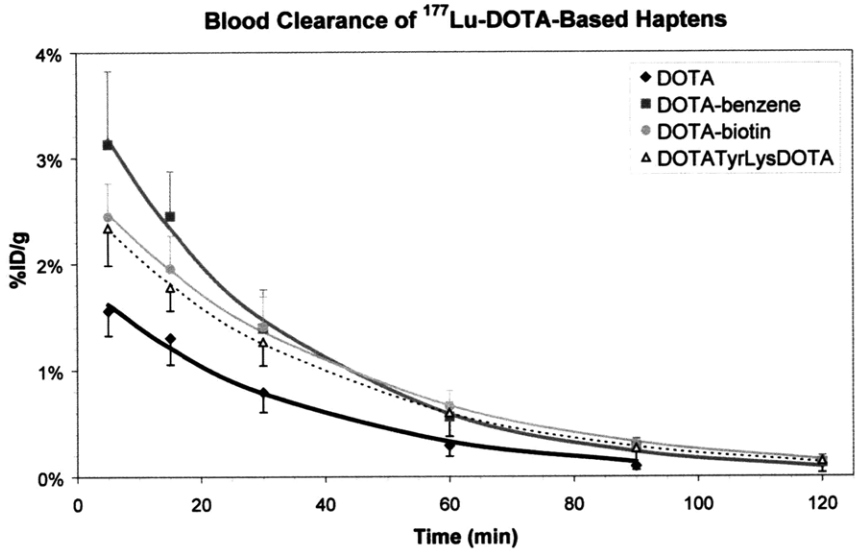

Figure 4.3 *In vivo* clearance of intravenously injected haptens. Blood %ID/g (mean ± s.d.) time profile of haptens after intravenous injection of 50-150 μCi in CD1 mice (n = 3–4). The lines represent fit exponential curves using least squares regression. By 2 h ^{177}Lu-DOTA blood activity was not distinguishable from background.

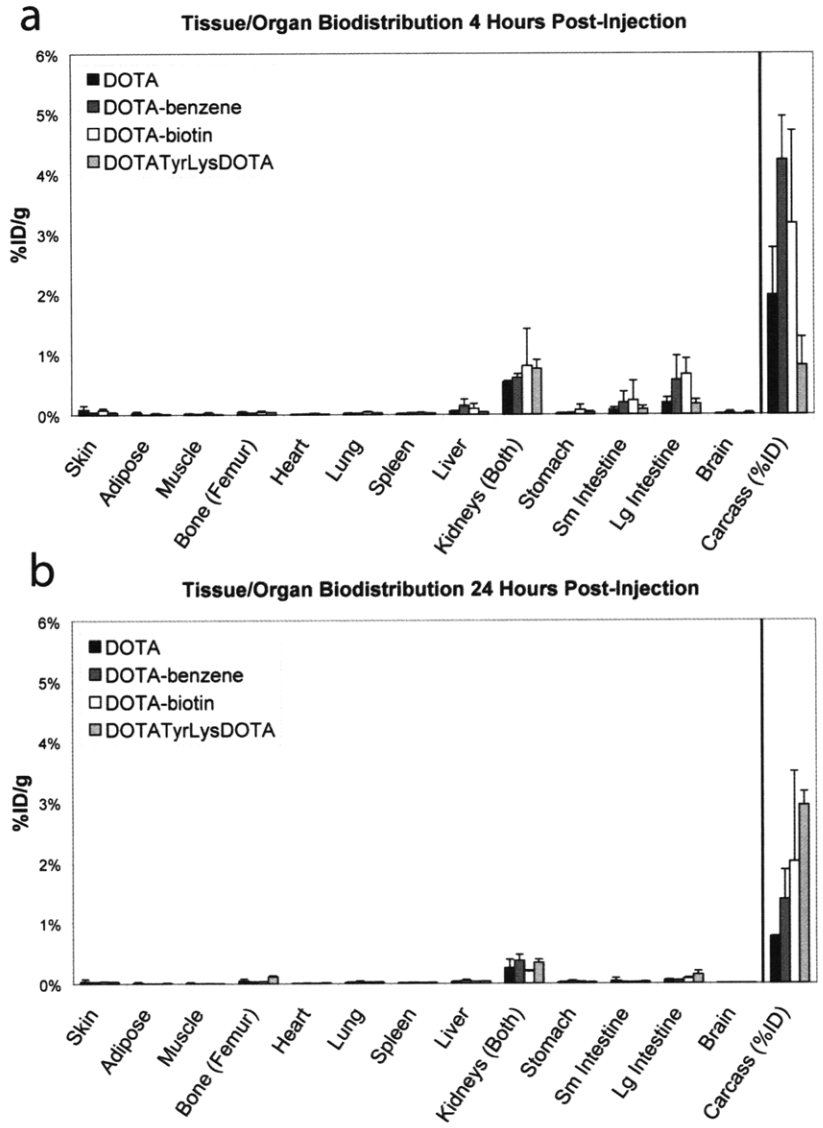

Figure 4.4 In vivo tissue/organ biodistribution of haptens. Tissue/organ %ID/g (mean ± s.d.) at 4 h post-injection (A) and 24 h post-injection (B) of 50-150 μCi hapten in CD1 mice (n = 3–4). Whole-body retention in carcass is presented as %ID.

From the organ biodistribution data, the radiation dose to the liver, kidney, and bone marrow was estimated for a 70 kg man for three radioisotopes, ^{90}Y, ^{131}I, and ^{177}Lu (Table 4.2). The self-dose and the total dose (self dose plus cross dose) are provided, where the whole-body activity was used to determine the cross dose. From the dose estimates, it is apparent that the cross-dose from the whole-body activity significantly impacts the dose, increasing the dose by 10- to 70-fold.

Table 4.2 Radiation dose estimates for DOTA-based chelates in selected organs

Hapten	Organ	Organ self-dose (mGy/MBq)			Organ self-dose and cross-dose (mGy/MBq)		
		^{90}Y	^{131}I	^{177}Lu	^{90}Y	^{131}I	^{177}Lu
DOTA	Liver	0.014	0.011	0.0053	0.035	0.023	0.010
	Kidney	0.17	0.11	0.067	0.19	0.12	0.071
	Red Marrow	0.00059	0.00014	0.000096	0.0079	0.0070	0.0015
DOTA-benzene	Liver	0.026	0.018	0.0091	0.052	0.035	0.016
	Kidney	0.24	0.16	0.096	0.27	0.17	0.10
	Red Marrow	0.0011	0.00027	0.00018	0.010	0.010	0.0021
DOTA-biotin	Liver	0.016	0.011	0.0055	0.045	0.033	0.014
	Kidney	0.15	0.088	0.054	0.18	0.11	0.063
	Red Marrow	0.0011	0.00025	0.00017	0.011	0.013	0.0026
DOTATyrLysDOTA	Liver	0.018	0.014	0.0068	0.052	0.043	0.018
	Kidney	0.23	0.14	0.087	0.26	0.17	0.098
	Red Marrow	0.00097	0.00023	0.00016	0.013	0.016	0.0032

The dose limiting toxicities ($TD_{5/5}$) for the liver, kidney, and red marrow estimated from external beam radiation are 30 Gy, 23 Gy, and 1.5 Gy, respectively (Emami et al. 1991). From the radiation dose estimates for the haptens, the dose-limiting organ is predicted to be the kidney for all ^{177}Lu-labeled haptens tested with an estimated kidney dose of approximately 0.1 mGy/MBq and liver and red marrow doses of approximately 0.01-0.02 mGy/MBq and 1-2 x 10^{-4} mGy/MBq, respectively. However, for ^{90}Y and ^{131}I isotopes, the dose limiting organ could be either the kidneys or the red marrow, with less than a two-fold difference predicted between the two organs for the estimated dose normalized to the respective organ $TD_{5/5}$. The estimated liver, kidney, and red marrow doses for ^{90}Y-labeled haptens are 0.04-0.05 mGy/MBq, 0.2-0.3 mGy/MBq, and 0.01 mGy/MBq, respectively, and 0.02-0.04 mGy/MBq, 0.1-0.2 mGy/MBq, and 0.01-0.02 mGy/MBq, respectively, for ^{131}I labeled haptens.

4.5. Discussion

In this study, we present a group of small molecule DOTA-based compounds that exhibit rapid blood clearance and result in exceptionally low whole-body retention within 4 h post-injection. While many small molecules exhibit fast blood clearance, they generally exhibit significant retention in normal tissues (Table 4.1). This background whole-body retention is typically 10-30% at 2-4 h and results in background radiation that limits signal to background ratios for imaging and nonspecific radiation that contributes to maximum tolerated dose for therapy applications. Identifying small molecules that exhibit whole-body retention less than 5% in only a few hours is thus necessary for improving both imaging and therapy using radionuclides. The DOTA molecules we present here should thus prove exceptionally useful for pretargeted applications with bispecific antibodies. The development of small molecules with even lower whole-body retention would further improve tumor to off-target ratios.

Other small molecules have been developed for pretargeted applications including DOTA-biotin as well as small peptide haptens (Barbet et al. 1998; Sharkey et al. 2003). The streptavidin/^{90}Y-DOTA-biotin PRIT system has been tested clinically and radiation doses have been estimated from whole-body scintigraphy at approximately 3.5 ± 1.0 and 0.04 ± 0.01 mGy/MBq for the kidneys and red marrow, respectively (Knox et al. 2000). The predicted dose estimates for the ^{90}Y-DOTA-biotin hapten presented here are 0.18 and 0.011 mGy/MBq for the kidney and red marrow, respectively. Thus, the kidney dose for the hapten is predicted to be about 20-fold lower than that measured in the clinical PRIT study. This is expected because streptavidin localizes to the kidneys where it remains accessible to binding by DOTA-biotin (Forster et al. 2006). In a mouse lymphoma xenograft study, pretargeted DOTA-biotin exhibited about five- to ten-fold higher kidney uptake than DOTA-biotin alone (Lin et al. 2006). A clinical trial of a pretargeted system without the use of streptavidin reported an average kidney dose of 0.7 mGy/MBq (Kraeber-Bodere et al. 2006), 5-fold lower than that observed for a streptavidin-based pretargeted clinical trial (Knox et al. 2000). In addition to high streptavidin uptake in the kidneys, streptavidin pretargeted systems also suffer from

endogenous biotin binding to streptavidin (Hamblett et al. 2002). Thus recent efforts have moved towards approaches using bispecific antibodies with peptide haptens. Sharkey et al. have developed an approach using peptide-based haptens and an antibody that recognizes the peptide epitope (Sharkey et al. 2003). While some of these peptide-based haptens exhibit fast clearance and low tissue uptake, others exhibit significantly slower whole-body clearance (Sharkey et al. 2003).

We are interested in developing a non-peptide approach using DOTA-based haptens. It was expected that an approach without using peptides would reduce kidney uptake, as it is known that peptides exhibit tubular reabsorption and resulting kidney retention (Behr et al. 1998). However, the data presented here shows no significant difference in kidney retention between DOTA and the DOTATyrLysDOTA peptide. From MIRD radiation dose estimates, similar red marrow doses are predicted for DOTA and the peptide. Nevertheless, DOTA presents some potential advantages as a hapten for PRIT. DOTA is commercially available in large quantities and thus no further synthesis before radiolabeling is required. In addition, Gd-DOTA, injected in millimolar quantities for MRI imaging, has an established safety profile in humans (Bourrinet et al. 2007).

From dosimetry estimates, it is predicted that the dose-limiting toxicity for all of the hapten molecules radiolabeled with ^{177}Lu is the kidney. However, for ^{90}Y and ^{131}I isotopes with longer path lengths, whole-body retention of the hapten contributes significantly to the red marrow dose, resulting in similar estimated doses to $TD_{5/5}$ ratios for the kidney and the red marrow. These estimates are for the hapten molecule alone. In PRIT, residual bispecific antibody in the blood and non-tumor tissue will bind to the hapten and may significantly alter clearance and biodistribution. Clinical PRIT studies with ^{131}I without a clearing or blocking agent report hematological toxicity as dose limiting (Kraeber-Bodere et al. 2006).

Directly radiolabeled antibodies in radioimmunotherapy trials exhibit dose limiting hematological toxicity, with estimated doses of 2.7 ± 0.9 mGy/MBq to the marrow and 2.4 ± 0.6 mGy/MBq dose to the kidneys when using ^{90}Y (Fisher et al. 2009). This suggests that if residual bispecific antibody is sufficiently low, PRIT will result in

significantly higher tumor to marrow and tumor to kidney ratios. In addition, the results presented here suggest that ^{177}Lu may result in lower off-target doses and may be preferred over ^{90}Y and ^{131}I in PRIT applications; this has also been suggested for radioimmunotherapy based on a xenograft study (Zacchetti et al. 2009).

In cases where the kidney proves to be the dose-limiting organ, kidney uptake and radiation dose may be reduced by using diuretics, catheterization, and/or renal protective agents (Jaggi et al. 2006).

The development of PRIT has allowed the delivery of higher doses of ionizing radiation to the tumor compared to directly-radiolabeled antibodies. However, these doses do not yet result in significant cure rates for heavily pre-treated patients with bulky disease. To fully realize the potential of PRIT, approaches that continue to improve tumor to normal tissue doses must be developed either through increasing tumor dose or decreasing normal tissue dose. In the next chapter, we present a novel method for PRIT using a CEA-specific bsAb, a dextran-based clearing agent, and radiolabeled DOTA. We demonstrate the best tumor to kidney ratios reported to date for CEA-targeted PRIT.

5. *IN VIVO* TUMOR TARGETING

5.1. Abstract

We have recently engineered a high-affinity antibody fragment to DOTA metal chelates with ~10 pM affinity to lutetium and yttrium chelates of DOTA-aminobenzene, ~100 pM affinity to lutetium and yttrium chelates of DOTA, ~1 nM affinity to indium chelates of DOTA-aminobenzene, and ~10 nM affinity to indium chelates of DOTA (Table 2.1). Here, we present a novel three-step method for PRIT using an IgG-scFv bispecific antibody, a dextran-based clearing agent, and radiolabeled DOTA, and test proof-of-principle of this system in a xenograft mouse model. In addition, we use this system to analyze *in vivo* the affect of small molecule affinity on tumor uptake. Biodistribution and tumor uptake were evaluated in xenograft mice with CEA-positive and CEA-negative tumors for ^{177}Lu-DOTA, ^{111}In-DOTA-Bn, and ^{111}In-DOTA after pretargeting with an anti-CEA bsAb. Kidney, liver, and bone marrow doses were estimated using standard Medical Internal Radiation Dose (MIRD) methodology. The PRIT method presented here resulted in tumor uptake of ^{177}Lu-DOTA of ~14 %ID/g at 24 h and 48 h, tumor-to-kidney ratios of ~20 at 24 h and 48 h, and tumor-to-blood ratios of greater than 300 at 24 h and 48 h. An affinity of ~100 pM resulted in 8-fold higher tumor uptake at 24 hours than an affinity of ~1 nM, and 28-fold higher uptake than ~10 nM affinity. We present here a novel PRIT method with the highest yet reported 48 h tumor-to-blood and tumor-to-kidney ratios for CEA targeting. In addition, we report for the first time a systematic study of the affect of small molecule affinity, over a span of three orders of magnitude, on tumor uptake.

5.2. Introduction

Directly radiolabeled tumor-specific antibodies have been investigated as delivery vehicles of radioisotopes to tumor cells for over 50 years (Pressman 1957; Larson et al. 1984; Boswell and Brechbiel 2007) and the first radiolabeled antibody was approved by the FDA for the treatment of Non-Hodgkin's lymphoma in 2002. Unfortunately, antibodies exhibit long half-lives in the blood resulting in low tumor to blood activity ratios and consequently low tumor to red marrow dose ratios. Antibody fragments and other smaller binding scaffolds exhibit faster blood clearance but result in high kidney and/or liver uptake. Radiolabeled small molecule ligands generally exhibit rapid blood clearance but result in relatively poor tumor accumulation due to low affinity and/or specificity for tumor antigen.

The premise of pretargeted radioimmunotherapy is that the exquisite binding specificity of antibodies can be coupled with the rapid clearance of radiolabeled small molecules to yield high tumor uptake, yet fast clearance from non-tumor tissue. Over the past 20 years, various methods of pretargeted radioimmunotherapy have been developed and tested in preclinical and clinical settings (Gautherot et al. 2000; Knox et al. 2000; DeNardo et al. 2001; Kraeber-Bodere et al. 2006; Lin et al. 2006; Sharkey et al. 2009).

We present here a novel method for pretargeted radioimmunotherapy using a three-step procedure with a bispecific antibody, a dextran clearing agent, and radiolabeled DOTA. To the best of our knowledge, this is the first PRIT method that uses an IgG-like bispecific antibody that can be produced using current antibody production and purification methods, eliminating additional development specific to the bsAb. High bsAb doses on the order required for antigenic saturation are used to achieve a high concentration of hapten binding sites in the tumor. Bsab dosing is followed by a dextran-based clearing agent to clear residual bsAb from the blood. The clearing step is followed by administration of radiolabeled DOTA, a small molecule metal chelate commercially available in large quantities with proven clinical safety in humans when chelated to gadolinium and used in millimolar concentrations as an MRI contrast agent (Bourrinet et

al. 2007). In the present study, we investigate the *in vivo* efficacy of this new PRIT system.

A unique feature of our engineered PRIT system is the ability of the anti-DOTA binding fragment to bind with varying affinities to different DOTA chelates (Chapter 2). This affords an unprecedented method to systematically analyze the affect of small molecule binding affinity on tumor uptake *in vivo* using the same bispecific antibody molecule with different radiolabeled DOTA chelates. We thus evaluate on a fundamental level the benefit of improving small molecule affinity in tumor targeting applications and compare the experimental results to mathematical predictions.

5.3. Materials and Methods

5.3.1. Reagents

1,4,7,10-Tetraazacyclododecane-1,4,7,10-tetraacetic acid (DOTA), *S*-2-(R-Aminobenzyl)-1,4,7,10-tetraazacyclododecane tetraacetic acid (DOTA-Bn), and *S*-2-(4-Isothiocyanatobenzyl)-1,4,7,10-tetraazacyclododecane tetraacetic acid (DOTA-SCN) were purchased from Macrocyclics (Dallas, TX). All other chemicals were purchased from Sigma-Aldrich (St. Louis, MO) or Thermo Fisher Scientific (Waltham, MA) unless specified otherwise.

5.3.2. Synthesis of Dextran-based Clearing Agent

5 mg (10 nmol) of 500 kDa amino dextran purchased from Invitrogen (Carlsbad, CA) with 136 moles of amine per mole dextran was reacted with 3.7 mg (5.3 μmol) DOTA-SCN in 1 mL DMSO with 1.9 μL (13.6 μmol) TEA overnight at room temperature with mild vortexing. The dextran reaction mixture was diluted with 14 mL 0.4 M sodium acetate pH 5.2 and 53 μmol yttrium nitrate was added. The mixture was incubated overnight at 37°C, dialyzed against water, and then dried down by vacuum centrifugation. The dried dextran compound was resuspended in PBS and purified by size exclusion chromatography using a Superdex 75 10/300 GL column. Fractions containing the dextran compound were combined, dialyzed against water twice, dried by vacuum centrifugation, resuspended in saline and 0.2 μm filtered. The final dextran-DOTA-Y contained approximately 130 DOTA molecules as assessed by a TNBSA assay (Thermo Fisher Scientific, Rockford, IL).

5.3.3. Radiolabeling

DOTA compounds were dissolved at 0.5 mM in ammonium acetate pH 5.6. 1-2 mCi $^{177}LuCl_3$ (PerkinElmer, Waltham, MA) or $^{111}InCl_3$ (Cardinal Health, Dublin, OH) were added to the metal chelate and incubated for 1-2 h at 85-95°C. The radiolabeled compounds were purified by RP-HPLC (Humblet et al. 2006; Misra et al. 2007) with gamma detection on a 4.6 x 75 mm Symmetry C18 column using a linear gradient from

0% to 40% B over 15 minutes, at a flow rate of 1 mL/min, where A = 10 mM TEAA and B = methanol. The purified compounds were dried under vacuum, resuspended in saline, and filter-sterilized.

IgG and bsAb protein were conjugated to p-SCN-Bn-DTPA (Macrocyclics) as described (Cooper et al. 2006). Concentrated DTPA-labeled protein was incubated with ~ 1 mCi $^{111}InCl_3$ for 30 min at room temperature. The protein was diluted with 500 µL saline and concentrated to approximately 50 µL using Vivaspin 5000 MWCO spin columns (Sartorius Stedim Biotech, Aubagne, France). The ^{111}In-labeled protein was diluted with 500 µL saline and concentrated twice more.

^{111}In-DOTA-dextran was prepared by synthesizing dextran-DOTA as described above, without loading with cold yttrium. Dextran-DOTA was incubated with 1-2 mCi $^{111}InCl_3$ for 1 h at 37°C followed by concentration and dilution with saline as described above.

5.3.4. Animal models

All animal handling was performed in accordance with BIDMC IACUC guidelines. Male NCRU-nu/nu mice were purchased from Taconic Farms (Germantown, NY). For biodistribution and tumor uptake, 100-150 µCi ^{177}Lu- or ^{111}In-labeled hapten was injected intravenously into the mice. Blood was collected from the tail vein using micro-capillary tubes and counted on a model 1470 Wallac Wizard (Perkin Elmer, Wellesley, MA) 10-detector gamma counter. Mice were euthanized by intraperitoneal injection of pentobarbital followed by cervical dislocation, a method consistent with the recommendations of the Panel on Euthanasia of the American Veterinary Medical Association. Organs and tumors were resected, washed in PBS thrice, weighed, and counted as described above.

5.3.5. Dosimetry

Radiation doses absorbed by normal tissues other than the red marrow were calculated according to the MIRD scheme. Percent injected activity in tumor, kidneys, liver, blood, and whole-body were calculated from activity measurements. The activity at

time 0 was assumed to be 4 %ID/g in the kidney and liver, 50 %ID/g in the blood, 0 %ID/g in the tumor and 100% in the whole-body. Isotope decay-adjusted activity was integrated over time, with a conservative assumption that the 48 h organ %ID remained constant thereafter. *S* values for ^{90}Y and ^{177}Lu were used to calculate dosimetry estimates in an adult male reference (Stabin and Siegel 2003). The red marrow dose was calculated as described (Wessels et al. 2004) from blood activity measurements. The activity in the whole-body was used to estimate the total body cumulative activity used for cross-dose calculations. Tumor doses were calculated from self-dose only using *S*-factors for a unit density sphere of size 500 g (the average LS174T tumor size scaled by 2000).

5.3.6. Imaging

SPECT/CT (single photon emission computed tomography/computed tomography) scans and image analyses were performed using a rodent scanner (NanoSPECT/CT, Bioscan, Washington, DC) equipped with an 8W x-ray source running at 45 kV (177 μA), and a 48 μm pitch CMOS-CCD x-ray detector. Mice were anesthetized in an anesthetic chamber with isoflurane and transferred to a bed on a gantry for imaging where gas anesthesia was maintained for the duration of the scan. After acquisition of a CT topogram, helical micro SPECT was performed using a four-headed gamma camera outfitted with multi-pinhole collimators (1.4 mm) and a total scan time of 45 min. SPECT images were acquired over 360° in 24 projections each using a 256 x 256 frame size (1.0 mm pixels). Images were reconstructed with Bioscan HiSPECT iterative reconstruction software and fused with CT images. Immediately after scanning, mice were sacrificed and tissues and tumors weighted and counted as described above.

5.4. Results

The Sm3e/C825 bsAb was produced and purified as described previously (Chapter 3). 24 h biodistribution of the bsAb and the parent Sm3e IgG in male nude mice bearing CEA-positive (LS174T) and CEA-negative (C6) tumors demonstrated similar specific accumulation in the antigen-positive tumor with ~4-fold higher uptake than the antigen-negative tumor (Table 5.1). In addition, high activity remained in the blood at 24 h, as expected, due to slow blood clearance of Fc-containing compounds.

Mice pretargeted with 500 ug bsAb were injected with ^{111}In-DOTA-Bn 24 h later. 4 h biodistribution showed significantly higher activity in all organs due to binding to bsAb (appendix Figure 7.1). Of particular note is the high activity in the blood and low tumor to blood ratio. The high blood activity motivated the development of a clearing/blocking agent.

We engineered a dextran-based clearing agent, using a 500 kDa aminodextran (~136 amino groups per dextran molecule) conjugated to DOTA. The resulting compound contained approximately 130 DOTA molecules per dextran. The dextran-DOTA compound was loaded with non-radioactive yttrium and when injected into pretargeted mice one hour prior to hapten administration resulted in hapten blood clearance essentially identical to that of hapten alone (appendix Figure 7.2) suggesting essentially complete blocking/clearance of residual bsAb in the blood. Dextran-DOTA was radiolabeled with ^{111}In to characterize the *in vivo* properties of the dextran agent alone. Biodistribution and blood clearance of ^{111}In-DOTA-dextran was analyzed in tumor-bearing mice (Figures 5.1 and 5.2). The dextran agent clears very rapidly from the blood and exhibits very high uptake in the liver and spleen at 4 h post-injection (p.i.).

Table 5.1 24 h biodistribution of 500 ug ^{111}In-bsAb and 500 ug ^{111}In-IgG.

Organ/tissue	Sm3e/C825 bsAb	Sm3e IgG
Blood	14 ± 1	13 ± 2
Skin	3.3 ± 0.1	2.6 ± 1.1
Adipose	5.2 ± 3.1	1.2 ± 0.1
Muscle	1.0 ± 0.1	1.0 ± 0.1
Bone (femur)	2.2 ± 0.4	1.4 ± 0.1
Heart	2.7 ± 0.1	3.0 ± 0.1
Lung	5.7 ± 0.0	3.9 ± 0.5
Spleen	7.2 ± 1.0	3.7 ± 0.5
Liver	3.5 ± 0.7	2.7 ± 0.6
Kidneys (both)	2.9 ± 0.2	2.5 ± 0.3
Stomach (with contents)	0.56 ± 0.09	0.62 ± 0.01
Sm Intestine	1.4 ± 0.1	1.1 ± 0.1
Lg Intestine	2.8 ± 0.5	2.6 ± 1.4
C6 Tumor	5.3 ± 1.8	4.0 ± 1.6
LS174T Tumor	19 ± 3	15 ± 3

%ID/g (mean ± s.d.), n = 2

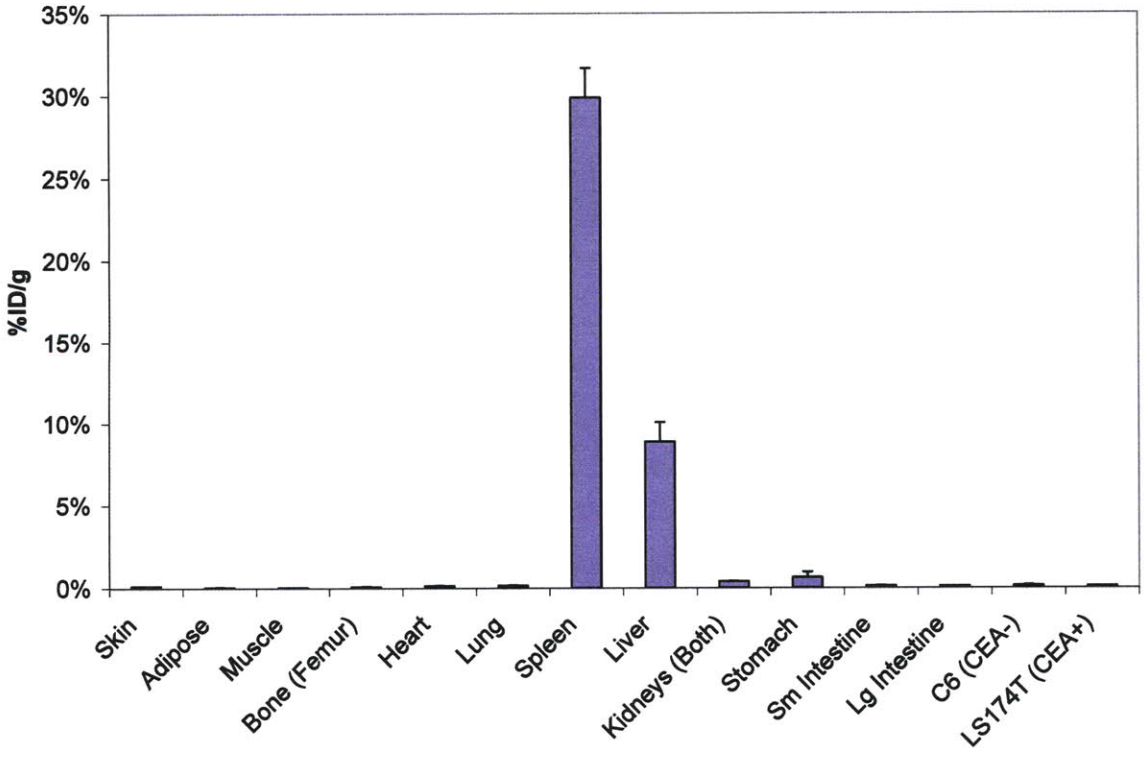

Figure 5.1. ^{111}In-DOTA-dextran organ/tissue biodistribution. Organ/tissue biodistribution (mean ± S.D., n=2) of ^{111}In-labeled DOTA-dextran clearing agent 4 h p.i. in tumor bearing mice.

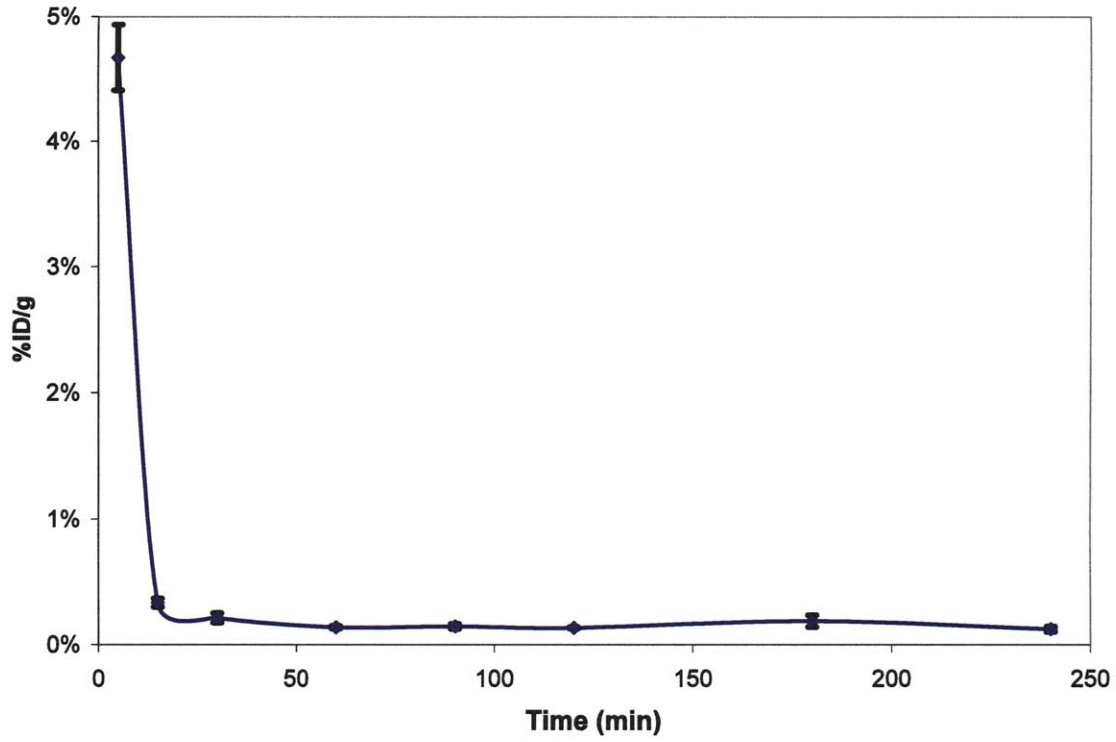

Figure 5.2 ^{111}In-DOTA-dextran Blood Clearance. Blood clearance (mean ± S.D., n=2) of ^{111}In-labeled DOTA-dextran clearing agent in tumor bearing mice.

We next tested a protocol involving all three reagents to determine the efficacy of our engineered PRIT system. We intravenously injected tumor-bearing mice with 500 μg bsAb followed by 250 ug of dextra-DOTA-Y clearing agent 24 h later. After an additional 1 h, 100-150 μCi ^{177}Lu-DOTA was injected intravenously. At 4 h post-injection of radiolabeled DOTA, tumor uptake was 7.44 ± 0.41 %ID/g in the antigen-positive tumor (Table 5.2 and Figure 5.3), 84-fold higher than the tumor uptake observed for ^{177}Lu-DOTA alone (Table 5.3). Activity was also higher in non-tumor tissue due to binding of ^{177}Lu-DOTA to residual bsAb in the extravascular compartment. Tumor uptake in the antigen-negative tumor was 9.82 ± 0.35 %ID/g at 4 h, similar to the antigen-positive tumor due to nonspecific uptake from enhanced permeability and retention (EPR) of the bsAb. Over time, the tumor activity in the antigen-negative tumor decreased to 4.23 ± 0.54 %ID/g at 24 h and 2.89 ± 2.28 %ID/g at 48 h while the tumor activity in the antigen-positive tumor increased to 14.3 ± 1.8 %ID/g at 24 h and remained essentially constant at 48 h. The LS174T tumor to blood ratio increased from 18 ± 2 at 4

h to 380 ± 90 at 24 h and was greater than 450 at 48 h (Table 5.4). At 48 h, the blood activity was not measurable above background. The LS174T tumor to kidney ratio increased from approximately 8 at 4 h to about 20 at 24 and 48 h (Figure 5.4). SPECT/CT images confirmed the quantitative biodistribution data with high SPECT signal in the CEA-positive tumors, lower signal in the CEA-negative tumor and no observable signal in non-tumor tissue (Figure 5.5).

From the PRIT organ biodistribution data, the radiation dose to the kidney, liver, red marrow, and antigen-positive tumor was estimated for a 70 kg man for ^{90}Y and ^{177}Lu (Table 5.5). It should be noted that these estimates are generated from mouse biodistribution data and are thus approximations; human clinical data will be required for more accurate dosimetry. The estimated doses to the kidney, liver, and red marrow were calculated from both the self-dose and cross-dose, where the whole-body activity was used to determine the cross-dose. The estimated dose to the tumor was determined from self-dose only. The dose limiting toxicities ($TD_{5/5}$) for the liver, kidney, and red marrow estimated from external beam radiation are 30 Gy, 23 Gy, and 1.5 Gy, respectively (Emami et al. 1991). From the radiation dose estimates, the dose-limiting organ is predicted to be the red marrow for both ^{90}Y-DOTA and ^{177}Lu-DOTA haptens. At a red marrow dose of 1.5 Gy, the estimated dose to the tumor is 98 Gy for ^{90}Y and 156 Gy for ^{177}Lu. A dose of greater than 50 Gy is generally thought to be sufficient to eradicate most tumors (Govindan et al. 2000).

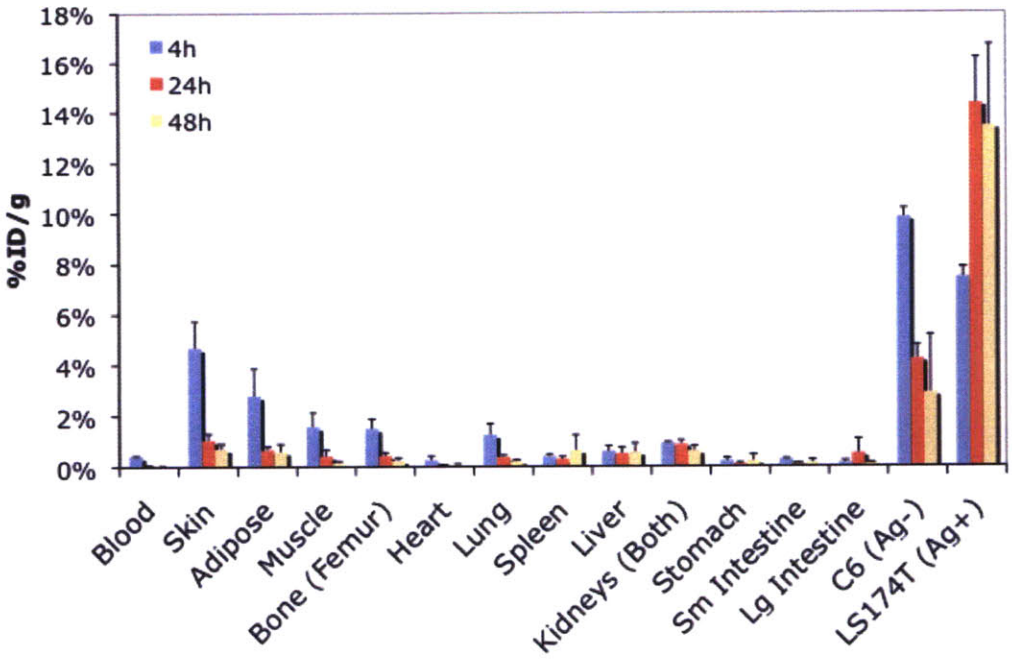

Figure 5.3 ^{177}Lu-DOTA Organ/tissue biodistribution. Organ/tissue biodistribution (mean ± s.d., n=3) of ^{177}Lu-labeled DOTA at 4, 24, and 48 h p.i. 500 ug Sm3e/C825 bsAb was injected followed by 250 ug Y-DOTA-dextran clearing agent 24 h later. 100-150 μCi ^{177}Lu-DOTA was injected 1 h after the clearing agent.

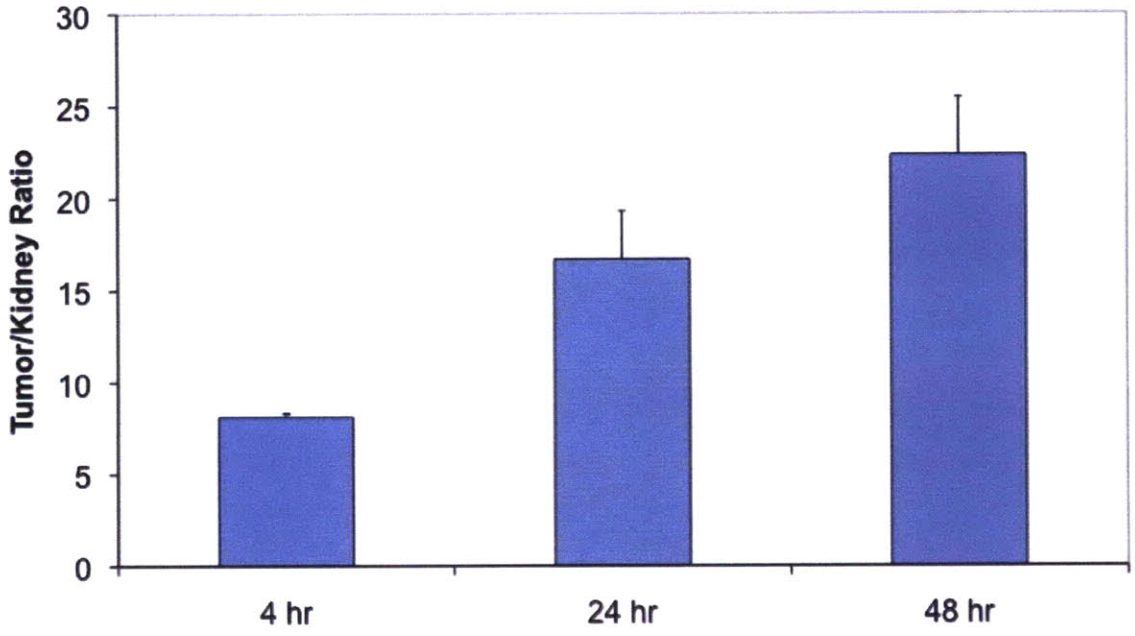

Figure 5.4 Pretargeted ^{177}Lu-DOTA tumor/kidney ratios. Tumor/kidney ratios (mean ± s.d., n=3) of ^{177}Lu-DOTA at various times.

Table 5.2 Biodistribution of pretargeted ^{177}Lu-DOTA

	Time post-injection[a]		
Organ/Tissue	4 h	24 h	48 h
Blood	0.42 ± 0.02	0.04 ± 0.01	< 0.03
Skin	4.68 ± 1.06	1.05 ± 0.25	0.71 ± 0.20
Adipose	2.78 ± 1.08	0.67 ± 0.12	0.60 ± 0.29
Muscle	1.56 ± 0.56	0.41 ± 0.24	0.15 ± 0.07
Bone (femur)	1.49 ± 0.38	0.43 ± 0.12	0.24 ± 0.10
Heart	0.25 ± 0.16	0.05 ± 0.01	0.07 ± 0.03
Lung	1.25 ± 0.43	0.37 ± 0.07	0.21 ± 0.04
Spleen	0.39 ± 0.09	0.29 ± 0.09	0.64 ± 0.60
Liver	0.59 ± 0.21	0.51 ± 0.23	0.56 ± 0.35
Kidneys (both)	0.92 ± 0.05	0.88 ± 0.16	0.62 ± 0.19
Stomach (with contents)	0.21 ± 0.12	0.09 ± 0.07	0.22 ± 0.24
Sm Intestine	0.28 ± 0.02	0.08 ± 0.04	0.14 ± 0.11
Lg Intestine	0.13 ± 0.09	0.52 ± 0.56	0.11 ± 0.04
C6 Tumor	9.82 ± 0.35 (0.26 ± 0.08 g)	4.23 ± 0.54 (0.26 ± 0.07 g)	2.89 ± 2.28 (0.28 ± 0.13 g)
LS174T Tumor	7.44 ± 0.41 (0.09 ± 0.03 g)	14.34 ± 1.83 (0.21 ± 0.10 g)	13.44 ± 3.25 (0.49 ± 0.09 g)

[a] Mice were injected with 500 ug bsAb i.v. 24 h later, mice received 250 ug dextran-DOTA i.v. 1 h later, mice received 100-150 uCi of ^{177}Lu-DOTA i.v. and were sacrificed at 4, 24, and 48 h p.i. Data given as mean ± s.d. (%ID/g, n=3). Tumor weights are provided as mean ± s.d. in parentheses.

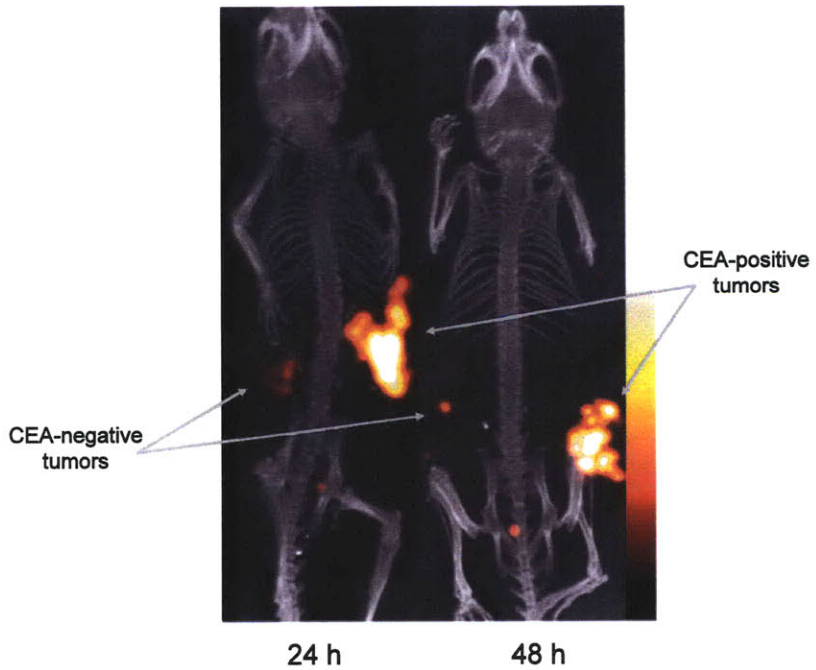

Figure 5.5 SPECT/CT images of pretargeted ^{177}Lu-DOTA. SPECT/CT maximum intensity projections of pretargeted tumor mice at 24 h (left) and 48 h (right) p.i. of ^{177}Lu-DOTA.

Table 5.3 Four hour Biodistribution of ^{177}Lu-DOTA in tumor mice.

Organ/tissue	**%ID/g[a]**
Blood	< 0.04
Skin	0.076 ± 0.021
Adipose	0.015 ± 0.009
Muscle	0.014 ± 0.004
Bone (femur)	0.030 ± 0.006
Heart	0.012 ± 0.000
Lung	0.029 ± 0.000
Spleen	0.030 ± 0.002
Liver	0.089 ± 0.010
Kidneys (both)	0.764 ± 0.011
Stomach (with contents)	0.227 ± 0.014
Sm Intestine	0.253 ± 0.072
Lg Intestine	0.080 ± 0.029
C6 Tumor (0.11 ± 0.01 g)	0.112 ± 0.034
LS174T Tumor (0.04 ± 0.02 g)	0.089 ± 0.005

[a] Mice were injected with 100-150 uCi of ^{177}Lu-DOTA i.v. Data given as mean ± s.d. (%ID/g, n=2). Tumor weights are provided as mean ± s.d. in parentheses.

Table 5.4 Pretargeted tumor/organ ratios.

	Time post-injection[a]		
Organ/tissue	4 h	24 h	48 h
Blood	18 ± 2	380 ± 90	> 450
Skin	1.7 ± 0.4	14 ± 2	20 ± 8
Adipose	3.2 ± 1.5	23 ± 6	28 ± 13
Muscle	5.3 ± 1.6	57 ± 41	105 ± 40
Bone (femur)	5.3 ± 1.6	38 ± 16	60 ± 19
Heart	49 ± 36	323 ± 108	244 ± 85
Lung	7.2 ± 3.7	39 ± 3	63 ± 6
Spleen	20 ± 5	52 ± 12	40 ± 21
Liver	13.9 ± 3.7	33 ± 11	32 ± 13
Kidneys (both)	8.1 ± 0.2	17 ± 3	22 ± 3
Stomach (with contents)	48 ± 22	252 ± 119	276 ± 236
Sm Intestine	27 ± 4	217 ± 76	183 ± 129
Lg Intestine	80 ± 36	83 ± 53	128 ± 16
C6 Tumor	0.7 ± 0.1	3.4 ± 0.3	10 ± 9
LS174T Tumor	1	1	1

[a] Tumor/organ ratios (mean ± s.d., n=3) [a] Mice were injected with 500 ug bsAb i.v. 24 h later, mice received 250 ug dextran-DOTA i.v. 1 h later, mice received 100-150 uCi of ^{177}Lu-DOTA i.v. and were sacrificed at 4, 24, and 48 h p.i.

Table 5.5 Radiation dose estimates in selected organs.

	Estimated Dose (mGy/MBq)	
	^{90}Y	^{177}Lu
Kidney	0.56	0.15
Liver	0.35	0.09
Red Marrow	0.05	0.01
Tumor	3.6	1.1

The pretargeted protocol described above was used to analyze the effect of affinity on the tumor uptake of radiolabled DOTA. The bsAb exhibits affinities of ~10 nM for ^{111}In-DOTA, ~1 nM for ^{111}In-DOTA-Bn, ~100 pM for ^{177}Lu-DOTA, and ~10 pM for ^{177}Lu-DOTA-Bn (Table 2.1). The 24 h organ/tissue biodistribution was determined in tumor-bearing mice with each of the four radiolabeled DOTA compounds (Figure 5.6 and Table 5.6). SPECT/CT images of one mouse from each set show that at least single digit nanomolar affinity is needed to observe signal in the antigen-positive tumor (Figure 5.7). The 24 h activity in the LS174T tumor increased from 0.5 ± 0.1 %ID/g for ~10 nM affinity to 1.6 ± 0.3 %ID/g for ~1 nM affinity to 14.3 ± 1.8 %ID/g for ~100 pM affinity. The tumor activity for ~10 pM affinity is not significantly different than that of ~100 pM affinity. The activity in the C6 antigen-negative tumor increased with affinity, presumably due to nonspecific uptake of bsAb. The activity in the non-tumor tissues is also higher for the higher affinity compounds due to the higher affinity binding to residual bsAb. The tumor to kidney ratio increased from 1.2 ± 0.4 for ~10 nM to 17 ± 3 for ~100 pM but then decreased to 10 ± 2 for ~10 pM affinity due to higher uptake in the kidney but similar tumor uptake.

The experimental results of 24 h tumor uptake versus affinity were compared to mathematical predictions based on a previously published compartmental model of tumor uptake (Schmidt and Wittrup 2009). Vascular permeability was estimated from the two-pore model of the capillary wall for a 1 kDa molecule. The surface density was estimated to be 2 x 10^5 DOTA binding sites per cell based on the 24 h tumor accumulation of bsAb (Table 5.1), the 24 h activity of the scFv in serum (chapter 3), and the 15 h internalization rate of CEA resulting in approximately half of the accumulated bsAb to be internalized and therefore inaccessible to binding. The blood clearance parameters were calculated from a biexponential fit of the *in vivo* blood clearance measured for ^{177}Lu-DOTA.

The experimental results compared well to the model prediction (Figure 5.8) with the 24 h tumor uptake increasing significantly from 1 nM to 100 pM affinity and then reaching a plateau with an additional improvement in affinity from 100 pM to 10 pM resulting in no significant improvement in 24 h tumor activity.

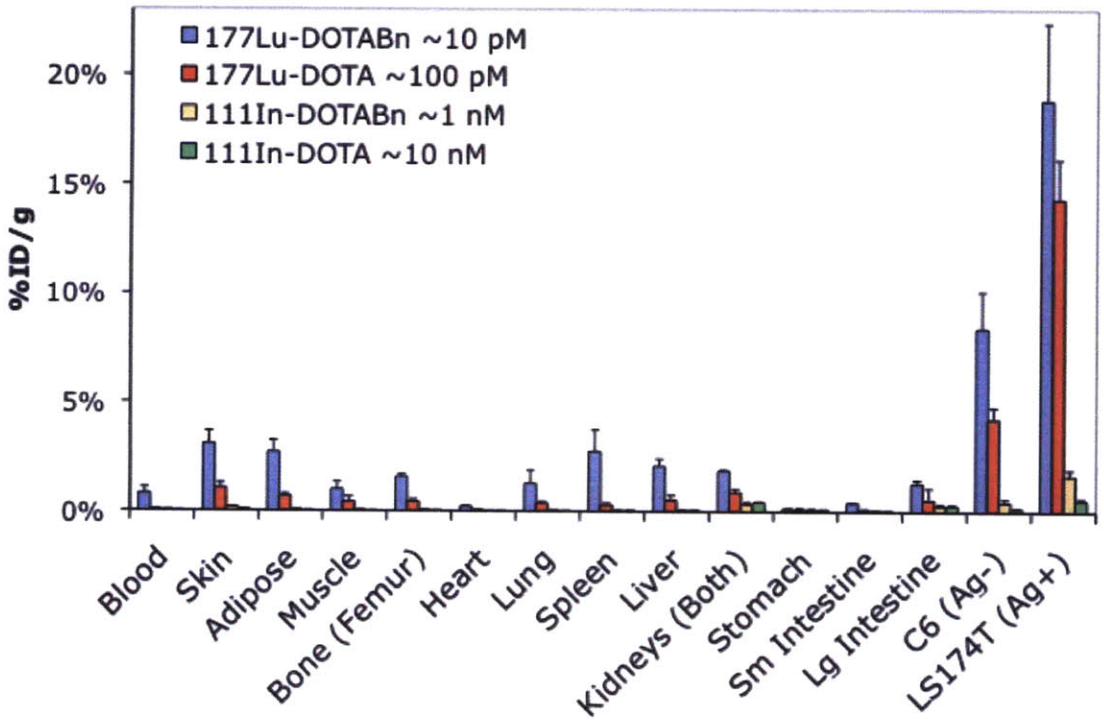

Figure 5.6 Biodistribution of DOTA compounds with varying affinities. Organ/tissue biodistribution 24 h p.i. (mean ± S.D., n=3) of ^{177}Lu-DOTA-Bn, ^{177}Lu-DOTA, ^{111}In-DOTA-Bn, and ^{111}In-DOTA. 500 ug Sm3e/C825 bsAb was injected followed by 250 ug Y-DOTA-dextran clearing agent 24 h later. Radiolabeled DOTA was injected 1 h after the clearing agent.

Table 5.6 24 h Biodistribution of pretargeted ^{177}Lu-DOTA-Bn, ^{177}Lu-DOTA, ^{111}In-DOTA-Bn, and ^{111}In-DOTA

	^{177}Lu-DOTA-Bn	^{177}Lu-DOTA	^{111}In-DOTA-Bn	^{111}In-DOTA
Blood	0.79 ± 0.29	0.04 ± 0.01	0.02 ± 0.00	< 0.01
Skin	3.1 ± 0.6	1.05 ± 0.25	0.16 ± 0.01	0.06 ± 0.01
Adipose	2.7 ± 0.5	0.67 ± 0.12	0.04 ± 0.00	0.01 ± 0.00
Muscle	1.0 ± 0.3	0.41 ± 0.24	0.04 ± 0.00	0.01 ± 0.00
Bone (femur)	1.6 ± 0.1	0.43 ± 0.12	0.04 ± 0.01	0.02 ± 0.00
Heart	0.22 ± 0.03	0.05 ± 0.01	0.01 ± 0.00	0.01 ± 0.00
Lung	1.3 ± 0.6	0.37 ± 0.07	0.03 ± 0.00	0.01 ± 0.01
Spleen	2.8 ± 1.0	0.29 ± 0.09	0.04 ± 0.01	0.03 ± 0.00
Liver	2.1 ± 0.3	0.51 ± 0.23	0.05 ± 0.01	0.04 ± 0.00
Kidneys (both)	1.9 ± 0.1	0.88 ± 0.16	0.33 ± 0.11	0.41 ± 0.03
Stomach (with contents)	0.12 ± 0.01	0.09 ± 0.07	0.08 ± 0.05	0.07 ± 0.04
Sm Intestine	0.40 ± 0.01	0.08 ± 0.04	0.04 ± 0.01	0.03 ± 0.00
Lg Intestine	1.3 ± 0.2	0.52 ± 0.56	0.26 ± 0.09	0.25 ± 0.07
C6 Tumor	8.4 ± 1.7 (0.21 ± 0.08)	4.2 ± 0.5 (0.26 ± 0.07 g)	0.42 ± 0.15 (0.50 ± 0.36 g)	0.14 ± 0.02 (0.48 ± 0.13 g)
LS174T Tumor	19 ± 4 (0.10 ± 0.01)	14.3 ± 1.8 (0.21 ± 0.10 g)	1.6 ± 0.3 (0.30 ± 0.18 g)	0.50 ± 0.12 (0.45 ± 0.24 g)

[a] Mice were injected with 500 ug bsAb i.v. followed 24 h later by 250 ug dextran-DOTA i.v. and 1 h later with 100-150 uCi of ^{177}Lu-DOTA-Bn, ^{177}Lu-DOTA, ^{111}In-DOTA-Bn, or ^{111}In-DOTA i.v. and sacrificed at 24 h p.i. Data is given as mean ± s.d. (%ID/g, n=3). Tumor weights are provided as mean ± s.d. in parentheses.

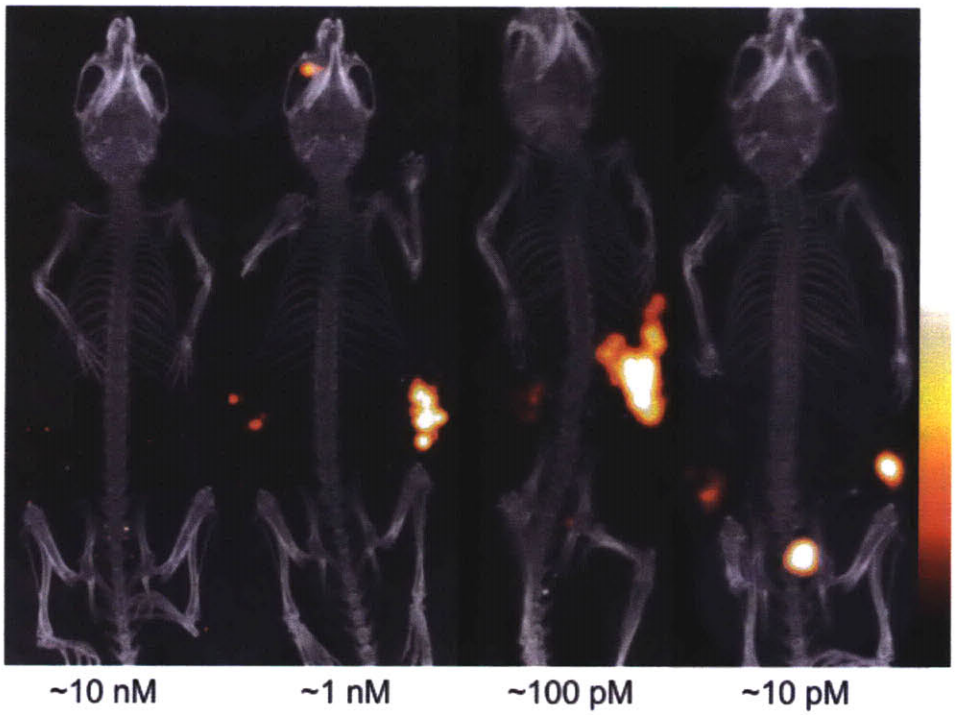

Figure 5.7 SPECT/CT images of pretargeted DOTA compounds with varying affinities. SPECT/CT maximum intensity projections of tumor mice pretargeted with ^{111}In-DOTA (left), ^{111}In-DOTA-Bn (left middle), ^{177}Lu-DOTA (right middle), and ^{177}Lu-DOTA-Bn (right) 24 h p.i.

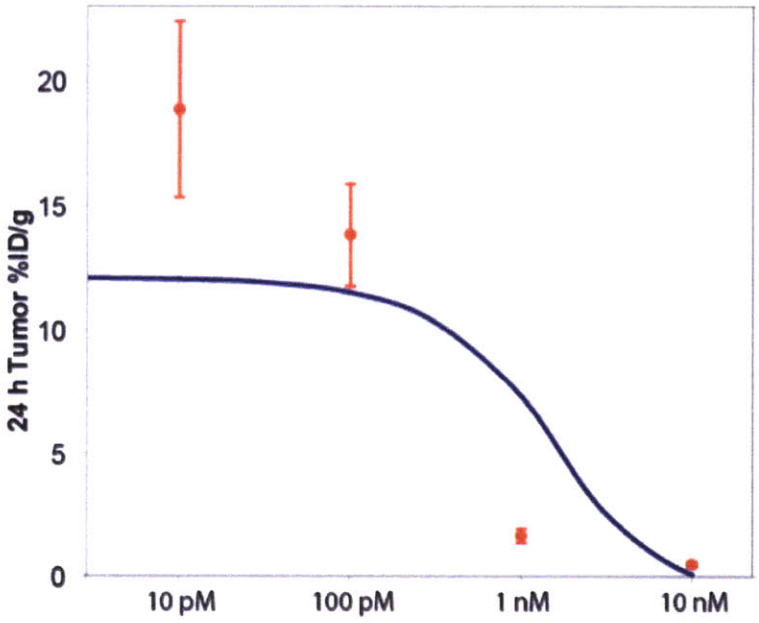

Figure 5.8 24 h tumor uptake for varying affinities: mathematical prediction versus experimental results. Mathematical prediction (navy line) and experimental data (red circles, mean ± s.d.) of 24 h tumor %ID/g for increasing affinity. Model parameters: $t_{1/2,\ ke}$ = 120 h, [Ag] = 13.3 x 10^{-8} M, ε = 0.44, $[Ab]_0$ = 1 nM, α = 0.096 s^{-1}, β = 0.00051 s^{-1}, A = 0.8, R_{cap} = 8 μm, R_{Krogh} = 75 μm, P = 2.4 x 10^{-7} m/s.

5.5. Discussion

Here we present a new method for pretargeted radioimmunotherapy that uses an IgG-scFv bsAb (Chapter 3), a dextran-based clearing agent, and radiolabeled DOTA. The engineered PRIT system was tested in xenograft mice bearing CEA-positive and CEA-negative tumors. The bsAb exhibits ~100 pM affinity for ^{177}Lu-DOTA. ^{177}Lu-DOTA has previously been shown to exhibit very rapid whole-body clearance from mice (Chapter 4). Here we demonstrate high LS174T tumor uptake and retention of ^{177}Lu-DOTA with fast clearance from non-tumor tissue resulting in the highest reported tumor-to-blood and tumor-to-kidney ratios at 48 h p.i. for CEA targeting.

A significant amount of ^{177}Lu-DOTA uptake is observed in the CEA-negative tumors at early times. Enhanced permeability and retention (EPR) results in nonspecific tumor accumulation of high-molecular weight compounds. While approximately 4-fold higher bsAb uptake is observed in LS174T tumors versus C6 tumors, the difference in hapten uptake at early times will be less because a significant fraction of the bsAb localized to the LS174T tumors will be inaccessible due to the 15 h internalization half-life of CEA (Schmidt et al. 2008), while all bsAb in the C6 tumors will be accessible to hapten binding. This is consistent with the observation of similar activities in the two tumors at early times. At later times, unbound antibody intravasates out of the CEA-negative tumor while CEA-bound antibody in the LS174T tumors internalizes ^{177}Lu-DOTA compounds where the radiolabel is trapped within the cell.

The PRIT approach presented here originates from a rational engineering design perspective. We used mathematical modeling to predict the affinity necessary for efficient hapten capture and retention at the site of the tumor (Chapter 2). We then engineered an IgG-like bsAb to retain slow blood clearance resulting in high tumor uptake, retain potentially beneficial secondary immune function, and to allow for production and purification identical to that of an IgG. We designed our system to use simply DOTA as the hapten, with no additional synthesis or modification required eliminating issues with linker cleavage and peptide stability (van Gog et al. 1998; van Schaijk et al. 2005). DOTA chelated to gadolinium has been administered to human

subjects in millimolar concentrations and has an established safety profile. DOTA metal chelates exhibit rapid blood clearance and whole-body clearance observed in mice (Chapter 4) and humans (Le Mignon et al. 1990). When systematically compared to other DOTA-based compounds, ^{177}Lu-DOTA exhibits slightly lower liver and intestine uptake at 4 h p.i. compared to radiolabeled DOTA-biotin and DOTA-Bn in normal CD1 mice (Chapter 4). This suggests that DOTA exhibits essentially complete renal clearance while DOTA-biotin and DOTA-Bn exhibit some clearance through bile. This effect may be more or less pronounced in humans.

The non-tumor tissue clearance of DOTA is not nearly as fast in mice pretargeted with bsAb, even with the addition of the dextran clearing agent, due to incomplete clearance resulting in residual antibody. Multiple doses of the clearing agent or infusion of the clearing agent over a period of time would likely result in more complete bsAb clearance from non-tumor tissue, as residual bsAb in the extravascular space will recycle back into the bloodstream over time (Press et al. 2001). A lower mass of dextran may also improve bsAb clearance; however, improved clearance will need to be balanced with possible tumor uptake of smaller agents resulting in blocked hapten binding sites.

Not only do we present here excellent tumor:blood ratios but they are demonstrated despite an exceptionally high dose of bsAb. Other reports of pretargeting methods report decreasing tumor/blood ratios with increasing bsAb doses (Sharkey et al. 2005; van Schaijk et al. 2005). Our method results in a high number of hapten binding sites in the tumor at the time of hapten dosing; this is important as the number of hapten binding sites is directly related to the number of radioisotopes that can be captured and retained at the site of the tumor, impacting the maximum possible dose. While three-step pretargeted radioimmunotherapy adds complexity over two-step procedures, it allows higher doses of bsAb to be administered resulting in higher achieved tumor doses as well as more homogenous distribution within the tumor. In addition, it allows for possible secondary immune effects resulting from the retained Fc domain that may prove significant (Sharkey et al. 2009). Two-step approaches may be sufficient for molecular imaging leading to improved cancer screening and staging (Sharkey et al. 2005; Sharkey et al.

2008). However, it is anticipated that the increased number of hapten binding sites afforded by three-step approaches will prove critical for therapy.

A unique advantage of the approach developed here is the ability to study the effect of affinity on the *in vivo* tumor uptake of radiolabeled DOTA. This is the first time, to our knowledge, that affinity alone has been analyzed *in vivo* over three orders of magnitude. We had the unique ability to parse out affinity, with unaltered internalization kinetics and B_{max}. We show here that ~100 picomolar affinity is required for high tumor uptake in this system with further affinity improvement resulting in no further improvement in tumor uptake. Based on our experimental results and their excellent correlation to mathematical prediction, we expect this affinity requirement to pertain to other systems of small molecule targeting with similar ~10^5 sites/cell surface density.

6. CONCLUDING REMARKS

Here, we present a novel PRIT approach, based on a systematic engineering design approach and mathematical modeling. DOTA was selected as the radionuclide-carrying hapten, based on its favorable pharmacokinetics and safety profile in humans. We engineered a high-affinity antibody fragment to DOTA with a target affinity motivated by mathematical modeling. A bispecific antibody construct was then engineered with the DOTA-binding moiety appended to the C-terminus of the light chain of an anti-CEA IgG. A three-step PRIT protocol with a dextran-based clearing agent demonstrated excellent tumor targeting of DOTA-chelated radioisotope and low background in tumor-bearing mice with tumor-to-blood ratios greater than 300 and tumor-to-kidney ratios of about 20 at 24 hours. This work shows that mathematical modeling can be used to motivate appropriate design criteria in developing improved agents for tumor targeting.

The promising biodistribution and imaging results presented here support further preclinical studies in anticipation of an investigational new drug (IND) application to the FDA. Thus, future work includes preclinical therapy experiments using ^{90}Y and/or ^{177}Lu in mouse tumor models. These studies will be performed in collaboration with Memorial Sloan Kettering Cancer Center (MSKCC) and the City of Hope.

Moving forward to clinical trial preparation, all three reagents will require preparation under current good manufacturing practices cGMP conditions. DOTA is already available in cGMP-grade from Macrocyclics. Many contract firms (and the City of Hope) have expertise in producing cGMP-grade antibodies for clinical studies. Because the bsAb used here is produced and purified in a manner identical to that of IgGs, scale-up and cGMP manufacturing should not be an issue. Contract organizations to synthesize cGMP grade compounds such as the dextran clearing agent also exist and this production should prove relatively straightforward. All three compounds will require successful completion of no observed adverse effect level (NOAEL) studies in two species (i.e. rat and dog). We predict no foreseeable issues with the IgG-like bsAb and DOTA compounds. However, high molecular weight iron-dextran compounds used to treat

anemia have been previously associated with a low but serious risk of anaphylaxis (Hayat 2008). If issues arise with the dextran compound, it should be relatively easy to develop a clearing agent with a lower molecular weight dextran or based on a different framework such as an albumin- or IgG-based compound. However, additional experimentation will be required to ensure efficacy.

Affinity maturation of the wild-type 2D12.5 DOTA-binding antibody used selection pressure for improved affinity to yttrium-chelated DOTA. The 2D12.5 antibody exhibits promiscuity in binding and binds to DOTA chelates of a variety of metals with varying affinities. It was not known *a priori* if the selection pressure during affinity maturation would result in clones with high specificity for yttrium-chelated DOTA and lose affinity to other DOTA chelates. The clone C8.2.5 that was selected with the highest measured affinity to yttrium-chelated DOTA also binds the 9-coordinate DOTA chelates of lutetium and gadolinium with similar affinity, a 1000-fold affinity improvement compared to the wild-type and no apparent change in promiscuity. In addition, the high affinity antibody binds 8-coordinate DOTA chelates of indium with nanomolar affinity, a similar three order of magnitude improvement in affinity. Thus, the engineered high-affinity antibody fragment may be used for imaging and therapy applications using a variety of isotopes with different radioactive properties.

^{90}Y, considered a hard beta due to its high energy emissions with maximum particle energy of 2.27 MeV and ~12 mm maximum particle range is currently one of the most widely used isotopes in radioimmunotherapy applications. Its long range in tissue may prove especially useful in treating bulk disease with large necrotic regions and heterogeneous distribution of radioisotope. ^{177}Lu is a soft beta (maximum particle energy of 0.5 MeV) and is especially promising as it was recently shown to exhibit lower off-target effects when compared to ^{90}Y in a radioimmunotherapy study in xenograft mice (Zacchetti et al. 2009) likely due to its shorter particle range (~2 mm maximum range). ^{177}Lu also emits gamma photons allowing imaging by SPECT. While ^{90}Y, a pure beta emitter, cannot be used for imaging, ^{86}Y can be used for PET imaging prior to or at the same time as ^{90}Y therapy. ^{111}In can also be used for imaging (SPECT) and has been used clinically for personalized dosimetry for ^{90}Y radioimmunotherapy (Fisher et al. 2009).

However, the weaker affinity of the ^{111}In-DOTA chelate for the bsAb will result in different biodistribution and thus dosimetry for ^{90}Y therapy is likely best performed using ^{86}Y PET.

There is also a very high likelihood that the PRIT system will be compatible with ^{225}Ac, a combined alpha and beta emitter (McDevitt et al. 2001). Nonradioactive actinium is not available, preventing confirmation of its compatibility thus far.

In addition to compatibility with a variety of radioisotopes, a second aspect of system modularity comes from the simple attachment of the DOTA-binding scFv to any IgG, allowing the approach to be used with any validated cancer-specific antibody. Indeed, we have already developed bispecific antibodies that target A33, a validated colon cancer antigen, and CD20, an antigen that is currently targeted by several FDA-approved antibodies for the treatment of Non-Hodgkin's lymphoma. Results from preliminary PRIT studies targeting A33 are very promising (see appendix 7.3.2) and demonstrate the versatility of our system.

Because the affinity maturation resulted in an antibody fragment with differing affinities for different DOTA chelates, we inadvertently developed an excellent system for the study of the affect of affinity of small molecules on tumor targeting *in vivo*. By using two different isotopes, ^{177}Lu and ^{111}In, and two different DOTA chelates, DOTA and DOTA-aminobenzene, we were able to analyze the affect of affinity over three orders of magnitude in a systematic fashion *in vivo* in tumor-bearing mice. This type of systematic study of the affect of affinity on small molecule tumor uptake *in vivo* has not been possible previously and we were thus able to fundamentally explore the affect of affinity on small molecule uptake for a constant B_{max} of approximately 10^5 binding sites per cell. We show here that improving affinity from single digit nanomolar to ~100 pM results in a 3-fold higher tumor to kidney ratio and a 4-fold higher tumor to blood ratio at 24 hours post injection. However, additional affinity improvement to ~10 pM results in no further increase in tumor uptake and lower tumor to background ratios due to higher binding and retention in non-tumor tissue to residual bsAb. It is important to note that

tumor uptake will be a function of both affinity and B_{max}, with lower numbers of binding sites requiring higher affinity to achieve the same tumor uptake.

As mentioned above, the PRIT system developed here can be used to target any surface receptor. Thus, an important question is which surface receptor(s) to target. A good target has 3 properties: 1) specific expression on malignant cells with little to no expression on normal cells, 2) a relatively slow internalization rate, and 3) high surface density. Most clinically validated cancer antigens (i.e. EGFR and HER2) are ubiquitous surface receptors expressed on normal cells and overexpressed on cancer cells. These are generally not good targets for PRIT. However, antibodies that bind to particular malignant-specific epitopes of ubiquitous receptors have been identified (Garrett et al. 2009). Other cancer antigens (i.e. CD20, A33, PSMA) are specific to particular tissues and may be useful targets if the tissue is expendable. One target that appears to be very specific to tumor cells is human aspartyl (asparaginyl) beta-hydroxylase (HAAH), as it is normally expressed intraceullarly but translocated to the cell surface in malignant cells (Lavaissiere et al. 1996; Ince et al. 2000). In addition, HAAH appears to be expressed on a large variety of tumor types and was detected in 99% of 1000 tumor specimens (Yeung 2005). Unfortunately, anti-HAAH antibodies exhibits a very fast internalization rate (Yeung et al. 2007) such that administered bsAb would be rapidly internalized and subsequently inaccessible to hapten binding. The number of hapten capture sites available at the time of hapten dosing is directly related to the antigen surface density and internalization rate. A relatively high surface density ($> 10^4$ per cell) and a slow internalization rate (~15 hour half-life or longer) are ideal.

One could imagine a tumor targeting approach that would yield the tumor-to-background ratios reported here but with a single step. A small molecule with high affinity for tumor antigen and rapid whole-body clearance would be necessary to achieve a one-step approach and would result in a much simpler and significantly more inexpensive therapy. Unfortunately, small molecule ligands developed to date for tumor targeting generally result in very high background retention (Table 4.1). In addition, most small molecules exhibit significantly lower affinities than antibodies and other protein scaffolds, due in part to a smaller surface area from which to derive necessary binding

contacts. To develop improved tumor-specific small molecules, one needs to focus on both reducing background in non-tumor tissue and improving affinity. A more fundamental and mechanistic understanding of the chemical properties that result in nonspecific binding and whole-body retention of small molecules and peptides is needed. Small molecules with high affinity for tumor antigens may be identified with technological improvements in small molecule library design combined with enhanced screening, selection, and the use of focused libraries. Affinity may be improved for identified compounds by using multivalent structures to improve affinity through avidity (Mammen et al. 1998; Misra et al. 2007; Humblet et al. 2009).

This thesis is evidence that mathematical modeling can be used to guide experimental efforts in drug development. Many parameters impact tumor targeting (i.e. B_{max}, affinity, vascular permeability, blood clearance, internalization rates) and it is important to understand on a fundamental level these mechanisms, how they can be manipulated, and how they interrelate with one another. For example, improving affinity using multivalent scaffolds has not yet resulted in the expected improvements in tumor uptake *in vivo* (Liu et al. 2009), likely due to a corresponding decrease in the vascular permeability of the molecule. Mathematical modeling needs to be incorporated into drug discovery and development in order to decrease experimentation by "trial and error" and to improve understanding when results are not as expected. A systematic method of mathematically motivated prediction followed by experimental validation should aid in developing rational, strategized approaches as well as highlight areas where mechanistic understanding is lacking.

7. APPENDIX

7.1. Mathematical Modeling

7.1.1. Micrometastasis Model

For micrometastases, the model equations were modified from Graff et al. (Graff and Wittrup 2003) to include a hapten species (Hap), a bound antibody/hapten complex (B_C), a free antibody/hapten complex (C), and an internalized hapten (HapI) in addition to the antibody (Ab), antigen (Ag), and bound antibody (B) species.

$$\frac{\partial[Ab]}{\partial t} = D_{Ab}\frac{1}{r^2}\frac{\partial}{\partial r}\left(r^2\frac{\partial[Ab]}{\partial r}\right) - \frac{k_{on\_Ab}}{\varepsilon_{Ab}}[Ab]\cdot[Ag] + k_{off\_Ab}[B] - \frac{k_{on\_Hap}}{\varepsilon_{Hap}}[Ab]\cdot[Hap] + k_{off\_Hap}[C]$$

$$\frac{\partial[Ag]}{\partial t} = R_{syn} - \frac{k_{on\_Ab}}{\varepsilon_{Ab}}[Ab]\cdot[Ag] + k_{off\_Ab}[B] - \frac{k_{on\_Ab}}{\varepsilon_{Ab}}[Ag]\cdot[C] + k_{off\_Ab}[B_C] - k_e[Ag]$$

$$\frac{\partial[B]}{\partial t} = \frac{k_{on\_Ab}}{\varepsilon_{Ab}}[Ab]\cdot[Ag] - k_{off\_Ab}[B] - \frac{k_{on\_Hap}}{\varepsilon_{Hap}}[B]\cdot[Hap] + k_{off\_Hap}[B_C] - k_e[B]$$

$$\frac{\partial[Hap]}{\partial t} = D_{Hap}\frac{1}{r^2}\frac{\partial}{\partial r}\left(r^2\frac{\partial[Hap]}{\partial r}\right) - \frac{k_{on\_Hap}}{\varepsilon_{Hap}}[Ab]\cdot[Hap] + k_{off\_Hap}[C] - \frac{k_{on\_Hap}}{\varepsilon_{Hap}}[B]\cdot[Hap] + k_{off\_Hap}[B_C]$$

$$\frac{\partial[B_C]}{\partial t} = \frac{k_{on\_Hap}}{\varepsilon_{Hap}}[B]\cdot[Hap] - k_{off\_Hap}[B_C] + \frac{k_{on\_Ab}}{\varepsilon_{Ab}}[Ag]\cdot[C] - k_{off\_Ab}[B_C] - k_e[B_C]$$

$$\frac{\partial[C]}{\partial t} = D_{Ab}\frac{1}{r^2}\frac{\partial}{\partial r}\left(r^2\frac{\partial[C]}{\partial r}\right) + \frac{k_{on\_Hap}}{\varepsilon_{Hap}}[Ab]\cdot[Hap] - k_{off\_Hap}[C] - \frac{k_{on\_Ab}}{\varepsilon_{Ab}}[Ag]\cdot[C] + k_{off\_Ab}[B_C]$$

$$\frac{\partial[HapI]}{\partial t} = k_e[B_C] - k_r[HapI]$$

D_{Ab} and D_{Hap} are the antibody and hapten diffusion constants, r is the radius, k_{on_Ab} and k_{off_Ab} are the association and dissociation rate constants for antibody binding to antigen, k_{on_Hap} and k_{off_Hap} are the association and dissociation rate constants for the antibody binding to hapten, k_e is the internalization rate constant for the antigen, R_{syn} is the synthesis rate of free antigen, and ε_{Ab} and ε_{Hap} are the void fractions for antibody and hapten.

The symmetry boundary condition for the unbound antibody (Ab) is the same at that in Graff et al. and also applies to the hapten (Hap) and free antibody/hapten complex (C).

$$\frac{\partial[Ab]}{\partial r}(0) = 0$$
$$\frac{\partial[Hap]}{\partial r}(0) = 0$$
$$\frac{\partial[C]}{\partial r}(0) = 0$$

The boundary condition for antibody at the edge of the sphere is the same as that in Thurber et al. (Thurber et al. 2007) and also applies to the hapten. The model equations for biexponential plasma concentrations are:

$$[Ab]_{plasma}(t) = [Ab]_{plasma,0}\left(A_{Ab}e^{-k_{1,Ab}t} + B_{Ab}e^{-k_{2,Ab}t}\right)$$
$$[Hap]_{plasma}(t) = [Hap]_{plasma,0}\left(A_{Hap}e^{-k_{1,Hap}t} + B_{Hap}e^{-k_{2,Hap}t}\right)$$

where $[Ab]_{plasma}$ and $[Hap]_{plasma}$ are the initial plasma concentrations of antibody and hapten, respectively, A_{Ab} and B_{Ab} are the fraction of alpha and beta antibody clearance, A_{Hap} and B_{Hap} are the fraction of alpha and beta hapten clearance, $k_{1,Ab}$ and $k_{2,Ab}$ are the antibody alpha and beta phase clearance rate constants, and $k_{1,Hap}$ and $k_{2,Hap}$ are the hapten alpha and beta phase clearance rate constants. The model equations for the normal tissue are:

$$\frac{d[Ab]_n}{dt} = \kappa[Ab]_{plasma}(t) - \lambda[Ab]_n(t)$$
$$\frac{d[Hap]_n}{dt} = \kappa[Hap]_{plasma}(t) - \lambda[Hap]_n(t)$$

where κ is the normal capillary transport rate, λ is the normal lymphatic clearance rate, and $[Ab]_n$ and $[Hap]_n$ are the interstitial normal tissue concentrations of antibody and hapten. κ and λ were calculated assuming two compartment pharmacokinetics.

$$\kappa = \frac{AB(k_2 - k_1)^2}{(A+B)(Ak_2 + Bk_1)}\frac{V_T}{V_P}$$
$$\lambda = \frac{Ak_2 + Bk_1}{A+B}$$

where V_T is the volume of the interstitial fluid compartment and V_P is the plasma volume. The initial conditions are $[Ab]_n(0) = 0$ and $[Hap]_n(0) = 0$. The boundary conditions are:

$$[Ab]_{r=R_{metastases}} = \varepsilon_{Ab} \cdot [Ab]_n$$
$$[Hap]_{r=R_{metastases}} = \varepsilon_{Hap} \cdot [Hap]_n$$

where ε_{Ab} and ε_{Hap} are the void fractions for the antibody and the hapten. Here, we assume that the concentration of free antibody/hapten complex in the well mixed normal tissue is zero.

$$[C]_{r=R_{metastases}} = 0$$

7.1.2. Vascularized Tumor Model

For the vascularized tumor model, the cylindrical geometry model equations were modified from Thurber et al. (Thurber et al. 2007):

$$\frac{\partial[Ab]}{\partial t} = D_{Ab}\frac{1}{r}\frac{\partial}{\partial r}\left(r\frac{\partial[Ab]}{\partial r}\right) - \frac{k_{on\_Ab}}{\varepsilon_{Ab}}[Ab]\cdot[Ag] + k_{off\_Ab}[B] - \frac{k_{on\_Hap}}{\varepsilon_{Hap}}[Ab]\cdot[Hap] + k_{off\_Hap}[C]$$

$$\frac{\partial[Ag]}{\partial t} = R_{syn} - \frac{k_{on\_Ab}}{\varepsilon_{Ab}}[Ab]\cdot[Ag] + k_{off\_Ab}[B] - \frac{k_{on\_Ab}}{\varepsilon_{Ab}}[Ag]\cdot[C] + k_{off\_Ab}[B_C] - k_e[Ag]$$

$$\frac{\partial[B]}{\partial t} = \frac{k_{on\_Ab}}{\varepsilon_{Ab}}[Ab]\cdot[Ag] - k_{off\_Ab}[B] - \frac{k_{on\_Hap}}{\varepsilon_{Hap}}[B]\cdot[Hap] + k_{off\_Hap}[B_C] - k_e[B]$$

$$\frac{\partial[Hap]}{\partial t} = D_{Hap}\frac{1}{r}\frac{\partial}{\partial r}\left(r\frac{\partial[Hap]}{\partial r}\right) - \frac{k_{on\_Hap}}{\varepsilon_{Hap}}[Ab]\cdot[Hap] + k_{off\_Hap}[C] - \frac{k_{on\_Hap}}{\varepsilon_{Hap}}[B]\cdot[Hap] + k_{off\_Hap}[B_C]$$

$$\frac{\partial[B_C]}{\partial t} = \frac{k_{on\_Hap}}{\varepsilon_{Hap}}[B]\cdot[Hap] - k_{off\_Hap}[B_C] + \frac{k_{on\_Ab}}{\varepsilon_{Ab}}[Ag]\cdot[C] - k_{off\_Ab}[B_C] - k_e[B_C]$$

$$\frac{\partial[C]}{\partial t} = D_{Ab}\frac{1}{r}\frac{\partial}{\partial r}\left(r\frac{\partial[C]}{\partial r}\right) + \frac{k_{on\_Hap}}{\varepsilon_{Hap}}[Ab]\cdot[Hap] - k_{off\_Hap}[C] - \frac{k_{on\_Ab}}{\varepsilon_{Ab}}[Ag]\cdot[C] + k_{off\_Ab}[B_C]$$

$$\frac{\partial[HapI]}{\partial t} = k_e[B_C] - k_r[HapI]$$

The boundary conditions for the free antibody are the same as that in Thurber et al. and are similarly applied to the hapten and free antibody/hapten complex. We assume that the concentration of free antibody/hapten complex in the plasma is zero. The boundary conditions at the outer edge of the cylinder are:

$$\frac{\partial[Ab]}{\partial r}(R_{tumor}) = 0$$
$$\frac{\partial[Hap]}{\partial r}(R_{tumor}) = 0$$
$$\frac{\partial[C]}{\partial r}(R_{tumor}) = 0$$

The boundary conditions at the inside edge of the cylinder are:

$$-\frac{D_{Ab}}{P_{Ab}}\left(\frac{d[Ab]}{dr}\right)\Bigg|_{r=R_{cap}} = [Ab]_{plasma} - \frac{[Ab]\big|_{r=R_{capillary}}}{\varepsilon_{Ab}}$$
$$-\frac{D_{Hap}}{P_{Hap}}\left(\frac{d[Hap]}{dr}\right)\Bigg|_{r=R_{cap}} = [Hap]_{plasma} - \frac{[Hap]\big|_{r=R_{capillary}}}{\varepsilon_{Hap}}$$
$$-\frac{D_{Ab}}{P_{Ab}}\left(\frac{d[C]}{dr}\right)\Bigg|_{r=R_{cap}} = -\frac{[C]\big|_{r=R_{capillary}}}{\varepsilon_{Ab}}$$

7.1.3. Model Equations for Activity

The total activity in the tumor as a function of time was calculated.

$$A(t) = \frac{A_0}{[Hap]_{plasma,0} \cdot V_p} e^{-\lambda_r t} Hap_{tot}(t) V_{tumor}$$

where A is the activity (MBq), A_0 is the initial activity (MBq), λ_r is the decay rate of the radionuclide, $Hap_{tot}(t)$ is the total hapten concentration in the tumor (Hap + B_C + C + HapI), and V_{tumor} is the volume of the tumor.

The cumulative activity in the tumor is therefore:

$$A_{cumulative} = \int_0^{\infty} A(t)dt$$

where $A_{cumulative}$ has units MBq·s.

7.1.4. Definition of Symbols and Model Parameters Used in Simulations

Table 7.1 Symbols and model parameters

Parameter	Definition	Value	Reference
$[Ab]_n$	Antibody concentration in normal tissue		
$[Ab]_{plasma}$	Antibody concentration in plasma		
$[Ab]_{plasma,0}$	Initial antibody concentration in plasma	2 μM	
[Ag]	Antigen concentration per total tumor volume		
$[Ag]_0$	Initial antigen concentration per total tumor volume	3×10^{-7} M	(Thurber et al. 2007; Thurber and Wittrup 2008)
[B]	Bound antibody-antigen complex concentration per total tumor volume		
$[B_C]$	Bound antigen-antibody-hapten complex concentration per total tumor volume		
[C]	Free antibody-hapten complex concentration per total tumor volume		
[Hap]	Free hapten concentration per total tumor volume		
$[Hap]_n$	Hapten concentration in normal tissue		
$[Hap]_{plasma}$	Hapten concentration in plasma		
$[Hap]_{plasma,0}$	Initial hapten concentration in plasma	100 nM	
[HapI]	Internalized hapten concentration per total tumor volume		
A	Tumor activity		
A_0	Initial hapten activity	5 GBq	
A_{Ab}	Antibody fraction (0-1) of alpha phase clearance	.43	(Thurber et al. 2007)
Ab	Free antibody concentration		
$A_{cumulative}$	Cumulative tumor activity		
A_{Hap}	Hapten fraction (0-1) of alpha phase clearance	.55	(Le Mignon et al. 1990)
D_{Ab}	Effective antibody diffusion coefficient	14×10^{-12} m^2/s	(Thurber et al. 2007)
D_{Hap}	Effective hapten diffusion coefficient	3×10^{-9} m^2/s	(Tofts 1997)
Hap_{tot}	Total hapten concentration per total tumor volume		
$k_{1,Ab}$	Antibody alpha phase clearance rate constant	1.5×10^{-5} s^{-1}	(Thurber et al. 2007)
$k_{1,Hap}$	Hapten alpha phase clearance rate constant	1.6×10^{-3} s^{-1}	(Le Mignon et al. 1990)
$k_{2,Ab}$	Antibody beta phase clearance rate constant	2.2×10^{-6} s^{-1}	(Thurber et al. 2007)
$k_{2,Hap}$	Hapten beta phase clearance rate	1.3×10^{-4} s^{-1}	(Le Mignon et al.

	constant		1990)
k_e	Endocytosis rate constant	1.3×10^{-5} s^{-1}	(Schmidt et al. 2008)
$k_{off,Ab}$	Antibody dissociation rate constant	.00001 s^{-1}	
$k_{off,Hap}$	Hapten dissociation rate constant	varies	
$k_{on,Ab}$	Antibody binding rate constant	10^5 $M^{-1}s^{-1}$	
$k_{on,Hap}$	Hapten binding rate constant	5×10^6 $M^{-1}s^{-1}$	
k_r	Residualizing rate constant	1.6×10^{-6} s^{-1}	(Shih et al. 1994)
P_{Ab}	Antibody capillary permeability	3×10^{-9} m/s	(Thurber et al. 2007)
P_{Hap}*	Hapten capillary permeability	1×10^{-7} m/s	(Daldrup et al. 1998)
r	radius		
R_{cap}	Capillary radius	10 μm	(Thurber et al. 2007)
$R_{metastases}$	Radius of micrometastasis	200 μm	
R_{syn}	Synthesis rate of antigen		
R_{tumor}	Radius of cylinder for vascularized tumor	50 μm	(Baish et al. 1996)
t	time		
V_P†	Plasma volume	3.5 liters	(Yang et al. 1978)
V_T	Interstitial fluid volume	12.5 liters	(Gauer et al. 1970)
$V_{tumor, vasc}$	Vascularized tumor volume	1 g	
ε_{Ab}	Antibody effective void fraction	.1	(Thurber et al. 2007)
ε_{Hap}	Hapten effective void fraction	.15 (metastasis), .38 (vascular)	(Bogin et al. 2002)
κ	Normal capillary transport rate		
λ	Normal lymphatic clearance rate		
λ_r (^{90}Y)	Decay rate constant	3×10^{-6} s^{-1}	(Snyder et al. 1975)

* It is assumed that the tumor capillary surface to volume ratio (S/V) is 200 cm^{-1} (Hilmas and Gillette 1974) and $P = K^{PS}/(S/V)$ where K^{PS} is the endothelial transfer coefficient

†For a 70 kg man

7.2. DNA Sequences for Gwiz Plasmids

7.2.1. Color Coded Legend

Pst1
Stop codons
Cmyc epitope tag
Variable light domain
Variable heavy domain
(Gly$_4$Ser) linker
Cκ
CH1-CH3
FLAG epitope tag
Leader Sequence
scFv fusion
Sal1

The DNA sequence for the Sm3e/C825 light chain plasmid is provided in section 7.2.2 and includes the sequence for the entire plasmid. For all other plasmids, only the DNA sequence of the insert is provided. All inserts reside between the Pst1 and Sal1 restriction sites in the gwiz plasmid. Key restriction enzyme sites within the insert are underlined.

7.2.2. Gwiz Plasmid with Sm3e/C825 Light Chain

TCGCGCGTTTCGGTGATGACGGTGAAAACCTCTGACACATGCAGCTCCCGGAGACGGTCACAG
CTTGTCTGTAAGCGGATGCCGGGAGCAGACAAGCCCGTCAGGGCGCGTCAGCGGGTGTTGGC
GGGTGTCGGGGCTGGCTTAACTATGCGGCATCAGAGCAGATTGTACTGAGAGTGCACCATATG
CGGTGTGAAATACCGCACAGATGCGTAAGGAGAAAATACCGCATCAGATTGGCTATTGGCCA
TTGCATACGTTGTATCCATATCATAATATGTACATTTATATTGGCTCATGTCCAACATTACCGC
CATGTTGACATTGATTATTGACTAGTTATTAATAGTAATCAATTACGGGGTCATTAGTTCATAG
CCCATATATGGAGTTCCGCGTTACATAACTTACGGTAAATGGCCCGCCTGGCTGACCGCCCAA
CGACCCCCGCCCATTGACGTCAATAATGACGTATGTTCCCATAGTAACGCCAATAGGGACTTT
CCATTGACGTCAATGGGTGGAGTATTTACGGTAAACTGCCCACTTGGCAGTACATCAAGTGTA
TCATATGCCAAGTACGCCCCCTATTGACGTCAATGACGGTAAATGGCCCGCCTGGCATTATGC
CCAGTACATGACCTTATGGGACTTTCCTACTTGGCAGTACATCTACGTATTAGTCATCGCTATT
ACCATGGTGATGCGGTTTTGGCAGTACATCAATGGGCGTGGATAGCGGTTTGACTCACGGGGA
TTTCCAAGTCTCCACCCCATTGACGTCAATGGGAGTTTGTTTTGGCACCAAAATCAACGGGAC
TTTCCAAAATGTCGTAACAACTCCGCCCCATTGACGCAAATGGGCGGTAGGCGTGTACGGTGG
GAGGTCTATATAAGCAGAGCTCGTTTAGTGAACCGTCAGATCGCCTGGAGACGCCATCCACGC
TGTTTTGACCTCCATAGAAGACACCGGGACCGATCCAGCCTCCGCGGCCGGGAACGGTGCATT
GGAACGCGGATTCCCCGTGCCAAGAGTGACGTAAGTACCGCCTATAGACTCTATAGGCACAC
CCCTTTGGCTCTTATGCATGCTATACTGTTTTTGGCTTGGGGCCTATACACCCCCGCTTCCTTAT
GCTATAGGTGATGGTATAGCTTAGCCTATAGGTGTGGGTTATTGACCATTATTGACCACTCCCC
TATTGGTGACGATACTTTCCATTACTAATCCATAACATGGCTCTTTGCCACAACTATCTCTATT

GGCTATATGCCAATACTCTGTCCTTCAGAGACTGACACGGACTCTGTATTTTTACAGGATGGG
GTCCCATTTATTATTTACAAATTCACATATACAACAACGCCGTCCCCCGTGCCCGCAGTTTTTA
TTAAACATAGCGTGGGATCTCCACGCGAATCTCGGGTACGTGTTCCGGACATGGGCTCTTCTC
CGGTAGCGGCGGAGCTTCCACATCCGAGCCCTGGTCCCATGCCTCCAGCGGCTCATGGTCGCT
CGGCAGCTCCTTGCTCCTAACAGTGGAGGCCAGACTTAGGCACAGCACAATGCCCACCACCAC
CAGTGTGCCGCACAAGGCCGTGGCGGTAGGGTATGTGTCTGAAAATGAGCGTGGAGATTGGG
CTCGCACGGCTGACGCAGATGGAAGACTTAAGGCAGCGGCAGAAGAAGATGCAGGCAGCTG
AGTTGTTGTATTCTGATAAGAGTCAGAGGTAACTCCCGTTGCGGTGCTGTTAACGGTGGAGGG
CAGTGTAGTCTGAGCAGTACTCGTTGCTGCCGCGCGCGCCACCAGACATAATAGCTGACAGAC
TAACAGACTGTTCCTTTCCATGGGTCTTTTCTGCAGATGAGGGTCCCCGCTCAGCTCCTGGGGC
TCCTGCTGCTCTGGCTCCCAGGTGCACGATGTCTCTTTGACTACAAGGACGACGATGACAAGC
CTAGGGAAAATGTGCTGACCCAATCTCCAAGCTCCATGTCTGTTTCTGTTGGCGATAGAGTAA
CCATCGCTTGTAGCGCATCCTCTAGTGTCCCATATATGCACTGGCTTCAACAGAAGCCAGGTA
AAAGCCCAAAGTTGTTGATTTATTTGACATCCAACTTGGCTTCTGGAGTGCCTTCAAGGTTTTC
TGGTTCCGGCTCAGGAACCGATTATAGTTTGACTATTAGCTCAGTGCAGCCAGAGGATGCTGC
AACCTACTATTGCCAGCAAAGGTCCTCATATCCACTGACTTTCGGGGGTGGAACGAAGTTGGA
AATCAAGCGTACGGTGGCTGCACCATCTGTCTTCATCTTCCCGCCATCTGATGAGCAGTTGAA
ATCTGGAACTGCCTCTGTTGTGTGCCTGCTGAATAACTTCTATCCCAGAGAGGCCAAAGTACA
GTGGAAGGTGGATAACGCCCTCCAATCGGGTAACTCCCAGGAGAGTGTCACAGAGCAGGACA
GCAAGGACAGCACCTACAGCCTCAGCAGCACCCTGACGCTGAGCAAAGCAGACTACGAGAAA
CACAAAGTCTACGCCTGCGAAGTCACCCATCAGGGCCTGAGCTCGCCCGTCACAAAGAGCTTC
AACAGGGGAGAGTGTACGCGTGGAGGTGGCGGTAGTGGCGGAGGTGGTTCTGCTAGCCACGT
TAAGTTGCAAGAATCTGGTCCAGGTTTGGTTCAGCCATCTCAATCTTTGTCTCTTACTTGTACT
GTTTCTGGTTTCTCTTTGACTGATTATGGTGTTCATTGGGTTAGACAATCTCCAGGTAAAGGTT
TGGAATGGTTGGGTGTTATTTGGTCTGGTGGAGGTACTGCTTATAATACTGCTTTGATTTCTAG
ATTGAATATTTATAGAGATAATTCTAAAAATCAAGTTTTTCTTGAAATGAATTCTTTGCAAGCT
GAAGATACTGCTATGTATTATTGTGCTAGAAGAGGTTCTTATCCATATAATTATTTTGATGCTT
GGGGTTGTGGTACTACTGTTACTGTTTCTTCTGGAGGCGGCGGATCTGGCGGTGGAGGTTCTG
GCGGCGGCGGATCTCAAGCTGTTGTTATTCAAGAATCTGCTTTGACTACTCCTCCAGGTGAAA
CCGTTACTTTGACTTGTGGATCTTCTACTGGTGCTGTTACTGCTTCTAATTATGCTAATTGGGTT
CAAGAAAAACCAGATCATTGCTTTACTGGTTTGATTGGTGGTCATAATAATAGACCACCAGGT
GTTCCGGCTAGATTTTCTGGTTCTTTGATTGGTGATAAAGCTGCTTTGACTATTGCTGGTACTC
AAACTGAAGATGAAGCTATTTATTTTTGTGCTTTGTGGTATTCTGATCATTGGGTTATTGGTGG
TGGTACTAGATTGACTGTTTTGGGCGGATCAGAACAAAAGCTTATTTCTGAAGAGGACTTGTA
ATAGGTCGACACGTGTGATCAGATATCGCGGCCGCTCTAGACCAGGCGCCTGGATCCAGATCA
CTTCTGGCTAATAAAAGATCAGAGCTCTAGAGATCTGTGTGTTGGTTTTTTGTGGATCTGCTGT
GCCTTCTAGTTGCCAGCCATCTGTTGTTTGCCCCTCCCCCGTGCCTTCCTTGACCCTGGAAGGT
GCCACTCCCACTGTCCTTTCCTAATAAAATGAGGAAATTGCATCGCATTGTCTGAGTAGGTGT
CATTCTATTCTGGGGGGTGGGGTGGGGCAGCACAGCAAGGGGGAGGATTGGGAAGACAATAG
CAGGCATGCTGGGGATGCGGTGGGCTCTATGGGTACCTCTCTCTCTCTCTCTCTCTCTCTCTCT
CTCTCTCTCTCTCGGTACCTCTCTCTCTCTCTCTCTCTCTCTCTCTCTCTCTCTCTCTCGGTACCA
GGTGCTGAAGAATTGACCCGGTTCCTCCTGGGCCAGAAAGAAGCAGGCACATCCCCTTCTCTG
TGACACACCCTGTCCACGCCCCTGGTTCTTAGTTCCAGCCCCACTCATAGGACACTCATAGCTC
AGGAGGGCTCCGCCTTCAATCCCACCCGCTAAAGTACTTGGAGCGGTCTCTCCCTCCCTCATC
AGCCCACCAAACCAAACCTAGCCTCCAAGAGTGGGAAGAAATTAAAGCAAGATAGGCTATTA
AGTGCAGAGGGAGAGAAAATGCCTCCAACATGTGAGGAAGTAATGAGAGAAATCATAGAATT
TCTTCCGCTTCCTCGCTCACTGACTCGCTGCGCTCGGTCGTTCGGCTGCGGCGAGCGGTATCAG
CTCACTCAAAGGCGGTAATACGGTTATCCACAGAATCAGGGGATAACGCAGGAAAGAACATG
TGAGCAAAAGGCCAGCAAAAGGCCAGGAACCGTAAAAAGGCCGCGTTGCTGGCGTTTTTCCA
TAGGCTCCGCCCCCCTGACGAGCATCACAAAAATCGACGCTCAAGTCAGAGGTGGCGAAACC
CGACAGGACTATAAAGATACCAGGCGTTTCCCCCTGGAAGCTCCCTCGTGCGCTCTCCTGTTC
CGACCCTGCCGCTTACCGGATACCTGTCCGCCTTTCTCCCTTCGGGAAGCGTGGCGCTTTCTCA
ATGCTCACGCTGTAGGTATCTCAGTTCGGTGTAGGTCGTTCGCTCCAAGCTGGGCTGTGTGCA
CGAACCCCCCGTTCAGCCCGACCGCTGCGCCTTATCCGGTAACTATCGTCTTGAGTCCAACCC
GGTAAGACACGACTTATCGCCACTGGCAGCAGCCACTGGTAACAGGATTAGCAGAGCGAGGT
ATGTAGGCGGTGCTACAGAGTTCTTGAAGTGGTGGCCTAACTACGGCTACACTAGAAGGACA

GTATTTGGTATCTGCGCTCTGCTGAAGCCAGTTACCTTCGGAAAAAGAGTTGGTAGCTCTTGA
TCCGGCAAACAAACCACCGCTGGTAGCGGTGGTTTTTTTGTTTGCAAGCAGCAGATTACGCGC
AGAAAAAAAGGATCTCAAGAAGATCCTTTGATCTTTTCTACGGGGTCTGACGCTCAGTGGAAC
GAAAACTCACGTTAAGGGATTTTGGTCATGAGATTATCAAAAAGGATCTTCACCTAGATCCTT
TTAAATTAAAAATGAAGTTTTAAATCAATCTAAAGTATATATGAGTAAACTTGGTCTGACAGT
TACCAATGCTTAATCAGTGAGGCACCTATCTCAGCGATCTGTCTATTTCGTTCATCCATAGTTG
CCTGACTCCGGGGGGGGGGGGCGCTGAGGTCTGCCTCGTGAAGAAGGTGTTGCTGACTCATA
CCAGGCCTGAATCGCCCCATCATCCAGCCAGAAAGTGAGGGAGCCACGGTTGATGAGAGCTT
TGTTGTAGGTGGACCAGTTGGTGATTTTGAACTTTTGCTTTGCCACGGAACGGTCTGCGTTGTC
GGGAAGATGCGTGATCTGATCCTTCAACTCAGCAAAAGTTCGATTTATTCAACAAAGCCGCCG
TCCCGTCAAGTCAGCGTAATGCTCTGCCAGTGTTACAACCAATTAACCAATTCTGATTAGAAA
AACTCATCGAGCATCAAATGAAACTGCAATTTATTCATATCAGGATTATCAATACCATATTTTT
GAAAAAGCCGTTTCTGTAATGAAGGAGAAAACTCACCGAGGCAGTTCCATAGGATGGCAAGA
TCCTGGTATCGGTCTGCGATTCCGACTCGTCCAACATCAATACAACCTATTAATTTCCCCTCGT
CAAAAATAAGGTTATCAAGTGAGAAATCACCATGAGTGACGACTGAATCCGGTGAGAATGGC
AAAAGCTTATGCATTTCTTTCCAGACTTGTTCAACAGGCCAGCCATTACGCTCGTCATCAAAAT
CACTCGCATCAACCAAACCGTTATTCATTCGTGATTGCGCCTGAGCGAGACGAAATACGCGAT
CGCTGTTAAAAGGACAATTACAAACAGGAATCGAATGCAACCGGCGCAGGAACACTGCCAGC
GCATCAACAATATTTTCACCTGAATCAGGATATTCTTCTAATACCTGGAATGCTGTTTTCCCGG
GGATCGCAGTGGTGAGTAACCATGCATCATCAGGAGTACGGATAAAATGCTTGATGGTCGGA
AGAGGCATAAATTCCGTCAGCCAGTTTAGTCTGACCATCTCATCTGTAACATCATTGGCAACG
CTACCTTTGCCATGTTTCAGAAACAACTCTGGCGCATCGGGCTTCCCATACAATCGATAGATT
GTCGCACCTGATTGCCCGACATTATCGCGAGCCCATTTATACCCATATAAATCAGCATCCATG
TTGGAATTTAATCGCGGCCTCGAGCAAGACGTTTCCCGTTGAATATGGCTCATAACACCCCTT
GTATTACTGTTTATGTAAGCAGACAGTTTTATTGTTCATGATGATATATTTTTATCTTGTGCAAT
GTAACATCAGAGATTTTGAGACACAACGTGGCTTTCCCCCCCCCCCCATTATTGAAGCATTTAT
CAGGGTTATTGTCTCATGAGCGGATACATATTTGAATGTATTTAGAAAAATAAACAAATAGGG
GTTCCGCGCACATTTCCCCGAAAAGTGCCACCTGACGTCTAAGAAACCATTATTATCATGACA
TTAACCTATAAAAATAGGCGTATCACGAGGCCCTTTCGTC

7.2.3. Sm3e Heavy Chain Insert

CTGCAGATGGGTTGGAGCCTCATCTTGCTCTTCCTTGTCGCTGTTGCTACGACGCGTCAAGTTA
AACTGGAACAGTCCGGTGCTGAAGTTGTCAAACCAGGTGCTTCCGTGAAGTTGTCCTGTAAAG
CCTCTGGTTTTAACATCAAGGATTCGTATATGCATTGGTTGAGACAAGGGCCAGGACAAAGAT
TGGAATGGATTGGCTGGATTGATCCAGAGAATGGTGATACCGAGTACGCTCCTAAATTTCAGG
GAAAGGCTACTTTTACTACCGACACTTCCGCTAATACCGCATACTTGGGCTTATCTTCCTTGAG
ACCAGAGGACACTGCCGTATACTACTGCAACGAAGGGACACCAACTGGTCCTTACTATTTCGA
CTACTGGGGACAAGGTACCTTAGTTACTGTCTCTAGCGCTAGCACCAAGGGCCCATCGGTCTT
CCCCCTGGCACCCTCCTCCAAGAGCACCTCTGGGGGCACAGCGGCCCTGGGCTGCCTGGTCAA
GGACTACTTCCCCGAACCGGTGACGGTGTCGTGGAACTCAGGCGCCCTGACCAGCGGCGTGC
ACACCTTCCCGGCTGTCCTACAGTCCTCAGGACTCTACTCCCTCAGCAGCGTGGTGACCGTGC
CCTCCAGCAGCTTGGGCACCCAGACCTACATCTGCAACGTGAATCACAAGCCCAGCAACACC
AAGGTGGACAAGAAAGTTGAGCCCAAATCTTGTGACAAAACTCACACATGCCCACCGTGCCC
AGCACCTGAACTCCTGGGGGGACCGTCAGTCTTCCTCTTCCCCCCAAAACCCAAGGACACCCT
CATGATCTCCCGGACCCCTGAGGTCACATGCGTGGTGGTGGACGTGAGCCACGAAGACCCTG
AGGTCAAGTTCAACTGGTACGTGGACGGCGTGGAGGTGCATAATGCCAAGACAAAGCCGCGG
GAGGAGCAGTACAACAGCACGTACCGTGTGGTCAGCGTCCTCACCGTCCTGCACCAGGACTG
GCTGAATGGCAAGGAGTACAAGTGCAAGGTCTCCAACAAAGCCCTCCCAGCCCCCATCGAGA
AAACCATCTCCAAAGCCAAAGGGCAGCCCCGAGAACCACAGGTGTACACCCTGCCCCCATCC
CGGGATGAGCTGACCAAGAACCAGGTCAGCCTGACCTGCCTGGTCAAAGGCTTCTATCCCAGC
GACATCGCCGTGGAGTGGGAGAGCAATGGGCAGCCGGAGAACAACTACAAGACCACGCCTCC
CGTGCTGGACTCCGACGGCTCCTTCTTCCTCTACAGCAAGCTCACCGTGGACAAGAGCAGGTG

GCAGCAGGGGAACGTCTTCTCATGCTCCGTGATGCATGAGGCTCTGCACAACCACTACACGCA
GAAGAGCCTCTCCCTGTCTCCGGGTAAATGATAAGTCGAC

7.2.4. A33 Heavy Chain Insert

CTGCAGATGGGTTGGAGCCTCATCTTGCTCTTCCTTGTCGCTGTTGCTACGACGCGTGAGGTGC
AGGTGATGGAGTCTGGGGGAGGCCTGGTCAAGCCTGGGGGGTCCCTGAGACTCTCCTGTGCA
GCCTCTGGAATCGGCTTCAGTCACTATGGCATTAGCTGGGTCCGCCAGGCTCCAGGGAAGGGG
CTGGAGTGGGTCGCCTACATTTATCCTAATTATGGGAGTGTAGACTACGCGAGCAGCGTGAAT
GGCCGATTCACCATCTCCCTCGACAACGCCCAGAACTCACTGTATCTGCAAATGAACAGCCTG
AGAGCCGAGGACACGGCCGTATATTTCTGTGCGAGAGATCGGGGTTATTATTCTGGTAGTAGG
GGGACTCGGTTGGATCTCTGGGGCCAGGGCACCCTGGTCACCGTCTCCTCAGCTAGCACCAAG
GGCCCATCGGTCTTCCCCCTGGCACCCTCCTCCAAGAGCACCTCTGGGGGCACAGCGGCCCTG
GGCTGCCTGGTCAAGGACTACTTCCCCGAACCGGTGACGGTGTCGTGGAACTCAGGCGCCCTG
ACCAGCGGCGTGCACACCTTCCCGGCTGTCCTACAGTCCTCAGGACTCTACTCCCTCAGCAGC
GTGGTGACCGTGCCCTCCAGCAGCTTGGGCACCCAGACCTACATCTGCAACGTGAATCACAAG
CCCAGCAACACCAAGGTGGACAAGAAAGTTGAGCCCAAATCTTGTGACAAAACTCACACATG
CCCACCGTGCCCAGCACCTGAACTCCTGGGGGGACCGTCAGTCTTCCTCTTCCCCCCAAAACC
CAAGGACACCCTCATGATCTCCCGGACCCCTGAGGTCACATGCGTGGTGGTGGACGTGAGCCA
CGAAGACCCTGAGGTCAAGTTCAACTGGTACGTGGACGGCGTGGAGGTGCATAATGCCAAGA
CAAAGCCGCGGGAGGAGCAGTACAACAGCACGTACCGTGTGGTCAGCGTCCTCACCGTCCTG
CACCAGGACTGGCTGAATGGCAAGGAGTACAAGTGCAAGGTCTCCAACAAAGCCCTCCCAGC
CCCCATCGAGAAAACCATCTCCAAAGCCAAAGGGCAGCCCCGAGAACCACAGGTGTACACCC
TGCCCCCATCCCGGGATGAGCTGACCAAGAACCAGGTCAGCCTGACCTGCCTGGTCAAAGGCT
TCTATCCCAGCGACATCGCCGTGGAGTGGGAGAGCAATGGGCAGCCGGAGAACAACTACAAG
ACCACGCCTCCCGTGCTGGACTCCGACGGCTCCTTCTTCCTCTACAGCAAGCTCACCGTGGAC
AAGAGCAGGTGGCAGCAGGGGAACGTCTTCTCATGCTCCGTGATGCATGAGGCTCTGCACAA
CCACTACACGCAGAAGAGCCTCTCCCTGTCTCCGGGTAAATGATAAGTCGAC

7.2.5. A33 Heavy Chain ds1 Insert

CTGCAGATGGGTTGGAGCCTCATCTTGCTCTTCCTTGTCGCTGTTGCTACGACGCGTGAGGTGC
AGGTGATGGAGTCTGGGGGAGGCCTGGTCAAGCCTGGGGGGTCCCTGAGACTCTCCTGTGCA
GCCTCTGGAATCGGCTTCAGTCACTATGGCATTAGCTGGGTCCGCCAGGCTCCAGGGAAGTGT
CTGGAGTGGGTCGCCTACATTTATCCTAATTATGGGAGTGTAGACTACGCGAGCAGCGTGAAT
GGCCGATTCACCATCTCCCTCGACAACGCCCAGAACTCACTGTATCTGCAAATGAACAGCCTG
AGAGCCGAGGACACGGCCGTATATTTCTGTGCGAGAGATCGGGGTTATTATTCTGGTAGTAGG
GGGACTCGGTTGGATCTCTGGGGCCAGGGCACCCTGGTCACCGTCTCCTCAGCTAGCACCAAG
GGCCCATCGGTCTTCCCCCTGGCACCCTCCTCCAAGAGCACCTCTGGGGGCACAGCGGCCCTG
GGCTGCCTGGTCAAGGACTACTTCCCCGAACCGGTGACGGTGTCGTGGAACTCAGGCGCCCTG
ACCAGCGGCGTGCACACCTTCCCGGCTGTCCTACAGTCCTCAGGACTCTACTCCCTCAGCAGC
GTGGTGACCGTGCCCTCCAGCAGCTTGGGCACCCAGACCTACATCTGCAACGTGAATCACAAG
CCCAGCAACACCAAGGTGGACAAGAAAGTTGAGCCCAAATCTTGTGACAAAACTCACACATG
CCCACCGTGCCCAGCACCTGAACTCCTGGGGGGACCGTCAGTCTTCCTCTTCCCCCCAAAACC
CAAGGACACCCTCATGATCTCCCGGACCCCTGAGGTCACATGCGTGGTGGTGGACGTGAGCCA
CGAAGACCCTGAGGTCAAGTTCAACTGGTACGTGGACGGCGTGGAGGTGCATAATGCCAAGA
CAAAGCCGCGGGAGGAGCAGTACAACAGCACGTACCGTGTGGTCAGCGTCCTCACCGTCCTG
CACCAGGACTGGCTGAATGGCAAGGAGTACAAGTGCAAGGTCTCCAACAAAGCCCTCCCAGC
CCCCATCGAGAAAACCATCTCCAAAGCCAAAGGGCAGCCCCGAGAACCACAGGTGTACACCC
TGCCCCCATCCCGGGATGAGCTGACCAAGAACCAGGTCAGCCTGACCTGCCTGGTCAAAGGCT
TCTATCCCAGCGACATCGCCGTGGAGTGGGAGAGCAATGGGCAGCCGGAGAACAACTACAAG

ACCACGCCTCCCGTGCTGGACTCCGACGGCTCCTTCTTCCTCTACAGCAAGCTCACCGTGGAC
AAGAGCAGGTGGCAGCAGGGGAACGTCTTCTCATGCTCCGTGATGCATGAGGCTCTGCACAA
CCACTACACGCAGAAGAGCCTCTCCCTGTCTCCGGGTAAATGATAAGTCGAC

7.2.6. A33 Heavy Chain ds2 Insert

CTGCAGATGGGTTGGAGCCTCATCTTGCTCTTCCTTGTCGCTGTTGCTACGACGCGTGAGGTGC
AGGTGATGGAGTCTGGGGGAGGCCTGGTCAAGCCTGGGGGGTCCCTGAGACTCTCCTGTGCA
GCCTCTGGAATCGGCTTCAGTCACTATGGCATTAGCTGGGTCCGCCAGGCTCCAGGGAAGGGG
CTGGAGTGGGTCGCCTACATTTATCCTAATTATGGGAGTGTAGACTACGCGAGCAGCGTGAAT
GGCCGATTCACCATCTCCCTCGACAACGCCCAGAACTCACTGTATCTGCAAATGAACAGCCTG
AGAGCCGAGGACACGGCCGTATATTTCTGTGCGAGAGATCGGGGTTATTATTCTGGTAGTAGG
GGGACTCGGTTGGATCTCTGGGGCTGTGGCACCCTGGTCACCGTCTCCTCAGCTAGCACCAAG
GGCCCATCGGTCTTCCCCCTGGCACCCTCCTCCAAGAGCACCTCTGGGGGCACAGCGGCCCTG
GGCTGCCTGGTCAAGGACTACTTCCCCGAACCGGTGACGGTGTCGTGGAACTCAGGCGCCCTG
ACCAGCGGCGTGCACACCTTCCCGGCTGTCCTACAGTCCTCAGGACTCTACTCCCTCAGCAGC
GTGGTGACCGTGCCCTCCAGCAGCTTGGGCACCCAGACCTACATCTGCAACGTGAATCACAAG
CCCAGCAACACCAAGGTGGACAAGAAAGTTGAGCCCAAATCTTGTGACAAAACTCACACATG
CCCACCGTGCCCAGCACCTGAACTCCTGGGGGGACCGTCAGTCTTCCTCTTCCCCCCAAAACC
CAAGGACACCCTCATGATCTCCCGGACCCCTGAGGTCACATGCGTGGTGGTGGACGTGAGCCA
CGAAGACCCTGAGGTCAAGTTCAACTGGTACGTGGACGGCGTGGAGGTGCATAATGCCAAGA
CAAAGCCGCGGGAGGAGCAGTACAACAGCACGTACCGTGTGGTCAGCGTCCTCACCGTCCTG
CACCAGGACTGGCTGAATGGCAAGGAGTACAAGTGCAAGGTCTCCAACAAAGCCCTCCCAGC
CCCCATCGAGAAAACCATCTCCAAAGCCAAAGGGCAGCCCCGAGAACCACAGGTGTACACCC
TGCCCCCATCCCGGGATGAGCTGACCAAGAACCAGGTCAGCCTGACCTGCCTGGTCAAAGGCT
TCTATCCCAGCGACATCGCCGTGGAGTGGGAGAGCAATGGGCAGCCGGAGAACAACTACAAG
ACCACGCCTCCCGTGCTGGACTCCGACGGCTCCTTCTTCCTCTACAGCAAGCTCACCGTGGAC
AAGAGCAGGTGGCAGCAGGGGAACGTCTTCTCATGCTCCGTGATGCATGAGGCTCTGCACAA
CCACTACACGCAGAAGAGCCTCTCCCTGTCTCCGGGTAAATGATAAGTCGAC

7.2.7. Sm3e/4M5.3 Light Chain Insert

CTGCAGATGAGGGTCCCCGCTCAGCTCCTGGGGCTCCTGCTGCTCTGGCTCCCAGGTGCAC
GATGTCTCTTTGACTACAAGGACGACGATGACAAGCCTAGGGAAAATGTGCTGACCCAATCTC
CAAGCTCCATGTCTGTTTCTGTTGGCGATAGAGTAACCATCGCTTGTAGCGCATCCTCTAGTGT
CCCATATATGCACTGGCTTCAACAGAAGCCAGGTAAAAGCCCAAAGTTGTTGATTTATTTGAC
ATCCAACTTGGCTTCTGGAGTGCCTTCAAGGTTTTCTGGTTCCGGCTCAGGAACCGATTATAGT
TTGACTATTAGCTCAGTGCAGCCAGAGGATGCTGCAACCTACTATTGCCAGCAAAGGTCCTCA
TATCCACTGACTTTCGGGGGTGGAACGAAGTTGGAAATCAAGCGTACGGTGGCTGCACCATCT
GTCTTCATCTTCCCGCCATCTGATGAGCAGTTGAAATCTGGAACTGCCTCTGTTGTGTGCCTGC
TGAATAACTTCTATCCCAGAGAGGCCAAAGTACAGTGGAAGGTGGATAACGCCCTCCAATCG
GGTAACTCCCAGGAGAGTGTCACAGAGCAGGACAGCAAGGACAGCACCTACAGCCTCAGCAG
CACCCTGACGCTGAGCAAAGCAGACTACGAGAAACACAAAGTCTACGCCTGCGAAGTCACCC
ATCAGGGCCTGAGCTCGCCCGTCACAAAGAGCTTCAACAGGGGAGAGTGTACGCGTGGAGGT
GGCGGTAGTGGCGGAGGTGGTTCTGCTAGCGACGTCGTTATGACTCAAACACCACTATCACTT
CCTGTTAGTCTAGGTGATCAAGCCTCCATCTCTTGCAGATCTAGTCAGAGCCTCGTACACAGT
AATGGAAACACCTATTTACGTTGGTACCTGCAGAAGCCAGGCCAGTgtCCAAAGGTCCTGATCT
ACAAAGTTTCCAACCGAGTTTCTGGGGTCCCAGACAGGTTCAGTGGCAGTGGATCAGGGACA
GATTTCACACTCAAGATCAACAGAGTGGAGGCTGAGGATCTGGGAGTTTATTTCTGCTCTCAA
AGTACACATGTTCCGTGGACGTTCGGTGGAGGCACCAAGCTTGAAATTAAGTCCTCTGCTGAT
GATGCTAAGAAGGATGCTGCTAAGAAGGATGATGCTAAGAAAGATGATGCTAAGAAAGATGG

TGGCGTCAAACTGGATGAGACTGGAGGAGGCTTGGTGCAACCTGGGGGGGCCATGAAACTCT
CCTGTGTTACCTCTGGATTCACTTTTGGTCACTACTGGATGAACTGGGTCCGCCAGTCTCCAGA
GAAAGGACTGGAGTGGGTAGCACAATTTAGAAACAAACCTTATAATTATGAAACATATTATTC
AGATTCTGTGAAAGGCAGATTCACCATCTCAAGAGATGATTCCAAAAGTAGTGTCTATCTGCA
AATGAACAACTTAAGAGTTGAAGACACGGGTATCTATTACTGTACGGGTGCTTCCTATGGTAT
GGAATACTTGGGTtgtGGAACCTCAGTCACCGTCTCCGGATCCGAACAAAAGCTTATTTCTGAA
GAGGACTTGTAATAGGTCGAC

7.2.8. A33/4M5.3 Light Chain Insert

CTGCAGATGAGGGTCCCCGCTCAGCTCCTGGGGCTCCTGCTGCTCTGGCTCCCAGGTGCAC
GATGTCTCTTTGACTACAAGGACGACGATGACAAGCCTAGTAGTGAGCTCCAGATGACCCAGT
CTCCATCCTCCCTGTCTGCATCTGTAGGAGACAGAGTCACCATCACTTGCCTGGCCAGTGAGTT
CCTTTTTAATGGTGTATCCTGGTATCAGCAGAAACCAGGGAAAGTTCCTAAGTTCCTGATCTAT
GGTGCATCCAATTTAGAATCTGGGGTCCCATCTCGGTTCAGTGGCAGTGGATCTGGGACAGAT
TTCACTCTCACCATCAGCAGCCTGCAGCCTGAAGATGTTGCAACTTATTACTGTCTAGGCGGTT
ATAGTGGTAGTAGTGGTTTGACTTTCGGCGGAGGGACCAAGGTGGAGATCAAACGTACGGTG
GCTGCACCATCTGTCTTCATCTTCCCGCCATCTGATGAGCAGTTGAAATCTGGAACTGCCTCTG
TTGTGTGCCTGCTGAATAACTTCTATCCCAGAGAGGCCAAAGTACAGTGGAAGGTGGATAACG
CCCTCCAATCGGGTAACTCCCAGGAGAGTGTCACAGAGCAGGACAGCAAGGACAGCACCTAC
AGCCTCAGCAGCACCCTGACGCTGAGCAAAGCAGACTACGAGAAACACAAAGTCTACGCCTG
CGAAGTCACCCATCAGGGCCTGAGCTCGCCCGTCACAAAGAGCTTCAACAGGGGAGAGTGTA
CGCGTGGAGGTGGCGGTAGTGGCGGAGGTGGTTCTGCTAGCGACGTCGTTATGACTCAAACA
CCACTATCACTTCCTGTTAGTCTAGGTGATCAAGCCTCCATCTCTTGCAGATCTAGTCAGAGCC
TCGTACACAGTAATGGAAACACCTATTTACGTTGGTACCTGCAGAAGCCAGGCCAGTgtCCAA
AGGTCCTGATCTACAAAGTTTCCAACCGAGTTTCTGGGGTCCCAGACAGGTTCAGTGGCAGTG
GATCAGGGACAGATTTCACACTCAAGATCAACAGAGTGGAGGCTGAGGATCTGGGAGTTTAT
TTCTGCTCTCAAAGTACACATGTTCCGTGGACGTTCGGTGGAGGCACCAAGCTTGAAATTAAG
TCCTCTGCTGATGATGCTAAGAAGGATGCTGCTAAGAAGGATGATGCTAAGAAAGATGATGC
TAAGAAAGATGGTGGCGTCAAACTGGATGAGACTGGAGGAGGCTTGGTGCAACCTGGGGGGG
CCATGAAACTCTCCTGTGTTACCTCTGGATTCACTTTTGGTCACTACTGGATGAACTGGGTCCG
CCAGTCTCCAGAGAAAGGACTGGAGTGGGTAGCACAATTTAGAAACAAACCTTATAATTATG
AAACATATTATTCAGATTCTGTGAAAGGCAGATTCACCATCTCAAGAGATGATTCCAAAAGTA
GTGTCTATCTGCAAATGAACAACTTAAGAGTTGAAGACACGGGTATCTATTACTGTACGGGTG
CTTCCTATGGTATGGAATACTTGGGTtgtGGAACCTCAGTCACCGTCTCCGGATCCGAACAAAA
GCTTATTTCTGAAGAGGACTTGTAATAGGTCGAC

7.2.9. A33 IgG + peptide Light Chain Insert

CTGCAGATGAGGGTCCCCGCTCAGCTCCTGGGGCTCCTGCTGCTCTGGCTCCCAGGTGCAC
GATGTCCTAGTAGTGAGCTCCAGATGACCCAGTCTCCATCCTCCCTGTCTGCATCTGTAGGAG
ACAGAGTCACCATCACTTGCCTGGCCAGTGAGTTCCTTTTTAATGGTGTATCCTGGTATCAGCA
GAAACCAGGGAAAGTTCCTAAGTTCCTGATCTATGGTGCATCCAATTTAGAATCTGGGGTCCC
ATCTCGGTTCAGTGGCAGTGGATCTGGGACAGATTTCACTCTCACCATCAGCAGCCTGCAGCC
TGAAGATGTTGCAACTTATTACTGTCTAGGCGGTTATAGTGGTAGTAGTGGTTTGACTTTCGGC
GGAGGGACCAAGGTGGAGATCAAACGTACGGTGGCTGCACCATCTGTCTTCATCTTCCCGCCA
TCTGATGAGCAGTTGAAATCTGGAACTGCCTCTGTTGTGTGCCTGCTGAATAACTTCTATCCCA
GAGAGGCCAAAGTACAGTGGAAGGTGGATAACGCCCTCCAATCGGGTAACTCCCAGGAGAGT
GTCACAGAGCAGGACAGCAAGGACAGCACCTACAGCCTCAGCAGCACCCTGACGCTGAGCAA
AGCAGACTACGAGAAACACAAAGTCTACGCCTGCGAAGTCACCCATCAGGGCCTGAGCTCGC

CCGTCACAAAGAGCTTCAACAGGGGAGAGTGTGGTGGAGGCGGTTCAGGCGGAGGTGGATCT
CTACCAGAAACTGGAGGTTCAGGTTAATAGGTCGAC

7.2.10. A33 IgG + peptide ds1 Light Chain Insert

CTGCAGATGAGGGTCCCCGCTCAGCTCCTGGGGCTCCTGCTGCTCTGGCTCCCAGGTGCAC
GATGTCCTAGTAGTGAGCTCCAGATGACCCAGTCTCCATCCTCCCTGTCTGCATCTGTAGGAG
ACAGAGTCACCATCACTTGCCTGGCCAGTGAGTTCCTTTTTAATGGTGTATCCTGGTATCAGCA
GAAACCAGGGAAAGTTCCTAAGTTCCTGATCTATGGTGCATCCAATTTAGAATCTGGGGTCCC
ATCTCGGTTCAGTGGCAGTGGATCTGGGACAGATTTCACTCTCACCATCAGCAGCCTGCAGCC
TGAAGATGTTGCAACTTATTACTGTCTAGGCGGTTATAGTGGTAGTAGTGGTTTGACTTTCGGC
TGTGGGACCAAGGTGGAGATCAAACGTACGGTGGCTGCACCATCTGTCTTCATCTTCCCGCCA
TCTGATGAGCAGTTGAAATCTGGAACTGCCTCTGTTGTGTGCCTGCTGAATAACTTCTATCCCA
GAGAGGCCAAAGTACAGTGGAAGGTGGATAACGCCCTCCAATCGGGTAACTCCCAGGAGAGT
GTCACAGAGCAGGACAGCAAGGACAGCACCTACAGCCTCAGCAGCACCCTGACGCTGAGCAA
AGCAGACTACGAGAAACACAAAGTCTACGCCTGCGAAGTCACCCATCAGGGCCTGAGCTCGC
CCGTCACAAAGAGCTTCAACAGGGGAGAGTGTGGTGGAGGCGGTTCAGGCGGAGGTGGATCT
CTACCAGAAACTGGAGGTTCAGGTTAATAGGTCGAC

7.2.11. A33 IgG + peptide ds2 Light Chain Insert

CTGCAGATGAGGGTCCCCGCTCAGCTCCTGGGGCTCCTGCTGCTCTGGCTCCCAGGTGCAC
GATGTCCTAGTAGTGAGCTCCAGATGACCCAGTCTCCATCCTCCCTGTCTGCATCTGTAGGAG
ACAGAGTCACCATCACTTGCCTGGCCAGTGAGTTCCTTTTTAATGGTGTATCCTGGTATCAGCA
GAAACCAGGGAAATGTCCTAAGTTCCTGATCTATGGTGCATCCAATTTAGAATCTGGGGTCCC
ATCTCGGTTCAGTGGCAGTGGATCTGGGACAGATTTCACTCTCACCATCAGCAGCCTGCAGCC
TGAAGATGTTGCAACTTATTACTGTCTAGGCGGTTATAGTGGTAGTAGTGGTTTGACTTTCGGC
GGAGGGACCAAGGTGGAGATCAAACGTACGGTGGCTGCACCATCTGTCTTCATCTTCCCGCCA
TCTGATGAGCAGTTGAAATCTGGAACTGCCTCTGTTGTGTGCCTGCTGAATAACTTCTATCCCA
GAGAGGCCAAAGTACAGTGGAAGGTGGATAACGCCCTCCAATCGGGTAACTCCCAGGAGAGT
GTCACAGAGCAGGACAGCAAGGACAGCACCTACAGCCTCAGCAGCACCCTGACGCTGAGCAA
AGCAGACTACGAGAAACACAAAGTCTACGCCTGCGAAGTCACCCATCAGGGCCTGAGCTCGC
CCGTCACAAAGAGCTTCAACAGGGGAGAGTGTGGTGGAGGCGGTTCAGGCGGAGGTGGATCT
CTACCAGAAACTGGAGGTTCAGGTTAATAGGTCGAC

7.3. Additional *In Vivo* Experiments

7.3.1. Pretargeted Experiments with ^{111}In-DOTA-Bn

Initial preliminary pretargeted experiments were performed with ^{111}In-DOTA-Bn, with an affinity of ~ 1 nM to the bsAb (chapter 2). Methods describing animal models are as described in Chapter 5. DOTA-Bn was dissolved at 0.5 mM in ammonium acetate pH 5.6. 1-2 mCi $^{111}InCl_3$ (Cardinal Health, Dublin, OH) were added to the metal chelate and incubated for 1-2 h at 85-95°C. The radiolabeled compounds were purified by RP-HPLC (Humblet et al. 2006; Misra et al. 2007) with gamma detection on a 4.6 x 75 mm Symmetry C18 column using a linear gradient from 0% to 90% B over 15 minutes, at a flow rate of 1 mL/min, where A = water + 0.01% formic acid (FA) and B = acetonitrile + 0.01% FA. The purified compound was injected as is. It was later determined that the formic acid and/or acetonitrile result in high spleen and liver uptake and slow blood clearance, possibly due to microaggregation with serum proteins. Thus, for all experiments presented in chapter 5, HPLC purification of DOTA compounds was performed with no formic acid present and compounds were subsequently dried under vacuum, resuspended in saline, and 0.2 μm filter purified before injection.

Figure 7.1 demonstrates that ^{111}In-DOTA-Bn binds to the Sm3e/C825 bsAb in vivo, resulting in significantly higher activity in almost all organs at 4 h p.i. As expected, blood activity is very high (~9 %ID/g at 4 h p.i.) for pretargeted ^{111}In-DOTA-Bn, due to binding to residual bsAb in the blood. A clearing/blocking step to remove or block residual bsAb at the time of hapten dosing will thus be necessary to improve tumor to background ratios.

We therefore synthesized a 500 kDa dextran-DOTA-Y clearing/blocking agent (see Chapter 5 for methods). This agent, dosed 24 h after bsAb administration and 1 h prior to hapten dosing was effective in reducing essentially all ^{111}In-DOTA-Bn binding to residual bsAb in the blood (Figure 7.2).

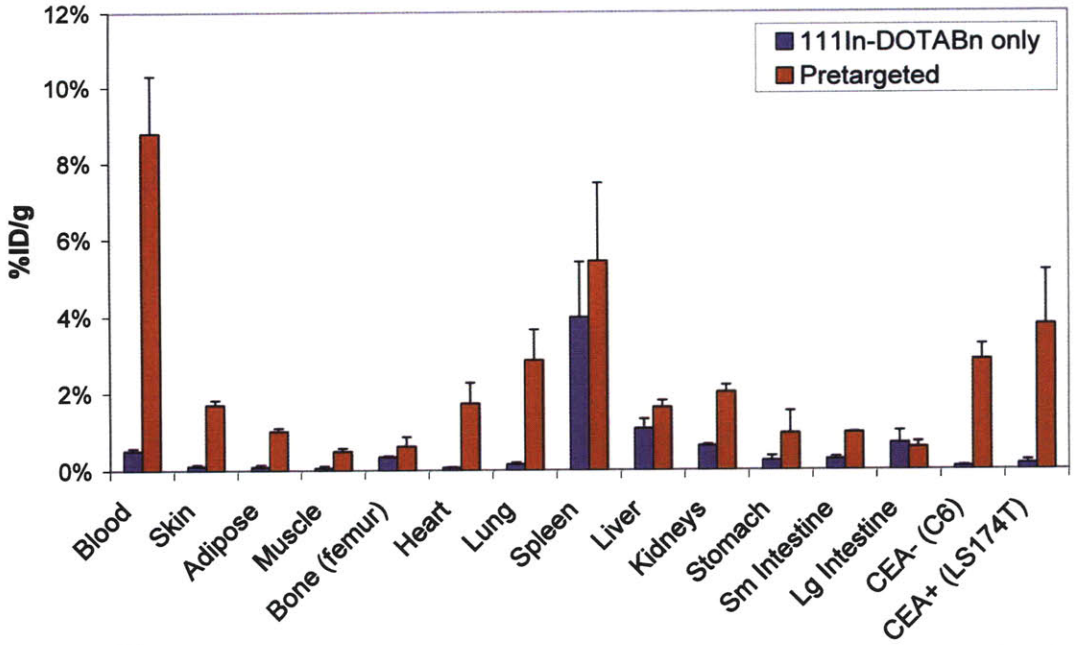

Figure 7.1 ^{111}In-DOTA-Bn Organ/Tissue Biodistribution. Organ/tissue activity (mean + s.d., n=2-3) at 4 h p.i. of ~ 2 pmol ^{111}In-DOTA-Bn only (blue) or ^{111}In-DOTA-Bn pretargeted 24 h earlier with 500 ug Sm3e/C825 bsAb.

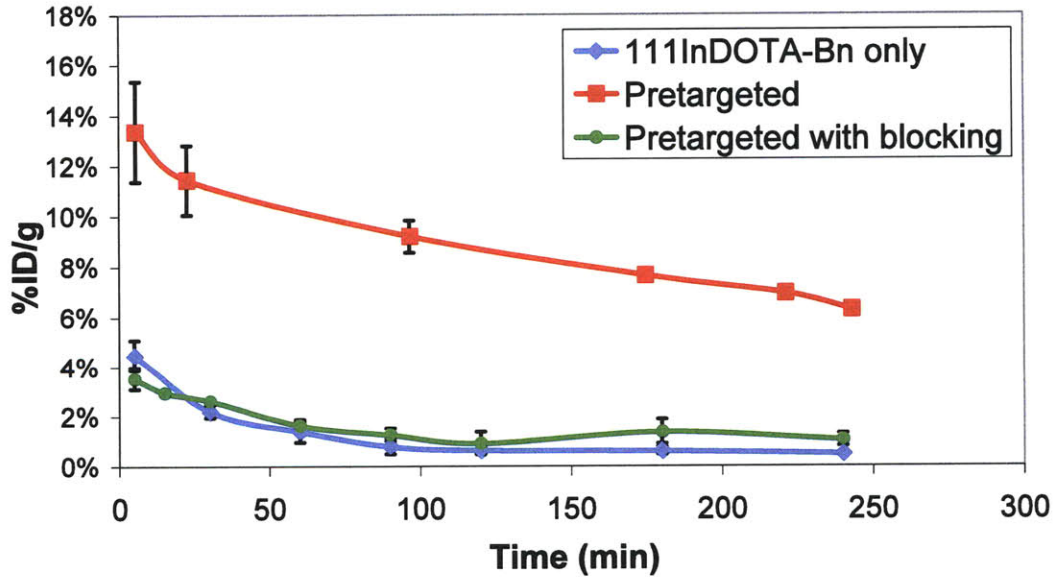

Figure 7.2 ^{111}In-DOTA-Bn Blood Clearance. Blood activity (mean ± s.d., n = 2-3) over time for ~ 2 pmol ^{111}In-DOTA-Bn only (blue), pretargeted 24 h earlier with 500 ug Sm3e/C825 bsAb (red), or pretargeted 25 h earlier with 500 ug bsAb with a blocking step of 18 ug dextran-DOTA-Y 1 h earlier (green).

7.3.2. Results of Pretargeted Experiments Conducted at Memorial Sloan Kettering Cancer Center (MSKCC)

MSKCC has performed preliminary experiments with both the Sm3e/C825 bsAb and an anti-A33 bsAb targeting SW1222 tumors that express both CEA and A33. The anti-A33 bsAb used here is different from that described in chapter 3, as the anti-A33 IgG variable domains are derived from the Ludwig humanized A33 antibody (Scott et al. 2005). The preliminary results presented below demonstrate that the engineered pretargeted radioimmunotherapy system can be used to target multiple antigens. Note that all bsAbs were iodinated prior to injection. The iodination appears to result in significantly faster blood clearance of the bsAb than that observed for ^{111}In-DTPA-labeled bsAb (see results from Chapter 3) and is likely the cause for the lower tumor uptake values.

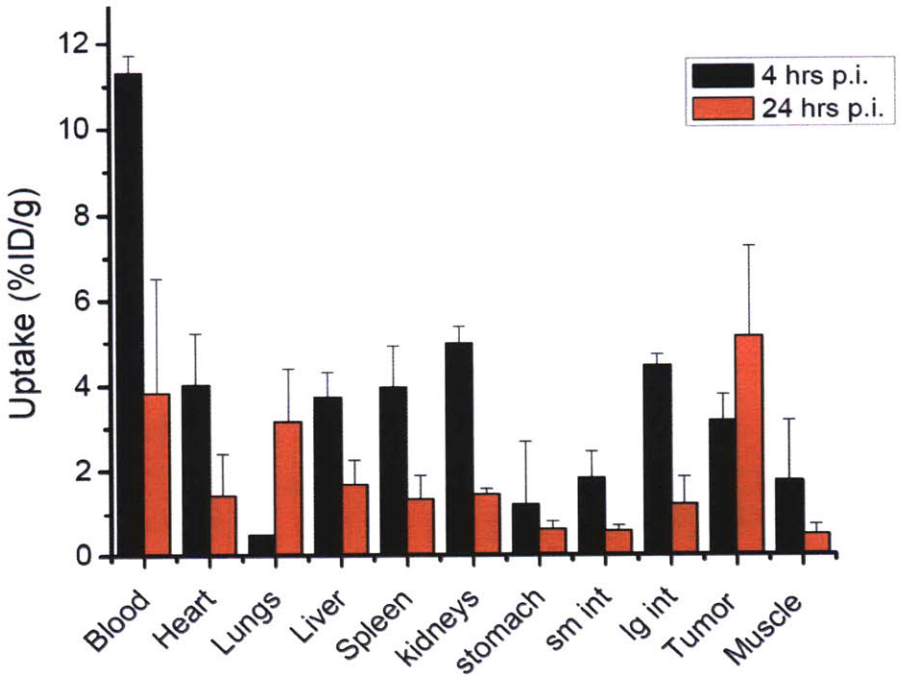

Figure 7.3 ^{131}I-Sm3e/C825 organ/tissue biodistribution at 4 and 24 h. Organ/tissue activity at 4 and 24 h p.i. of 0.02 mg of ^{131}I-Sm3e/C825 bsAb in SW1222 tumor bearing mice.

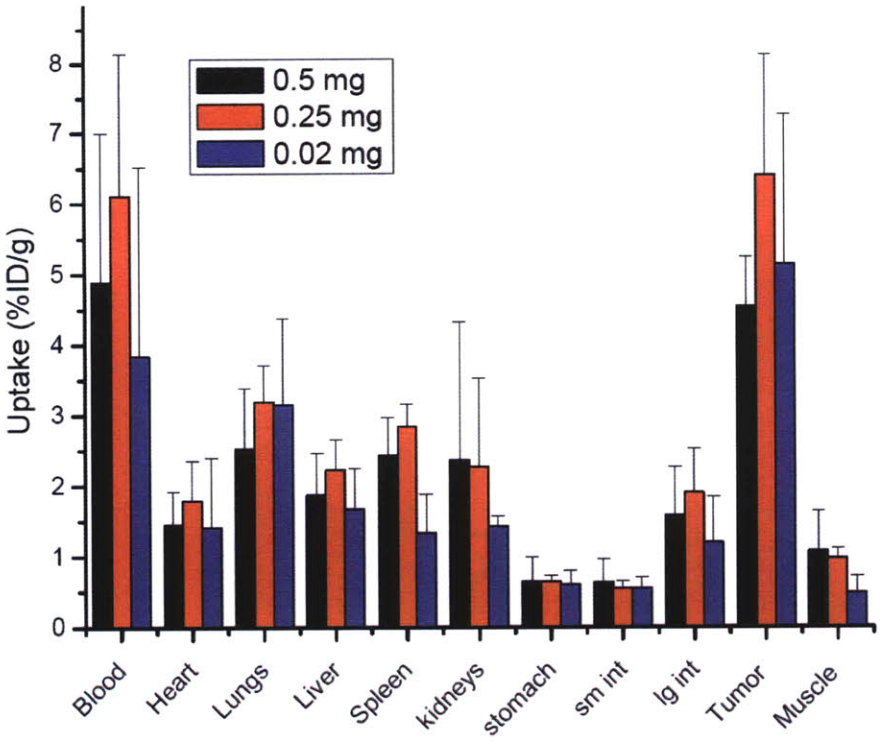

Figure 7.4 ^{131}I-Sm3e/C825 dose response. Organ/tissue activity at 24 h p.i. of various doses of ^{131}I-Sm3e/C825 bsAb in SW1222 tumor bearing mice.

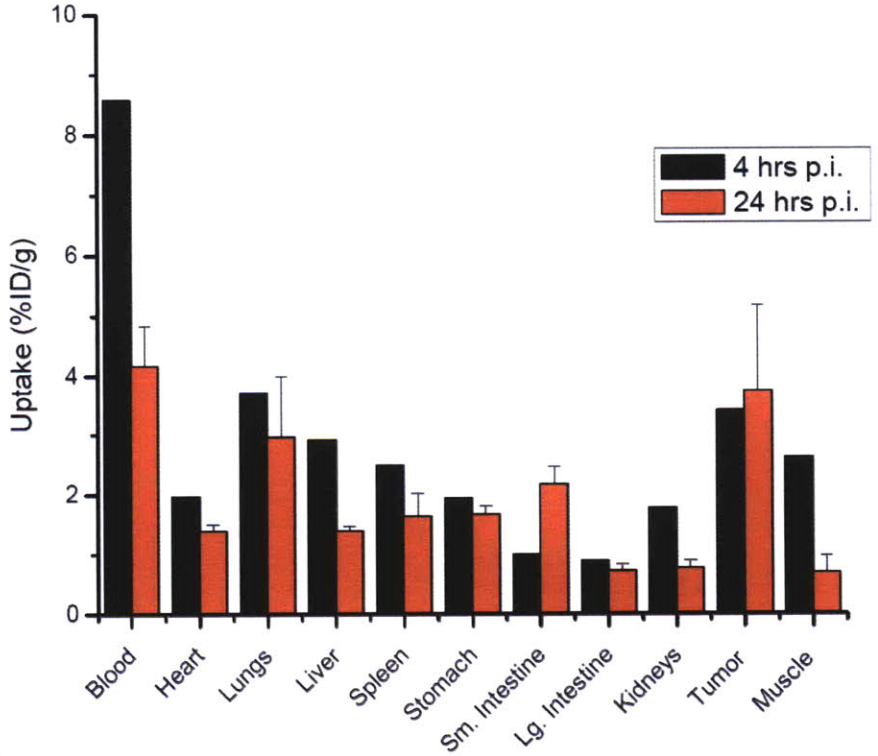

Figure 7.5 ^{131}I-A33/C825 organ/tissue biodistribution at 4 and 24 h. Organ/tissue activity at 4 and 24 h p.i. of 0.02 of ^{131}I-A33/C825 bsAb in SW1222 tumor bearing mice.

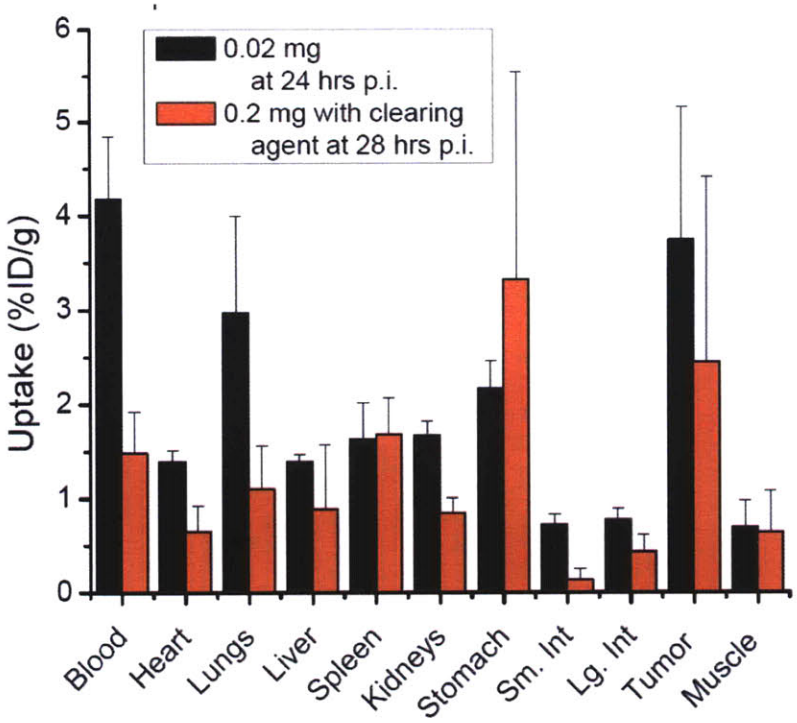

Figure 7.6 ^{131}I-A33/C825 organ/tissue biodistribution with clearing agent. Organ/tissue activity of ^{131}I-A33/C825 bsAb with and without dextran-DOTA-Y clearing agent in SW1222 tumor bearing mice.

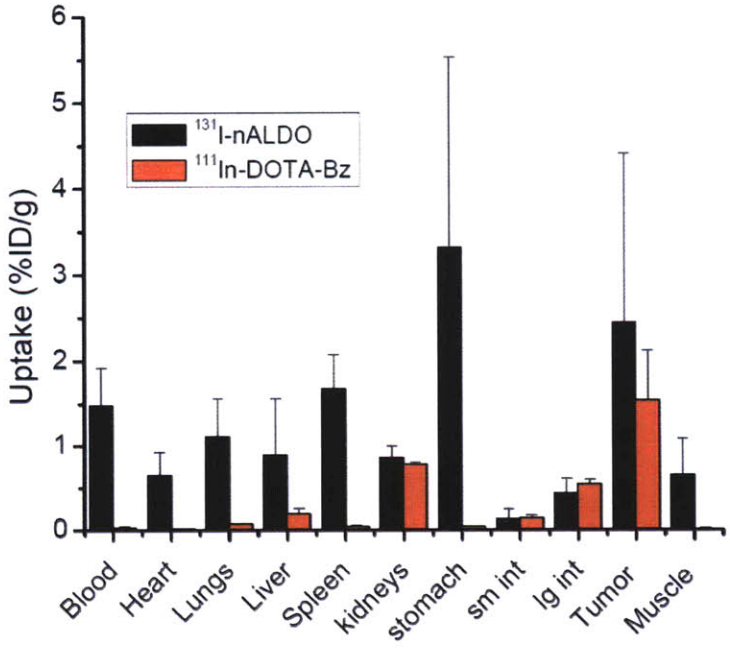

Figure 7.7 BsAb and ^{111}In-DOTA-Bn organ/tissue biodistribution. Organ/tissue activity of ^{131}I-A33/C825 (nALDO) and ^{111}In-DOTA-Bn in SW1222 tumor bearing mice. 0.2 mg ^{131}I-A33/C825 was administered at t = 0 h. 31 pmoles dextran-DOTA-Y was administered at t = 24 h and ^{111}In-DOTA-Bn was administered at t = 28 h. Animals were sacrificed at t = 29 h.

7.4. HEK293-F Transfection Agents

The expression level of the Sm3e/C825 bsAb in HEK293 cells using various transfection agents was tested. The results are presented in Table 7.2.

Table 7.2 Sm3e/C825 bsAb HEK293 secretion with different transfection agents

	Yield
PEI (25 mL culture, 7 d)	7.4 mg/L
jetPEI (25 mL culture, 7 d)	0.76 mg/L
PEI (1/2 L culture, 7 d)	6 mg/L
XpressNow (1/2 L culture, 7 d)	160 ug/L
PEI (32 mL culture, 15 d)	2.6 mg/L
PEI + 3 mM sodium butyrate + suppl day 8 (32 mL culture, 15 d)	12.6 mg/L

8. BIBLIOGRAPHY

Ashweek, N. J., I. Coldham, et al. (2003). "Preparation of diamines by lithiation-substitution of imidazolidines and pyrimidines." Organic & Biomolecular Chemistry **1**(9): 1532-1544.

Axworthy, D. B., J. M. Reno, et al. (2000). "Cure of human carcinoma xenografts by a single dose of pretargeted yttrium-90 with negligible toxicity." Proc Natl Acad Sci U S A **97**(4): 1802-7.

Bagshawe, K. D. (2006). "Antibody-directed enzyme prodrug therapy (ADEPT) for cancer." Expert Rev Anticancer Ther **6**(10): 1421-31.

Baish, J. W., Y. Gazit, et al. (1996). "Role of tumor vascular architecture in nutrient and drug delivery: an invasion percolation-based network model." Microvasc Res **51**(3): 327-46.

Banerjee, S. R., C. A. Foss, et al. (2008). "Synthesis and evaluation of technetium-99m- and rhenium-labeled inhibitors of the prostate-specific membrane antigen (PSMA)." J Med Chem **51**(15): 4504-17.

Barbet, J., P. Peltier, et al. (1998). "Radioimmunodetection of medullary thyroid carcinoma using indium-111 bivalent hapten and anti-CEA x anti-DTPA-indium bispecific antibody." J Nucl Med **39**(7): 1172-8.

Baxter, L. T. and R. K. Jain (1989). "Transport of fluid and macromolecules in tumors. I. Role of interstitial pressure and convection." Microvasc Res **37**(1): 77-104.

Behr, T. M., D. M. Goldenberg, et al. (1998). "Reducing the renal uptake of radiolabeled antibody fragments and peptides for diagnosis and therapy: present status, future prospects and limitations." Eur J Nucl Med **25**(2): 201-12.

Blake, D. A., R. M. Jones, et al. (2001). "Antibody-based sensors for heavy metal ions." Biosens Bioelectron **16**(9-12): 799-809.

Boder, E. T., K. S. Midelfort, et al. (2000). "Directed evolution of antibody fragments with monovalent femtomolar antigen-binding affinity." Proc Natl Acad Sci U S A **97**(20): 10701-5.

Boerman, O. C., F. G. van Schaijk, et al. (2003). "Pretargeted radioimmunotherapy of cancer: progress step by step." J Nucl Med **44**(3): 400-11.

Bogin, L., R. Margalit, et al. (2002). "Parametric imaging of tumor perfusion using flow- and permeability-limited tracers." J Magn Reson Imaging **16**(3): 289-99.

Boswell, C. A. and M. W. Brechbiel (2007). "Development of radioimmunotherapeutic and diagnostic antibodies: an inside-out view." Nucl Med Biol **34**(7): 757-78.

Bourrinet, P., E. Martel, et al. (2007). "Cardiovascular safety of gadoterate meglumine (Gd-DOTA)." Invest Radiol **42**(2): 63-77.

Bowley, D. R., A. F. Labrijn, et al. (2007). "Antigen selection from an HIV-1 immune antibody library displayed on yeast yields many novel antibodies compared to selection from the same library displayed on phage." Protein Eng Des Sel **20**(2): 81-90.

Butlin, N. G. and C. F. Meares (2006). "Antibodies with infinite affinity: origins and applications." Acc Chem Res **39**(10): 780-7.

Byegard, J., G. Skarnemark, et al. (1999). "The stability of some metal EDTA, DTPA and DOTA complexes: Application as tracers in groundwater studies." Journal of Radioanalytical and Nuclear Chemistry **241**(2): 281-290.

Camera, L., S. Kinuya, et al. (1994). "Evaluation of the serum stability and in vivo biodistribution of CHX-DTPA and other ligands for yttrium labeling of monoclonal antibodies." J Nucl Med **35**(5): 882-9.

Capdevila, J., E. Elez, et al. (2009). "Anti-epidermal growth factor receptor monoclonal antibodies in cancer treatment." Cancer Treat Rev **35**(4): 354-63.

Chao, G., W. L. Lau, et al. (2006). "Isolating and engineering human antibodies using yeast surface display." Nat Protoc **1**(2): 755-68.

Chen, X., R. Park, et al. (2004). "MicroPET and autoradiographic imaging of breast cancer alpha v-integrin expression using 18F- and 64Cu-labeled RGD peptide." Bioconjug Chem **15**(1): 41-9.

Chen, X., E. Sievers, et al. (2005). "Integrin alpha v beta 3-targeted imaging of lung cancer." Neoplasia **7**(3): 271-9.

Coloma, M. J. and S. L. Morrison (1997). "Design and production of novel tetravalent bispecific antibodies." Nat Biotechnol **15**(2): 159-63.

Cooper, M. S., E. Sabbah, et al. (2006). "Conjugation of chelating agents to proteins and radiolabeling with trivalent metallic isotopes." Nat Protoc **1**(1): 314-7.

Corneillie, T. M., A. J. Fisher, et al. (2003). "Crystal structures of two complexes of the rare-earth-DOTA-binding antibody 2D12.5: ligand generality from a chiral system." J Am Chem Soc **125**(49): 15039-48.

Corneillie, T. M., P. A. Whetstone, et al. (2003). "A rare earth-DOTA-binding antibody: probe properties and binding affinity across the lanthanide series." J Am Chem Soc **125**(12): 3436-7.

Corneillie, T. M., P. A. Whetstone, et al. (2004). "Converting weak binders into infinite binders." Bioconjug Chem **15**(6): 1389-91.

Cox, J. P. L., A. S. Craig, et al. (1990). "SYNTHESIS OF C-FUNCTIONALIZED AND N-FUNCTIONALIZED DERIVATIVES OF 1,4,7-TRIAZACYCLONONANE-1,4,7-TRIYLTRIACETIC ACID (NOTA), 1,4,7,10-TETRA-AZACYCLODODECANE-1,4,7,10-TETRAYLTETRA-ACETIC ACID (DOTA), AND DIETHYLENENETRIAMINEPENTA-ACETIC ACID (DTPA) - BIFUNCTIONAL COMPLEXING AGENTS FOR THE DERIVATIZATION OF ANTIBODIES." Journal of the Chemical Society-Perkin Transactions 1(9): 2567-2576.

Cutler, C. S., C. J. Smith, et al. (2000). "Current and potential therapeutic uses of lanthanide radioisotopes." Cancer Biother Radiopharm **15**(6): 531-45.

Daldrup, H., D. M. Shames, et al. (1998). "Correlation of dynamic contrast-enhanced MR imaging with histologic tumor grade: comparison of macromolecular and small-molecular contrast media." AJR Am J Roentgenol **171**(4): 941-9.

DeNardo, D. G., C. Y. Xiong, et al. (2001). "Anti-HLA-DR/anti-DOTA diabody construction in a modular gene design platform: bispecific antibodies for pretargeted radioimmunotherapy." Cancer Biother Radiopharm **16**(6): 525-35.

Emami, B., J. Lyman, et al. (1991). "Tolerance of normal tissue to therapeutic irradiation." Int J Radiat Oncol Biol Phys **21**(1): 109-22.

Fenwick, J. R., G. W. Philpott, et al. (1989). "Biodistribution and histological localization of anti-human colon cancer monoclonal antibody (MAb) 1A3: the influence of administered MAb dose on tumor uptake." Int J Cancer **44**(6): 1017-27.

Fisher, D. R., S. Shen, et al. (2009). "MIRD dose estimate report No. 20: radiation absorbed-dose estimates for 111In- and 90Y-ibritumomab tiuxetan." J Nucl Med **50**(4): 644-52.

Ford, C. H., P. A. Osborne, et al. (2001). "Bispecific antibody targeting of doxorubicin to carcinoembryonic antigen-expressing colon cancer cell lines in vitro and in vivo." Int J Cancer **92**(6): 851-5.

Forster, G. J., E. B. Santos, et al. (2006). "Pretargeted radioimmunotherapy with a single-chain antibody/streptavidin construct and radiolabeled DOTA-biotin: strategies for reduction of the renal dose." J Nucl Med **47**(1): 140-9.

Garber, K. (2003). "Lymphoma market turf war imminent, pending Bexxar approval." Nat Biotechnol **21**(2): 115-6.

Garcia de Palazzo, I., M. Holmes, et al. (1992). "Antitumor effects of a bispecific antibody targeting CA19-9 antigen and CD16." Cancer Res **52**(20): 5713-9.

Garrett, T. P., A. W. Burgess, et al. (2009). "Antibodies specifically targeting a locally misfolded region of tumor associated EGFR." Proc Natl Acad Sci U S A **106**(13): 5082-7.

Garrison, J. C., T. L. Rold, et al. (2007). "In vivo evaluation and small-animal PET/CT of a prostate cancer mouse model using 64Cu bombesin analogs: side-by-side comparison of the CB-TE2A and DOTA chelation systems." J Nucl Med **48**(8): 1327-37.

Gauer, O. H., J. P. Henry, et al. (1970). "The regulation of extracellular fluid volume." Annu Rev Physiol **32**: 547-95.

Gautherot, E., E. Rouvier, et al. (2000). "Pretargeted radioimmunotherapy of human colorectal xenografts with bispecific antibody and 131I-labeled bivalent hapten." J Nucl Med **41**(3): 480-7.

Goldenberg, D. M., J. F. Chatal, et al. (2007). "Cancer Imaging and Therapy with Bispecific Antibody Pretargeting." Update Cancer Ther **2**(1): 19-31.

Goldenberg, D. M., E. A. Rossi, et al. (2008). "Multifunctional antibodies by the Dock-and-Lock method for improved cancer imaging and therapy by pretargeting." J Nucl Med **49**(1): 158-63.

Goodwin, D. A., C. F. Meares, et al. (1988). "Pre-targeted immunoscintigraphy of murine tumors with indium-111-labeled bifunctional haptens." J Nucl Med **29**(2): 226-34.

Goodwin, D. A., C. F. Meares, et al. (1994). "Pharmacokinetics of Pretargeted Monoclonal-Antibody 2d12.5 and Y-88 Janus-2-(P-Nitrobenzyl)-1,4,7,10-Tetraazacyclododecanetetraacetic Acid (Dota) in Balb/C Mice with Khjj Mouse Adenocarcinoma - a Model for Y-90 Radioimmunotherapy." Cancer Research **54**(22): 5937-5946.

Govindan, S. V., D. M. Goldenberg, et al. (2000). "Advances in the use of monoclonal antibodies in cancer radiotherapy." Pharm Sci Technolo Today **3**(3): 90-98.

Graff, C. P., K. Chester, et al. (2004). "Directed evolution of an anti-carcinoembryonic antigen scFv with a 4-day monovalent dissociation half-time at 37 degrees C." Protein Eng Des Sel **17**(4): 293-304.

Graff, C. P. and K. D. Wittrup (2003). "Theoretical analysis of antibody targeting of tumor spheroids: importance of dosage for penetration, and affinity for retention." Cancer Res **63**(6): 1288-96.

Graziano, R. F. and P. Guptill (2004). "Chemical production of bispecific antibodies." Methods Mol Biol **283**: 71-85.

Hackel, B. J., A. Kapila, et al. (2008). "Picomolar affinity fibronectin domains engineered utilizing loop length diversity, recursive mutagenesis, and loop shuffling." J Mol Biol **381**(5): 1238-52.

Hamblett, K. J., B. B. Kegley, et al. (2002). "A streptavidin-biotin binding system that minimizes blocking by endogenous biotin." Bioconjug Chem **13**(3): 588-98.

Harmsen, M. M. and H. J. De Haard (2007). "Properties, production, and applications of camelid single-domain antibody fragments." Appl Microbiol Biotechnol **77**(1): 13-22.

Hayat, A. (2008). "Safety issues with intravenous iron products in the management of anemia in chronic kidney disease." Clin Med Res **6**(3-4): 93-102.

Hilmas, D. E. and E. L. Gillette (1974). "Morphometric analyses of the microvasculature of tumors during growth and after x-irradiation." Cancer **33**(1): 103-10.

Hopper-Borge, E. A., R. E. Nasto, et al. (2009). "Mechanisms of tumor resistance to EGFR-targeted therapies." Expert Opin Ther Targets **13**(3): 339-62.

Horning, S. J., A. Younes, et al. (2005). "Efficacy and safety of tositumomab and iodine-131 tositumomab (Bexxar) in B-cell lymphoma, progressive after rituximab." J Clin Oncol **23**(4): 712-9.

Hudson, P. J. and C. Souriau (2003). "Engineered antibodies." Nat Med **9**(1): 129-34.

Humblet, V., P. Misra, et al. (2009). "Multivalent scaffolds for affinity maturation of small molecule cell surface binders and their application to prostate tumor targeting." J Med Chem **52**(2): 544-50.

Humblet, V., P. Misra, et al. (2006). "An HPLC/mass spectrometry platform for the development of multimodality contrast agents and targeted therapeutics: prostate-specific membrane antigen small molecule derivatives." Contrast Media Mol Imaging **1**(5): 196-211.

Iannello, A. and A. Ahmad (2005). "Role of antibody-dependent cell-mediated cytotoxicity in the efficacy of therapeutic anti-cancer monoclonal antibodies." Cancer Metastasis Rev **24**(4): 487-99.

Ince, N., S. M. de la Monte, et al. (2000). "Overexpression of human aspartyl (asparaginyl) beta-hydroxylase is associated with malignant transformation." Cancer Res **60**(5): 1261-6.

Jaggi, J. S., S. V. Seshan, et al. (2006). "Mitigation of radiation nephropathy after internal alpha-particle irradiation of kidneys." Int J Radiat Oncol Biol Phys **64**(5): 1503-12.

Janevik-Ivanovska, E., E. Gautherot, et al. (1997). "Bivalent hapten-bearing peptides designed for iodine-131 pretargeted radioimmunotherapy." Bioconjug Chem **8**(4): 526-33.

Joosten, C. E., L. S. Cohen, et al. (2004). "Glycosylation profiles of the human colorectal cancer A33 antigen naturally expressed in the human colorectal cancer cell line SW1222 and expressed as recombinant protein in different insect cell lines." Biotechnol Prog **20**(4): 1273-9.

Karacay, H., P. Y. Brard, et al. (2005). "Therapeutic advantage of pretargeted radioimmunotherapy using a recombinant bispecific antibody in a human colon cancer xenograft." Clin Cancer Res **11**(21): 7879-85.

Kenanova, V., T. Olafsen, et al. (2005). "Tailoring the pharmacokinetics and positron emission tomography imaging properties of anti-carcinoembryonic antigen single-chain Fv-Fc antibody fragments." Cancer Res **65**(2): 622-31.

Knox, S. J., M. L. Goris, et al. (2000). "Phase II trial of yttrium-90-DOTA-biotin pretargeted by NR-LU-10 antibody/streptavidin in patients with metastatic colon cancer." Clin Cancer Res **6**(2): 406-14.

Kontermann, R. E. (2005). "Recombinant bispecific antibodies for cancer therapy." Acta Pharmacol Sin **26**(1): 1-9.

Kraeber-Bodere, F., A. Faivre-Chauvet, et al. (1999). "Toxicity and efficacy of radioimmunotherapy in carcinoembryonic antigen-producing medullary thyroid cancer xenograft: comparison of iodine 131-labeled F(ab')2 and pretargeted bivalent hapten and evaluation of repeated injections." Clin Cancer Res **5**(10 Suppl): 3183s-3189s.

Kraeber-Bodere, F., C. Rousseau, et al. (2006). "Targeting, toxicity, and efficacy of 2-step, pretargeted radioimmunotherapy using a chimeric bispecific antibody and 131I-labeled bivalent hapten in a phase I optimization clinical trial." J Nucl Med **47**(2): 247-55.

Larson, S. M., J. A. Carrasquillo, et al. (1984). "Radioimmunodetection and radioimmunotherapy." Cancer Invest **2**(5): 363-81.

Lavaissiere, L., S. Jia, et al. (1996). "Overexpression of human aspartyl(asparaginyl)beta-hydroxylase in hepatocellular carcinoma and cholangiocarcinoma." J Clin Invest **98**(6): 1313-23.

Le Doussal, J. M., M. Martin, et al. (1989). "In vitro and in vivo targeting of radiolabeled monovalent and divalent haptens with dual specificity monoclonal antibody conjugates: enhanced divalent hapten affinity for cell-bound antibody conjugate." J Nucl Med **30**(8): 1358-66.

Le Mignon, M. M., C. Chambon, et al. (1990). "Gd-DOTA. Pharmacokinetics and tolerability after intravenous injection into healthy volunteers." Invest Radiol **25**(8): 933-7.

Lin, Y., J. M. Pagel, et al. (2006). "A genetically engineered anti-CD45 single-chain antibody-streptavidin fusion protein for pretargeted radioimmunotherapy of hematologic malignancies." Cancer Res **66**(7): 3884-92.

Liu, G., S. Dou, et al. (2007). "Predicting the biodistribution of radiolabeled cMORF effector in MORF-pretargeted mice." Eur J Nucl Med Mol Imaging **34**(2): 237-46.

Liu, H., Z. Miao, et al. (2009). "In vivo evaluation of melanoma targeted multivalent alpha-melanocyte-stimulating hormone analogs using microPET studies." J Nucl Med **50**(Supplement 2): 1586.

Love, R. A., J. E. Villafranca, et al. (1993). "How the anti-(metal chelate) antibody CHA255 is specific for the metal ion of its antigen: X-ray structures for two Fab'/hapten complexes with different metals in the chelate." Biochemistry **32**(41): 10950-9.

Lu, D., H. Zhang, et al. (2005). "A fully human recombinant IgG-like bispecific antibody to both the epidermal growth factor receptor and the insulin-like growth factor receptor for enhanced antitumor activity." J Biol Chem **280**(20): 19665-72.

Lubic, S. P., D. A. Goodwin, et al. (2001). "Biodistribution and dosimetry of pretargeted monoclonal antibody 2D12.5 and Y-Janus-DOTA in BALB/c mice with KHJJ mouse adenocarcinoma." J Nucl Med **42**(4): 670-8.

Mammen, M., S. K. Choi, et al. (1998). "Polyvalent interactions in biological systems: Implications for design and use of multivalent ligands and inhibitors." Angew. Chem., Int. Ed. Eng. **37**: 2755.

Marvin, J. S. and Z. Zhu (2005). "Recombinant approaches to IgG-like bispecific antibodies." Acta Pharmacol Sin **26**(6): 649-58.

McCall, A. M., L. Shahied, et al. (2001). "Increasing the affinity for tumor antigen enhances bispecific antibody cytotoxicity." J Immunol **166**(10): 6112-7.

McDevitt, M. R., D. Ma, et al. (2001). "Tumor therapy with targeted atomic nanogenerators." Science **294**(5546): 1537-40.

Menard, S., S. Canevari, et al. (1989). "Hybrid antibodies in cancer diagnosis and therapy." Int J Biol Markers **4**(3): 131-4.

Midelfort, K. S., H. H. Hernandez, et al. (2004). "Substantial energetic improvement with minimal structural perturbation in a high affinity mutant antibody." J Mol Biol **343**(3): 685-701.

Misra, P., V. Humblet, et al. (2007). "Production of multimeric prostate-specific membrane antigen small-molecule radiotracers using a solid-phase 99mTc preloading strategy." J Nucl Med **48**(8): 1379-89.

Moreau, J., E. Guillon, et al. (2004). "Complexing mechanism of the lanthanide cations Eu3+, Gd3+, and Tb3+ with 1,4,7,10-tetrakis(carboxymethyl)-1,4,7,10-tetraazacyclododecane (dota)-characterization of three successive complexing phases: study of the thermodynamic and structural properties of the complexes by potentiometry, luminescence spectroscopy, and EXAFS." Chemistry **10**(20): 5218-32.

Nayeem, M. S. and R. H. Khan (2006). "Recombinant antibodies in cancer therapy." Curr Protein Pept Sci **7**(2): 165-70.

Nygren, P. A. (2008). "Alternative binding proteins: affibody binding proteins developed from a small three-helix bundle scaffold." FEBS J **275**(11): 2668-76.

Olafsen, T., V. E. Kenanova, et al. (2006). "Tunable pharmacokinetics: modifying the in vivo half-life of antibodies by directed mutagenesis of the Fc fragment." Nat Protoc **1**(4): 2048-60.

Paganelli, G., P. Magnani, et al. (1991). "Three-step monoclonal antibody tumor targeting in carcinoembryonic antigen-positive patients." Cancer Res **51**(21): 5960-6.

Pagel, J. M., N. Hedin, et al. (2003). "Comparison of anti-CD20 and anti-CD45 antibodies for conventional and pretargeted radioimmunotherapy of B-cell lymphomas." Blood **101**(6): 2340-8.

Park, S. I. and O. W. Press (2007). "Radioimmunotherapy for treatment of B-cell lymphomas and other hematologic malignancies." Curr Opin Hematol **14**(6): 632-8.

Penfield, J. G. and R. F. Reilly (2008). "Nephrogenic systemic fibrosis risk: is there a difference between gadolinium-based contrast agents?" Semin Dial **21**(2): 129-34.

Press, O. W., M. Corcoran, et al. (2001). "A comparative evaluation of conventional and pretargeted radioimmunotherapy of CD20-expressing lymphoma xenografts." Blood **98**(8): 2535-43.

Pressman, D. (1957). "Radiolabeled antibodies." Ann N Y Acad Sci **69**(4): 644-50.

Rader, C., G. Ritter, et al. (2000). "The rabbit antibody repertoire as a novel source for the generation of therapeutic human antibodies." J Biol Chem **275**(18): 13668-76.

Reiter, Y., U. Brinkmann, et al. (1994). "Stabilization of the Fv fragments in recombinant immunotoxins by disulfide bonds engineered into conserved framework regions." Biochemistry **33**(18): 5451-9.

Reiter, Y., U. Brinkmann, et al. (1996). "Engineering antibody Fv fragments for cancer detection and therapy: disulfide-stabilized Fv fragments." Nat Biotechnol **14**(10): 1239-45.

Rossi, E. A., D. M. Goldenberg, et al. (2006). "Stably tethered multifunctional structures of defined composition made by the dock and lock method for use in cancer targeting." Proc Natl Acad Sci U S A **103**(18): 6841-6.

Schmidt, M. M., G. M. Thurber, et al. (2008). "Kinetics of anti-carcinoembryonic antigen antibody internalization: effects of affinity, bivalency, and stability." Cancer Immunol Immunother.

Schmidt, M. M. and K. D. Wittrup (2009). "A modeling analysis of the effects of molecular size and binding affinity on tumor targeting." Mol Cancer Ther **8**(10): 2861-2871.

Schmitt, A., P. Bernhardt, et al. (2005). "Differences in biodistribution between 99mTc-depreotide, 111In-DTPA-octreotide, and 177Lu-DOTA-Tyr3-octreotate in a small cell lung cancer animal model." Cancer Biother Radiopharm **20**(2): 231-6.

Schneider, D. W., T. Heitner, et al. (2009). "In vivo biodistribution, PET imaging, and tumor accumulation of 86Y- and 111In-antimindin/RG-1, engineered antibody fragments in LNCaP tumor-bearing nude mice." J Nucl Med **50**(3): 435-43.

Scott, A. M., F. T. Lee, et al. (2005). "A phase I trial of humanized monoclonal antibody A33 in patients with colorectal carcinoma: biodistribution, pharmacokinetics, and quantitative tumor uptake." Clin Cancer Res **11**(13): 4810-7.

Sharkey, R. M., T. M. Cardillo, et al. (2005). "Signal amplification in molecular imaging by pretargeting a multivalent, bispecific antibody." Nat Med **11**(11): 1250-5.

Sharkey, R. M., H. Karacay, et al. (2009). "Pretargeted versus directly targeted radioimmunotherapy combined with anti-CD20 antibody consolidation therapy of non-Hodgkin lymphoma." J Nucl Med **50**(3): 444-53.

Sharkey, R. M., H. Karacay, et al. (2008). "Metastatic human colonic carcinoma: molecular imaging with pretargeted SPECT and PET in a mouse model." Radiology **246**(2): 497-507.

Sharkey, R. M., W. J. McBride, et al. (2003). "A universal pretargeting system for cancer detection and therapy using bispecific antibody." Cancer Res **63**(2): 354-63.

Shen, J., M. D. Vil, et al. (2007). "Single variable domain antibody as a versatile building block for the construction of IgG-like bispecific antibodies." J Immunol Methods **318**(1-2): 65-74.

Shih, L. B., S. R. Thorpe, et al. (1994). "The processing and fate of antibodies and their radiolabels bound to the surface of tumor cells in vitro: a comparison of nine radiolabels." J Nucl Med **35**(5): 899-908.

Siegel, J. A. and M. G. Stabin (1994). "Absorbed fractions for electrons and beta particles in spheres of various sizes." J Nucl Med **35**(1): 152-6.

Snyder, W. S., M. R. Ford, et al. (1975). "S," absorbed dose per unit cumulated activity for selected radionuclides and organs. New York, Society of Nuclear Medicine: 1-257.

Stabin, M. G. and J. A. Siegel (2003). "Physical models and dose factors for use in internal dose assessment." Health Phys **85**(3): 294-310.

Stickney, D. R., L. D. Anderson, et al. (1991). "Bifunctional antibody: a binary radiopharmaceutical delivery system for imaging colorectal carcinoma." Cancer Res **51**(24): 6650-5.

Takenouchi, K., K. Watanabe, et al. (1993). "Novel Bifunctional Macrocyclic Chelating-Agents Appended With A Pendant-Type Carboxymethylamino Ligand And Nitrobenzyl Group And Sability Of The Y-88(III) Complexes." Journal of Organic Chemistry **58**(7): 1955-1958.

Tassev, D. V. and N. K. Cheung (2009). "Monoclonal antibody therapies for solid tumors." Expert Opin Biol Ther **9**(3): 341-53.

Thurber, G. M., M. M. Schmidt, et al. (2008). "Antibody tumor penetration: transport opposed by systemic and antigen-mediated clearance." Adv Drug Deliv Rev **60**(12): 1421-34.

Thurber, G. M. and K. D. Wittrup (2008). "Quantitative spatiotemporal analysis of antibody fragment diffusion and endocytic consumption in tumor spheroids." Cancer Res **68**(9): 3334-41.

Thurber, G. M., S. C. Zajic, et al. (2007). "Theoretic criteria for antibody penetration into solid tumors and micrometastases." J Nucl Med **48**(6): 995-9.

Tofts, P. S. (1997). "Modeling tracer kinetics in dynamic Gd-DTPA MR imaging." J Magn Reson Imaging **7**(1): 91-101.

van Gog, F. B., G. W. Visser, et al. (1998). "Synthesis and evaluation of 99mTc/99Tc-MAG3-biotin conjugates for antibody pretargeting strategies." Nucl Med Biol **25**(7): 611-9.

van Schaijk, F. G., E. Oosterwijk, et al. (2005). "Pretargeting of carcinoembryonic antigen-expressing tumors with a biologically produced bispecific anticarcinoembryonic antigen x anti-indium-labeled diethylenetriaminepentaacetic acid antibody." Clin Cancer Res **11**(19 Pt 2): 7130s-7136s.

VanAntwerp, J. J. and K. D. Wittrup (2000). "Fine affinity discrimination by yeast surface display and flow cytometry." Biotechnol Prog **16**(1): 31-7.

Weiner, L. M., M. V. Dhodapkar, et al. (2009). "Monoclonal antibodies for cancer immunotherapy." Lancet **373**(9668): 1033-40.

Welt, S., C. R. Divgi, et al. (1990). "Quantitative analysis of antibody localization in human metastatic colon cancer: a phase I study of monoclonal antibody A33." J Clin Oncol **8**(11): 1894-906.

Wessels, B. W., W. E. Bolch, et al. (2004). "Bone marrow dosimetry using blood-based models for radiolabeled antibody therapy: a multiinstitutional comparison." J Nucl Med **45**(10): 1725-33.

Wild, D., M. Behe, et al. (2006). "[Lys40(Ahx-DTPA-111In)NH2]exendin-4, a very promising ligand for glucagon-like peptide-1 (GLP-1) receptor targeting." J Nucl Med **47**(12): 2025-33.

Worn, A. and A. Pluckthun (2001). "Stability engineering of antibody single-chain Fv fragments." J Mol Biol **305**(5): 989-1010.

Wu, C., H. Ying, et al. (2007). "Simultaneous targeting of multiple disease mediators by a dual-variable-domain immunoglobulin." Nat Biotechnol **25**(11): 1290-7.

Yang, S. S., E. L. Nickoloff, et al. (1978). "Tc-99m human serum albumin: a suitable agent for plasma volume measurements in man." J Nucl Med **19**(7): 804-7.

Yeung, Y. A. (2005). Antibody Engineering for Cancer Therapy. Chemical Engineering. Cambridge, Massachusetts Institute of Technology.

Yeung, Y. A., A. H. Finney, et al. (2007). "Isolation and characterization of human antibodies targeting human aspartyl (asparaginyl) beta-hydroxylase." Hum Antibodies **16**(3-4): 163-76.

Zacchetti, A., A. Coliva, et al. (2009). "(177)Lu- labeled MOv18 as compared to (131)I- or (90)Y-labeled MOv18 has the better therapeutic effect in eradication of alpha folate receptor-expressing tumor xenografts." Nucl Med Biol **36**(7): 759-70.

Zhang, H., J. Schuhmacher, et al. (2007). "DOTA-PESIN, a DOTA-conjugated bombesin derivative designed for the imaging and targeted radionuclide treatment of bombesin receptor-positive tumours." Eur J Nucl Med Mol Imaging **34**(8): 1198-208.

Zhu, H., R. K. Jain, et al. (1998). "Tumor pretargeting for radioimmunodetection and radioimmunotherapy." J Nucl Med **39**(1): 65-76.